Master Thesis

Haptic Shared Control in Deep Sea Mining – Enhancing Teleoperation of a Subsea Crawler

Kang Wang

Delft, August 2014

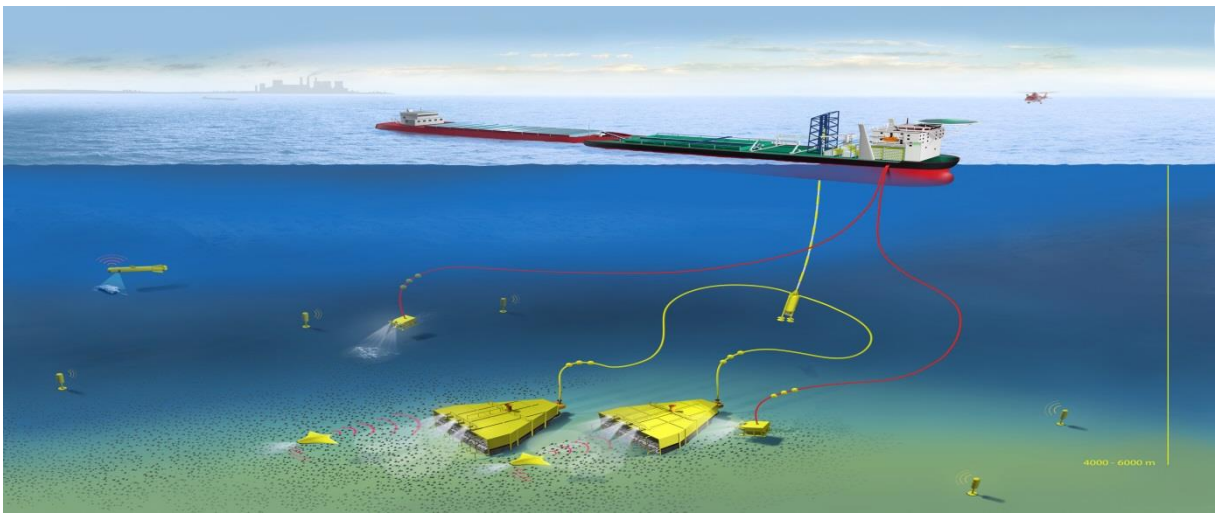

Student No.: 4249194
BioMechanical Design
Department of Mechanical Engineering
Delft University of Technology

The picture on the cover page comes from:
http://www.austmine.com.au/News/tabid/790/articleType/ArticleView/articleId/1540/The-future-of-deep-sea-mining.aspx

Haptic Shared Control in Deep Sea Mining – Enhancing Teleoperation of a Subsea Crawler

Kang Wang

Committee:

Dr.Ir. D. A. Abbink	*BioMechanical Engineering, Department of Mechanical Engineering, 3ME.*
Dr. T.L.Gibo	*BioMechanical Engineering, Department of Mechanical Engineering, 3ME*
Ir. R.J. Kuiper	*BioMechanical Engineering, Department of Mechanical Engineering,3ME.*
Dr.Ir. D.M. Pool	*Aerospace Engineering, Department of Control and Simulation, LR.*

Supervisor: *Ir. R.J. Kuiper*
Dr. T. Gibo
Dr.Ir. D.A. Abbink

Preface

During my Master's study, I have become fascinated by the interaction between human and machine. The methodology of haptic shared control combines precision of automated controller and operator's higher intelligence, which I believe is a promising approach to improve control performance in various engineering applications. Personally I was very passionate to study the efficacy of such a novel principle in specific applications. One of these possible implementations is teleoperation of subsea vehicles supporting future deep sea mining. In this study, I focus on investigating the strength of haptic shared control into driving a simulated subsea crawler, by comparing its performance with manual control and supervisory control.

The main content of my thesis was studying and simulating dynamics of subsea crawler under seabed scenario, constructing novel master device to carry out bi-manual control of such a vehicle, designing the man-machine interface and executing the man-machine experiment. Besides the report itself, the appendices enclosed to this report provide more details about the background information and adversities I encountered during this project, along with extra results from the man-machine experiment.

I'd like to specially thank Ir. Roel Kuiper for the time and patience he spent on my work throughout my project. Although once as a student with barely any knowledge in offshore engineering, with Roel's continuous guidance and explanations, I learned quite a lot about both deep sea and real engineering installations. The special course on Bachmann real time computer given by Roel really saved me a lot of time during interface construction. Also I'd like to express my highest gratitude to Dr. David Abbink and Dr. Tricia Gibo, for their countless feedbacks and suggestions on my every single step through our regular discussions. I'd also like to thank all members in the Delft haptic lab, Joroen Wildenbeest, Henri Boessenkool, Patrice Lambert, Jack Schorsch, Teun Hoevenaars, Bram Onneweer and Eline van der Kruk, who provided me with advices intermittently and also considerable cups of free coffee all the time. Moreover, I'd like to applaud to all the subjects who were willing to offer their precious time in participating in my long time experiment even during the exam period. Last but not least, I would like to thank my family members in China for their supports through weekly video chats, which empowered me spiritually every time when I felt defeated or stressed by either the problems in project or the nostalgia.

A USB-disk containing all raw data from the experiment, software, GUI files, literature and analysing scripts has been submitted to the depository in department of BioMechanical Engineering, all of which are available on request.

Haptic Shared Control in Deep Sea Mining – Enhacing Teleoperation of Subsea Crawler

Kang Wang[*], Roel J.Kuiper[*†], Tricia Gibo[*], David A.Abbink[*]

Abstract— Deep sea mining is currently being investigated as a possibility to harvest valuable materials from mineral-rich areas located in water depths up to 2000 meters. One promising mining method is to employ a large crawler on the seabed, remotely controlled by an operator on the supporting vessel. Controlling such a vehicle is expected to be difficult due to unpredictable seabed conditions and limited situation awareness of the operator. In addition, the optimal human-machine interface for controlling the crawler is yet to be determined. A common approach in marine operation is to automate the task as much as possible, leaving the operator in a supervisory role. An alternative approach is haptic shared control, which has shown to be beneficial in vehicle control tasks (automotive, UAVs), yielding improved performance but mitigating traditional human-automation interaction issues such as skill degradation, reduced situation awareness and overreliance. This study aims to compare supervisory control and haptic shared control to manual control of a teleoperated subsea crawler. A simulator was constructed, including a bi-manual control interface capable of rendering haptic feedback, two virtual displays showing primary and secondary task-related information, a mathematical model simulating the dynamics of the slow vehicle, and unpredictable soil properties of the seabed. In a human factor experiment, subjects (n=12) controlled the simulated crawler to complete normal steering, repeated obstacle avoidance, and an unexpected slip event at the end; all with manual control, haptic shared control and supervisory control. During normal steering between obstacles, both haptic shared control and supervisory control improved subjects' performance and supervisory control allowed a significant decrease in control effort. However, during slip recovery and obstacle avoidance, supervisory control appreciably reduced subjects' situation awareness. Therefore haptic shared control is a promising approach to assist the operator in underwater teleoperation with improved task performance but not the side-effects from the automation.

Index Terms— Haptic shared control; Deep sea mining; Teleoperation; Supervisory control.

1 Introduction

Reseach on deep sea mining has been stimulated in recent years due to depletion of on-land mineral resources and detected promising amount of mineral deposits in deep sea. However it is an extremely harsh working environment because of the overwhelming hydrostatic pressure, deprivation of natural lighting and rough seabed bathymetry caused by tectonic activities. Those factors are causing problems on the excavation and mineral rising process, which impede the realization of actual deep see mining. Large water depth also induced further question on operator's system awareness and control transmission due to the long distance between the control station and the slave system. Thus a better approach to support future operator's control performance should be investigated.

The realization of deep sea mining has been studied for years, though all remain in the prototyping and experimental period. A popularly accepted architecture of deep sea mining includes a supporting vessel, a slurry rising system, and mineral recovery machines [1]–[3]. A tracked vehicle equipped with cutting tools, also called a subsea crawler, is believed suitable to serve as a mineral recovery machine. A subsea crawler is supposed to execute rock-cutting under tremendous hydrostatic pressure and move smoothly on seabed terrain, but in this study we only focused on the mobility of the crawler. Because the seabed environment is ever-changing due to unpredictable soil properties and turbidity, preprogrammed autonomous controllers may not be able to solve newly emerged problem. Therefore such a costly system should be controlled by an experienced operator. However the harsh environment of the deep sea mostly precludes human's direct presence in-situ manipulation, teleoperation is a much cheaper and safer option to realize human's manipulation of the mineral recovery machine than costly manned submersibles.

A subsea crawler has special dynamics which are difficult to control due to the unique soil-track interaction. The varying soil properties and unstructured terrain make the steering task challenging. Since no real system has ever been built yet, a simulation is constructed that vividly represents a scenario of deep sea mining. Popular prototypes of a subsea crawler are mainly inspired from the designs of off-road tracked vehicles and trenchers used in offshore pipeline burial [4], [5]. The study of terramechanics gives insight to the soil-track interaction of these tracked vehicles [6], [7]. Several analytical models were proposed to predict the off-road vehicle's responses to variables like sinkage depth, traction effort, and bulldozing resistance, which had a satisfactory match with results from in-situ measurements [8], [9]. Based on terramechanics theory, simulations of underwater remotely operated vehicle (ROV) based on the mathematic model have also been proposed [4], [10]–[12]. Both simulations and lab experiments have found that slip is much easier to occur in a seabed environment than a terrestrial vehicle,

since several mechanical properties of pelagic soil are weaker than that of continental soil. More importantly, the heterogeneity of seabed soil could result into sudden loss of traction force. Without accurate soil properties, preprogrammed autonomous controllers could hardly control the vehicle during a severe slip event. Nevertheless, research of deep sea mining has quite a number of outcomes about the dynamics of underwater vehicles, yet the human's control performance of such a vehicle hasn't been investigated.

A subsea crawler should be controlled so as to track a prescribed optimal path. An optimal path is determined based on early underwater investigations (e.g. pre-scan by multibeam and side scan, drilling samples) for the sake of both maximum production and vehicle safety. The most often used steering mechanism in controlling off-road vehicles is skid steering, in which steering is controlled by the relative speed difference between the left and right tracks of a vehicle [13]. Using skid steering is also believed to be the approach for controlling a subsea crawler to trace the optimal path, such that the speeds of the left and right track become two separate control inputs. Hong et al proposed a control algorithm that simultaneously determines the vehicle's desired heading angle by calculating the relative position between vehicle and closest point on the optimal path [14]. The desired heading angle can be adjusted by these two speed inputs according to pre-determined soil-track interaction. Alternatively, a more intelligent vehicle can be achieved by a successive learning algorithm to overcome the uncertainties in soil friction and hydrodynamic resistance, while keep the human monitoring the whole learning process[15]. However this method needs further validation, and there is the added possibility that the vehicle can deviate from the safe path during the learning process. Nevertheless, an optimal path tracking is not enough for a realistic simulation. Because the seabed is ever-changing, at the time of real excavation, the terrain could be different from previous terrain investigation. Subsea crawler may then run into other unexpected issues, such as newly emerged obstacles, and severe slip. These factors presented in the literatures should be better included into the simulation to test the robustness of the control maneuver.

Human's Control Approaches

As the subsea crawler needs to be teleoperated, authority of the operator's involvement in the control loop remains an open question. According to Sheridan's theory of level of automation [16], control methods for a teleoperation system spread along a spectrum with supervisory control at one end and manual (or bilateral) control at the other end. The concept of supervisory control was first proposed due to the time delay in command transmission in teleoperation tasks, which may limit the teleoperator to a 'wait-and-see' approach [17]. In supervisory control, the slave system could execute autonomously under certain phases, controlled by a local controller. The operator continuously receives a variety of information concerning the working status of the slave system, and only intervenes in the control loop in case of special needs or an emergency. Most of the time, supervisory control relies on automation, which is well known to reduce workload. But disadvantages of automation have been also reported [18], which may further result in misuse, disuse and abuse of automation [19]. Operator may use the automation to perform tasks it is not designed to handle (misuse), operator becomes too skeptical about the automation and refuses to use the automation (disuse), or implement the automation without sufficiently considering its effect to the human operator (abuse). Moreover, because the underwater slave system moves relatively slow, operator's vigilance towards unexpected events under supervisory control is highly questionable due to complacency and reduced system awareness. The control performance during unexpected events (e.g. obstacles, slip) may be much more deteriorated with higher level of automation. In contrast, these side-effects from automation can be significantly reduced in manual control. As in manual control, the operator takes full responsibility of the system and controls the movements of actuators via a master device, while the system continuously responds to the control inputs. Yet the system under manual control will be prone to human errors and operator's increased control effort will cause other problems, such as fatigue.

As the control authority changes intermittently between the operator and automation system in supervisory control, shared control emerges as an alternative to make the best use of human-machine cooperation [20]–[22]. Shared control keeps the human in the loop and combines the benefits from automation's precision and human's intelligence. Haptics is a more intuitive and less-occupied way than other sensory channels (e.g. auditory, visual) to provide a human-machine interaction [23]. The machine generates active force feedback on the control interface to guide human, where the forces are calculated by combining the dynamics of haptic interface with optimal control inputs. Haptic shared control has been proven to yield performance improvement and control effort relief in various applications like car driving [24]–[27] and telemanipulation [28], [29]. For example, in a path tracking task, if the operator conforms to the guidance, the machine will also follow the optimal path accurately. In this way, HSC is advantageous in more accurate path tracking, and indirectly reduced control activities and workload. HSC was also explored in the control of a suspended grab for deep sea mining, but only reduced control effort and some indirectly measured improved situation awareness was found [30]. The concept of using artificial guidance while keeping the human in the loop has not been implemented yet in an underwater vehicle where tricky soil-vehicle interaction exists.

Unlike steering a car, the heading angle of the subsea crawler is adjusted by the relative speed difference between two speed inputs. Former studies on shared control in assisting car driving constrains the vehicle to a constant speed such that the human only needed to con-

centrate on the single degree of freedom steering itself [31]–[33]. For a subsea crawler where skid steering is used, controlling the velocity of the vehicle is coupled with its heading angle; hence the operator also has the ability to adjust the vehicle speed. Therefore the steering guidance is achieved by the cooperation between two control inputs, so that operator should understand the guidance on a higher level. As the subsea crawler's change in movement is driven by a sequence of integrated tractive force, there will be lags between the operator's inputs and system outcome, i.e. the system does not respond immediately to a control input. Thus, the operator needs to predict the system's outcome with a self-built internal model of the causal relation between the control input and slow-changing system output [34].

Furthermore, in a control station, multiple screens are needed to represent all aspects of the working scenarios at the remote site. Thus the operator needs to perform a secondary task while steering a ROV. A secondary task could also be an approach to evaluate the subject's mental workload, i.e. how much processing capability is left for an additional task. An auditory recognition task was tested as secondary task in car driving, where only slightly shorter reaction time was found under HSC than manual control [32]. However resting visual processing ability is more interesting than auditory sense in underwater engineering applications as most of the information is delivered through visual perception. Thus a visual recognition task is preferred in this study.

Hypotheses

In order to solve all these aforementioned potential problems on a subsea crawler, the most suitable control maneuver needs to be found. In this study we are interested in comparing HSC and supervisory control to manual control in controlling a simulated subsea crawler. It is hypothesized that:

1. *A higher level of automation will lead to improve both primary steering performance and secondary task performance, while reduce the control effort.*
2. *Supervisory control will deteriorate the steering performance during unexpected events, but not for HSC.*

A human subject experiment was designed and executed to compare the effects of HSC and supervisory control with manual control. The operator was presented with a virtual environment of the remote site and a virtual subsea crawler. The operator's control commands on two single degree of freedom joysticks are acquired and translated into velocity commands of both tracks on each side of the virtual vehicle. The experiment in this study consists of steering a virtual vehicle to track a prescribed path and avoid sudden popped-up obstacles, while responding to a secondary visual recognition task, which will be described in details in section II. Different metrics used to evaluate results on steering performance and control activity are presented in section III. . Section IV further discusses the results and limitations of this experiment, and conclusions of this study are drawn in section V.

2 METHODS

2.1 Apparatus

This experiment setup consists of a pair of 1DOF joysticks as haptic interface, with which subjects could control the speed of each side of the tracks. Two identical *HP-1940* monitors, with 38.0×30.5 cm area of screen opening and 1280×1024 pixels resolution, are presented to the subjects, one showing a 3D representation of the camera view in virtual reality. The other display shows an integrated control panel, providing supplementary information about the status of the subsea crawler, such as global positioning, vehicle speed, control input, etc. A secondary visual recognition task is also presented on the virtual control panel. The simulated vehicle dynamics including soil-track interaction and single body dynamic modelling are calculated by real time computer and updated continuously on these two screens.

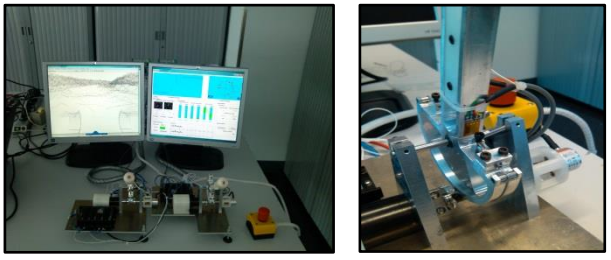

Figure 1. *Left:* Custom built experimental setup, including a bi-manual interface (two haptic joysticks), a 3d visualization of the primary steering task (left screen) and secondary task (right screen). *Right*: A close picture of the joystick. The handle is connected to the DC motor by a Capstan drive though steel cables.

The simulation in this study was based on the calculation of a virtual subsea crawler weighing 16 tons, with a maximum velocity on both tracks at 1m/s underwater. Ductile clay was chosen as the typical soil (soil cohesion at 10 Kpa, and soil angle of internal friction at 6 deg) to calculates the soil-track interaction. The guidance force and vehicle dynamics were calculated by a local real time computer (*Bachmann MH212/S*) at 500Hz. The maximum and minimum throttle on the joystick generated track speed at 1m/s and 0.05m/s respectively. Subjects were controlling the task via visual feedback on these two screens in front of the haptic interface. The 3D representation shown to the subjects are updated at 10Hz, according to parameters of vehicle status calculated from the virtual model in real time computer. On the top of each handle was mounted with a tactile single pole N/O pushbutton for answering the secondary task.

2.2 Task Description

In this study, the task of mobilizing the subsea crawler between mining fields was simulated. The subjects were asked to complete a path tracking task, where the prescribed optimal path was displayed on both 3D virtual environment (red curve in figure 3) and sub-screen on control panel. During the experiment, slave's lateral error and estimated time of arrival (ETA) were shown on the control panel as well.

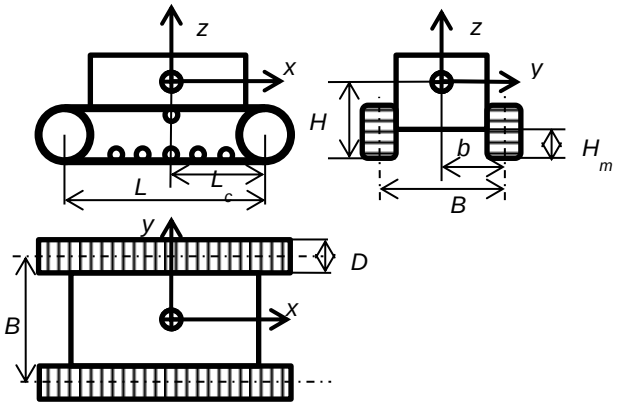

Figure 2. Parameterization of the virtual vehicle used in the dynamic model.

Track Length	**L**	6 m	Mass Center	$\mathbf{H_c}$	1.5 m
Track Width	**D**	0.6 m		$\mathbf{L_c}$	3 m
Thread Width	**b**	3.5 m		$\mathbf{B_c}$	1.75m
Vehicle Mass (in water)	**M**	16 ton	Moment of Inertia	$\mathbf{I_{xx}}$	$3.5e^4$ Kg/m^2
Projection Area	$\mathbf{A_p}$	10 m^2		$\mathbf{I_{yy}}$	$8.2e^4$ Kg/m^2
Chassis height	$\mathbf{H_{min}}$	0.5 m		$\mathbf{I_{zz}}$	$8.6e^4$ Kg/m^2

Table 1. Parameters of the virtual vehicle used in the dynamic model.

Because the seabed is ever-changing, there will be some differences in terrain status between preliminary investigation and actual conditions. It simulates the scenario that a local sensing system equipped on the crawler continuously acquires the terrain variations in vehicle's proximity, and updates the 3D virtual environment on the screen at the same time. Thus when the vehicle is moving, even without the obstacle, the virtual terrain in front of the vehicle hood still varies in elevation. Inevitably, some parts of the newly updated terrain may be insurmountable to the crawler, which is represented by a ditch in this simulator. Totally 12 obstacles were randomly distributed along the path, but not necessarily on the center of the path. Subjects were supposed to avoid such obstacles by skid steering (i.e. full throttle for one track and possibly minimum for the other), The simulation determined the moment to present the obstacle based on the speed of the vehicle:

$$L_{dist} = ttc \times v' \quad (1)$$

where $\boldsymbol{ttc}$ stands for time to collide, v' is the vehicle's heading speed with respect to the obstacle center. In this experiment we set $\boldsymbol{ttc}$ at 7 seconds, and once the simulator detects the distance between vehicle center and obstacle edge falls into this range $\boldsymbol{L_{dist}}$, the obstacle will be presented on the screen.

At the same time, subjects' workload was measured by a secondary visual recognition task. On the upper right side of the control panel, eight red markers are shown each time, whose positions were randomly updated once per four seconds. Participants were asked to identify the number of markers that fall into the specified range, represented by the black dashed circle (figure 3). Two tactile switches on the top of the handles were used by subjects to indicate their judgment. If the number is less or equal to 4, they were supposed to press switch on the left handle, otherwise the right one.

Aside from the obstacle avoidance and secondary task, an extra slip event was triggered at the end of the map, where the optimal path requires a left turn. On dynamic aspects, the left and right tracks lose 20% and 40% of maximum traction force respectively during this slip event. Subjects were not informed of the slip event in advance during the actual experiment, yet they experienced the slip event and practiced recovering from it during the training session once. Subjects were told that the guidance in both HSC and supervisory control could neither avoid the obstacle nor recover from the slip event by itself, so that their intervention was necessary during these unexpected events.

2.3 Experimental Conditions

Three experimental conditions are offered to the subjects during the experiment. The pure manual control was taken as the baseline to compare with HSC and supervisory control. The calculation of optimal vehicle's track speeds in HSC and supervisory control was mainly adapted from former study on path tracking for tracked vehicle [14]. Because the vehicle speed and heading angle are coupled, with a desired heading speed and heading angle, optimal net traction force $\overline{\boldsymbol{F_L}}$ and $\overline{\boldsymbol{F_R}}$ on two sides can be solved. According to terramechanics for tracked vehicle, if the mechanical properties of soil are determined, the desired slip ratio $(\boldsymbol{i_L}, \boldsymbol{i_R})$ can be obtained from the experiment measurement on the curve relates vehicle's net traction force with slip ratio. For the sake of brevity, we assumed a relatively flattened pavement on seabed in the simulated environment and neglected pitch and roll rotation of the vehicle. As the slip ratio of a track is defined as the ratio between the slip speed and theoreti

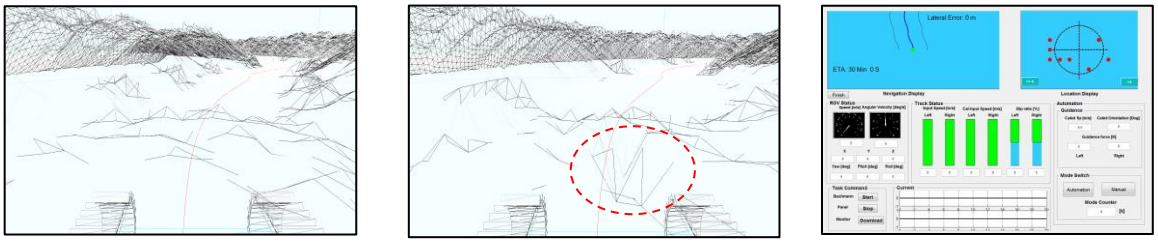

Figure 3. 3D representation through the viewpoint in virtual reality. *Left*: steering the vehicle in normal operation without obstacles. The subject aims to follow the red optimal path. *Middle*: One of the 12 obstacle avoidances. Within the red highlighted circle is the ditch which the subject is supposed to get rid of. The red circle is not visible in real experiment. The subject needs to distinguish such a ditch from other normal terrain variations. *Right:* the control panel where supplementary information and secondary task is shown.

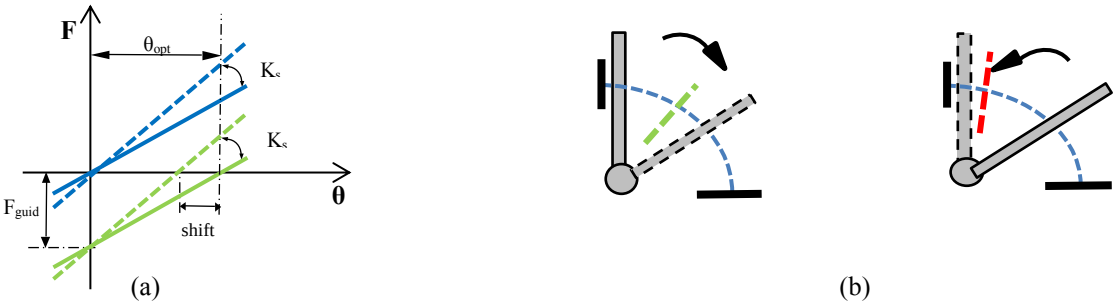

Figure 4. (a) Illustration of stiffness and force feedback design. Blue solid force-angle line represents the centering stiffness (virtual spring) of the handle in manual control. The green solid line depicts the force feedback where the neutral point of former virtual spring is shifted to the optimal angle. The blue dashed line denotes the stiffness feedback, in which the former centering stiffness (solid blue line) is increased by K_s according to the lateral deviation. If both the force feedback and stiffness feedback are implemented, the force-angle relationship is akin to the green dashed line. (b) The operator's intervention approach in supervisory control. *Left*: The system gives the control authority back to the operator once either of the two handle is pull back so that the corresponding speed input is below 0.6m/s. *Right*: The system restores full automation mode when the vehicle recovers back to the optimal path, and speed inputs on both sides return up to 0.9m/s.

-cal speed, where the slip occurs when there is a difference between actual and theoretical speed [7]:

$$i_L = \frac{\omega_L r - (\dot{x} - b\dot{\psi})}{\omega_L r}$$
$$i_R = \frac{\omega_R r - (\dot{x} + b\dot{\psi})}{\omega_R r} \quad (2)$$

Where r is the effective radius of the drive sprocket on the track, ω_L, ω_R are the input speed controlled by either operator or the controller, $\dot{x}$ is the heading speed of the vehicle, and $\dot{\psi}$ is the yaw rate of the vehicle. If the symmetry of the crawler is assumed, the local actual speed of left and right track becomes $(\dot{x} - b\dot{\psi})$ and $(\dot{x} + b\dot{\psi})$ respectively. In this way the desired track input speeds on both sides can be calculated as:

$$\omega_L = \frac{\dot{x}_d - b\dot{\psi}_d}{r(1-i_L)}$$
$$\omega_R = \frac{\dot{x}_d + b\dot{\psi}_d}{r(1-i_L)} \quad (3)$$

The desired input track speed was then proportionally projected to the turning angle of the corresponding handle of the joystick operated by the human operator.

The methodology to generate guidance according to the desired turning angle in HSC was inspired from force plus stiffness feedback, which had been proven to have even more improved performance at the same level of control activity than pure force feedback [35]. Additional stiffness feedback could also avoid the instability problem in pure force feedback. First of all, the joystick has a self-centering stiffness K_0 with neural position at zero point to prevent erroneous input by accidental touch. Force feedback is applied to the joystick by altering the equilibrium point from initial zero point to optimal turning angle θ_{opt} calculated by the controller (figure 4.a). Thus in an ideal case in force feedback, operator should continuously seek for the shifting neutral position while the intercept of the shifted force-position characteristic on force axis will be the guidance force applied to the haptic interface (figure 4.a). Apart from the shifting optimal steering angle θ_{opt}, an additional stiffness feedback was applied to increase the stiffness based on the absolute lateral deviation $e(t)$ times c_s. Therefore more resistance force will be provided when operator steers away from the optimal steering angle.

$$F_{HSC} = K_0 \cdot (\theta_{steer} - \theta_{opt}) + c_s |e(t)| \cdot (\theta_{steer} - \theta_{opt}) \quad (4)$$

To establish the control algorithm for the crawler, a reference speed needs to be set for both HSC and supervisory control. Here we set a constant reference speed at 0.8m/s for HSC design so that an extra speed range of 0.2m/s was left for operator's improvisation.

In supervisory control, the automation system has a default full throttle on both handle (1m/s), but the crawler is controlled by a separate internal loop instead of the

actual handle, with reference speed also at 1m/s. In this case, operator was supposed to only respond to the secondary task while monitor the steering task. However operator may intervene into the control loop by pulling back either of the two handles so that the corresponding input speed falls into a switch tolerance at 0.6m/s (figure 4.b). Some gap was left between the full throttle and the switch tolerance to prevent sudden subconscious hand jitter when holding the handles for answering of the secondary task. After intervention, operator could also return the control authority back to full automation by pushing both handles forwards to full throttle. System will restore internal automation once the vehicle returns to the optimal path with absolute lateral deviation less than 0.6m (which is the same tolerance used to distinguish task modules), and both throttle speeds exceed 0.9m/s are detected.

Since three experimental conditions were tested, there were six permutated condition orders. Each subject needed to complete the whole virtual map three times, once per condition, according to the condition order. Participants were asked to steer the simulated crawler to avoid obstacles which shown up intermittently, while keep tracking the predefined optimal path as closely as possible between obstacles. Subjects' mental load is measured by a secondary task, where they were asked to recognize the number of markers within the reference range during steering. A training session was set before the experiment for each subject, where the subject learnt to drive the crawler in manual control mode. Obstacles and slip event were also included in the training session.

2.4 Subjects

Twelve male subjects, all were right handed and students from Delft University of Technology, between the ages of 23 to 34 (M=26.2, STD=2.9 years) volunteered for the experiment. All participants had normal or corrected-to-normal sight. These participants had no prior experience in controlling teleoperation tasks. All subjects were given a written task instruction about the experiment protocol and apparatus before the experiment. They were not remunerated financially for their participation. Subjects were randomly divided into six groups, one condition order each, so as to minimize the learning effect. Each participated in one experiment lasting for approximately 1.5 hours, including training session. Before the formal measurement, each subject familiarized with the skid steering by completing a training session, where three accumulative avoidances and one successful slip recovery was recognized as completion. The device and experimental protocol had been proved by the Delft Ethics Committee (HREC).

2.4 Data Analysis

To objectively evaluate the effect of HSC and supervisory control in steering a subsea crawler, a series of raw data about the vehicle status and operator's control activities was logged from the real time computer at 500Hz. The raw data collected from the experiment was partitioned into separate segments, labeled as within obstacle, between obstacles and slip recovery. Within-obstacles-module starts when an obstacle appeared on the screen, and ends when the vehicle's center position recovered back within ±0.6m (black dashed lines in figure 5) in lateral deviation for the first time after the corresponding obstacle avoidance. Slip recovery starts when the slip event was triggered and finishes at the place the left turn ends.

Based on the results, in total eight different metrics were calculated to determine the differences between experimental conditions.

1. *Root Mean Square (RMS) of the lateral deviation between obstacles:* Vehicle's lateral deviation is the most straightforward way to evaluate the subject's performance in path tracking. Since the lateral deviation have both positive and negative values, the root mean square of the lateral deviation is suitable to measure the magnitude it throughout the path tracking.
2. *Maximum absolute lateral deviation in slip:* maximum absolute lateral deviation the simulated vehicle performs during slip event.
3. *Mean length traversed in obstacle avoidance:* The averaged length the vehicle traversed in avoiding one obstacle with respect to the optimal path. Only successful avoidances are taken into account.
4. *Total number of collisions:* The number of collisions is directly resulted from the subject's vigilance and situation awareness in the primary path tracking task.
5. *Mean reaction time towards the obstacle:* The duration it takes for the subject to respond to the obstacle. More specific, it is the time period between the moment the obstacle presented to the subject and the moment the subject generates a significant steering change (the absolute difference between two speed inputs exceeds 0.4 m/s).
6. *Accuracies in secondary task:* The subject's response accuracy (percentage of correct answers) in the secondary task, which is a supplementary approach to evaluate the subject's mental workload in the path tracking task.
7. *Standard deviation (STD) of the difference in turning angles:* The difference between left and right turning angles is related to the skid steering. The higher variation of the difference in turning angles, the more intense of the control activities.
8. *Standard deviation (STD) of the torque on the handle:* The variation of the torque the subject inserted onto these two handles directly determines the subject's physical workload.

The data of the experiment was calculated using each subject's data per condition. The comparisons between experimental conditions are shown with the group mean per condition, along with the 95% confidence interval. The statistical differences were determined by using one way repeated ANOVA, except the maximum slip event and torques on handles. It is because the slip was triggered at the end of the path, the subject may have expectation on the slip event after one trial. In order to mini-

mize the expectation effect, the data analysis only took each subject's performance in the first time the slip was triggered (in the first condition presented), and one way independent ANOVA was used. For the torques on the handles, left-or-right hand was taken as a factor and two ways repeated ANOVA was calculated. Results were regarded as statistically significant when $p \leq 0.05$.

3 RESULTS

Figure 5 plots a typical subject's performance in primary steering task under three experimental conditions. The section of trajectory selected 300 meters in length. The top trace illustrates the curvatures of the predefined path, indicating both left, right turns and straight segments on the prescribed path. The distance between vehicle center and an obstacle center falls within 3 meters was recognized as collision. Comparing the directions the subject decided to avoid each obstacle across three conditions, the avoidance strategy conducted by each subject is not noticeably affected by the experimental conditions. The main effect locates on lateral deviation of the vehicle from the desired path between obstacles. As indicated in figure 5, the maximum lateral deviations seem to decrease with HSC and supervisory control while vehicle's trajectories are also much smoother, when compared with that in manual control.

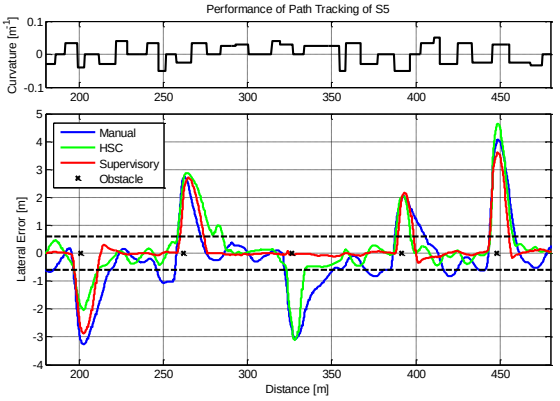

Figure. 5. Plot of a typical subject's lateral deviation during a 300 m section of the seabed path under three experimental conditions. The top trace indicates the curvatures of predefined optimal path and asterisk markers represent the location of these obstacles. Two parallel black dashed lines refer to tolerance of lateral deviation at ±0.6m with respect to centerline, to distinguish between within obstacle and between obstacles task module.

Path tracking between obstacles

When subjects steered the vehicle between obstacles, it was regarded as normal path tracking operation. Both individual subject's result and group mean with 95% confidence interval are shown in figure 6. RMS of lateral deviation under HSC (M=0.352, STD=0.050 [m]) and supervisory (M=0.217, STD=0.099 [m]) is smaller than manual control (M=0.451, STD=0.107 [m]). There is a statistical significant difference ($F(2,22) = 7{,}11$, $p<0.01$) in RMS of lateral deviation. Post-hoc analysis revealed differences between all three conditions, where HSC and supervisory control result in a reduction of 22% and 52%

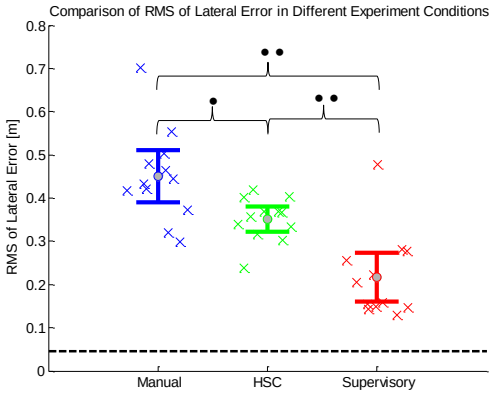

Figure 6. Comparison of root mean square (RMS) of lateral errors in three between obstacles with respect to the optimal path. Each subject's individual result is represented by cross markers. Group means are shown with 95% confidence interval. The black horizontal dashed line represents the hypothetical RMS value when the system is run by full automation throughout the experiment. '●' ,'● ●' means a significance with $p<0.05$ and $p<0.01$, respectively.

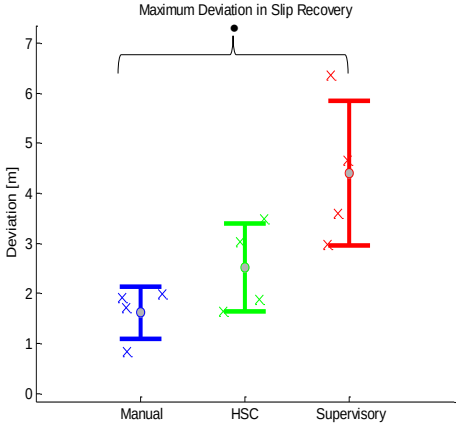

Figure 7. Maximum absolute lateral deviation during slip recovery. '●' ,'● ●' means a significance with $p<0.05$ and $p<0.01$, respectively.

lateral deviation, respectively.

Maximum Deviation in Slip Event

The slip event was set to measure operator's vigilance and situation awareness towards unexpected event under different assist conditions. To fairly evaluate the dependence of maximum lateral deviation in slip recovery on experimental conditions, we only compared each subject's response for the first time the slip event was triggered, so as to remove the expectation effect (figure 7). One way ANOVA was solely calculated on maximal lateral deviation in this case. A significant difference was found ($F(2,9)=7.429$, $p<0.05$), and post-hoc analysis gave a significant difference between manual and supervisory control ($p<0.05$) and a trend can be seen between HSC and supervisory control ($p=0.089$), but not between HSC and manual control. Regarding the fact that there were only 4 subjects in each group, the difference between HSC and supervisory control is also reasonably evident. Larger subject volume is needed to determine the statistical dif-

ference between HSC and s control.

Obstacle Avoidance

Figure 8 illustrates the minimum distance of the vehicle's center to the center of obstacle, for all 12 obstacles for all 12 subjects' individual results for all three conditions. Theoretically a collision occurs if the vehicle center falls within 3 meters of an obstacle center. This gave an averaged hit rate of: (M=14.6%, STD=8.0%) in manual control, (M = 25.7%, STD= 14.4%) in HSC and (M=18.8%, STD=15.1%) in supervisory control. No statistical significance was found for the hit rate between conditions. However since the simulation determined the moment to present the obstacles based on the speed of the vehicle, which caused an inconsistency in difficulty of avoidance under three conditions. To best mitigate the bias introduced by the experiment design, operators' reaction time was calculated as a more sensitive metric on operator's response to obstacles. An absolute difference exceeds 0.4m/s between the speed inputs of two handles is defined as the beginning of operator's intervention. The reaction time is then the duration between the moment

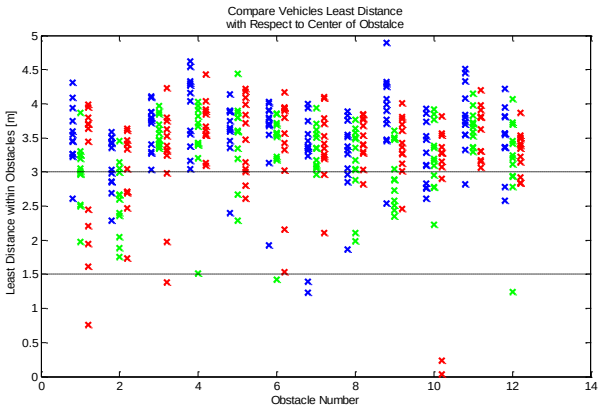

Figure 8. Overview of each subject's performance of the least distance between vehicle center and obstacle center over 12 obstacles. *Blue*: Manual control. *Green*: HSC. *Red*: Supervisory control. It's because the subject could pass through the obstacle after the collision, such that there existed some cases where the least distance is below 3m.

obstacles showed up, and the moment intervention started. However since the input speed has certain range, the vehicle's skid steering ability is limited. If we assumed maximum speed (1m/s) on one track and a minimum speed (0.05m/s) on the other side as maximum steering ability during avoiding obstacle, this results into four different potential situations:

1. Operator didn't detect the obstacle at all so that did not react to the obstacle (***type I collision***).
2. Operator responded before the collision but it was impossible to avoid the obstacle, even with maximum steering (***type II collision***).
3. Operator responded in time but still hit the obstacle while it was still possible to avoid it with maximum steering, because wrong steering maneuver was taken (***type III collision***).
4. Operator responded in time and successfully avoided the obstacle.

Numbers of collision in different experimental conditions are shown in figure 9-a, categorized according to collision type. Type I collision only occurred once in manual and twice in HSC control, and none in supervisory control. Type II collisions occurred substantially more during HSC (9 times) than during manual (1 times) and supervisory control (2 times). Operators under HSC (27 times) and supervisory control (25 times) conducted more type III collisions than during manual control (19 times) in total. The reaction time during type II and type III collisions are shown in the scatter plot (figure 9b). Even though the sample volume is not equal in different conditions, the operators still showed shorter reaction time for type II collisions during HSC than during supervisory control. For type III collisions (figure 9-b, right), among majority of the collisions under manual and HSC, subjects still had pretty low reaction time (manual: *M = 1.45, SE=0.145*; HSC: *M=1.54, SE=0.157*). However subjects' averaged reaction time was longer in supervisory control (*M = 2.13, SE=0.169*). If we average subjects' reaction time regardless of the collision (figure 9-c), there existed a

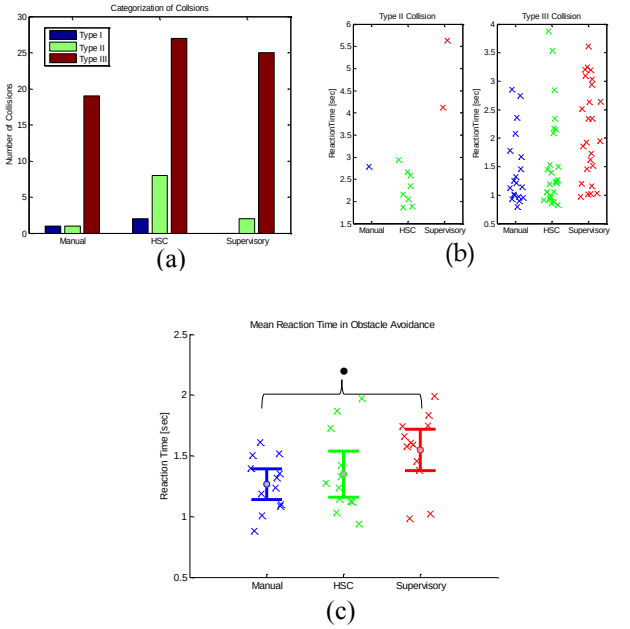

Figure 9. (a) Total number of collisions in three experimental conditions by 12 subjects, categorized by collision type. (b) Distribution of the subjects' reaction towards the obstacles in type II and type III collisions. (c) Each subject's mean reaction times towards the obstacles in three experimental conditions, with group mean and 95% of confidence interval.

statistically significant difference across the conditions ($F(2,22) = 4.67$, $p=0.02$), which mainly attributes to the difference between supervisory control (M=1.55, STD=0.30) and manual control (M=1.27, STD=0.22, $p<0.01$). It is questionable that subjects ran into type II error much more often in HSC, though their reaction time was not significantly increased compared to manual control. This discrepancy will be further discussed in the next section.

The mean length the vehicle traversed in avoiding ob-

stacles also reported a significant difference between conditions using a one way repeated ANOVA ($F(2,22)=7.53$, $p<0.01$), as shown in figure 10. Post hoc analysis showed that the subjects with HSC spent less length in obstacle avoidance than manual control ($p<0.05$), but not between other comparisons. This indicates that operator steered the vehicle back to the centerline with shorter distance under HSC. Also significant differences were found in mean vehicle speed when the obstacle appeared between all three conditions ($F(1.1,12)=122.3$, $p<0.01$), since subjects showed certain obedience to the

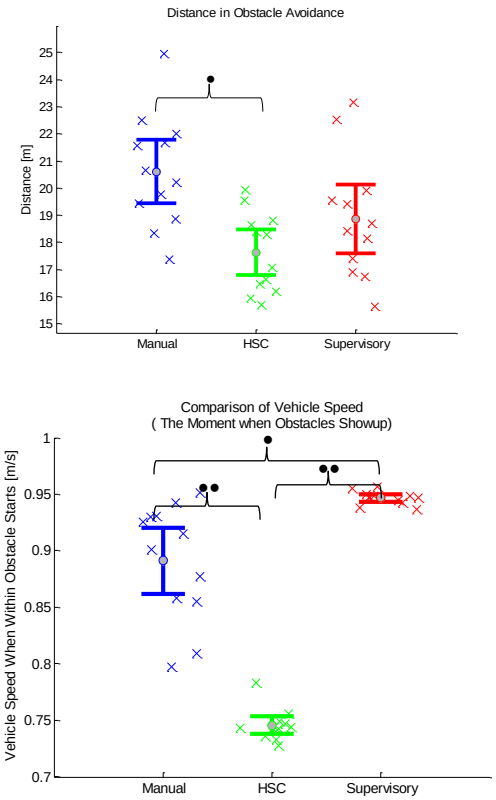

Figure 10. *Upper:* Averaged length the vehicle traversed during obstacle avoidances. *Bottom:* vehicle's mean heading speed when the obstacle was presented to the subject. '●' ,'● ●' means a significance with $p<0.05$ and $p<0.01$, respectively.

predefined speed in HSC, which made the vehicle relatively slower than the speeds in manual control and even supervisory control.

Secondary Task

Figure 11 illustrates subjects' accuracies for the secondary task under different experimental conditions, categorized by task modules: total, within obstacle, between obstacles and slip recovery. Aside from the experimental conditions, the individual difference and task module are two main factors that influencing performance of secondary task. Subjects' performance in secondary task was influenced by task module. Taking the task module as a factor, a two-way repeated ANOVA showed a significant difference between task modules, $F(2,22) =55.8$, $p<0.01$). Subjects had higher accuracies during normal operation (between obstacles) than during unexpected events (i.e. obstacle avoidances and slip event, $p<0.01$). In within obstacle and slip recovery task modules, subjects' accuracies vary regardless of the assist conditions, so that no statistical difference was found in these two task modules. However a statistical difference is found on response accuracy between obstacles ($F(2,22=4.81$, $p<0.05$)), post-hoc tests revealed a statistical difference ($p=0.04$) between supervisory ($M=89.9\%$, $STD=7.0\%$) and manual control ($M=84.2\%$, $STD=12.2\%$). It is noticeable that subjects who responded badly between obstacles in manual had an appreciable improvement in both assist conditions, while other subjects remained a relatively high accuracy level across all conditions. A further comparison only selected those subjects whose accuracies in manual control were less than 90% (6 subjects in total) and further compare the effects from assist conditions, we find statistically significant improvement in both HSC and supervisory control against manual control ($p<0.05$). Therefore it is possible that these two assist conditions could bring more benefits

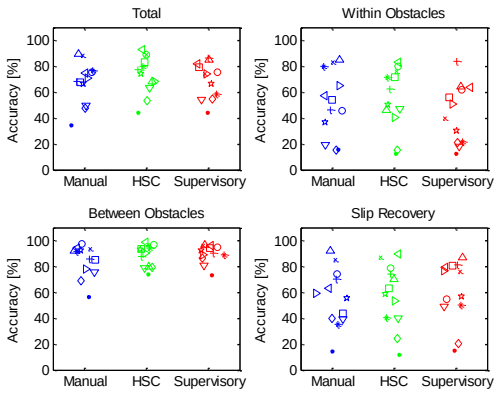

Figure 11. Overview of each subjects' response accuracies categorized by task module and experimental conditions. Each subject is marked with different identifier, 1~12 from left to right. *Top left*: Subject's response accuracies in total. *Top right:* Subject's response accuracies within obstacles. *Bottom left:* Subject's response accuracies between obstacles. *Bottom right:* Subject's response accuracies during slip recovery.

to subjects who need improvements in secondary tasks, while others could maintain their accuracies under assist conditions.

Control Effort

The STD of the difference in turning angles was categorized according to the task modules (figure 12). No significant difference between conditions was found within obstacles. However one-way repeated ANOVA reported a significant main effect between three experimental conditions for the normal operation between obstacles, ($F(2,22=52.07)$, $p<0.01$). Post-hoc comparison of the three groups indicated strong difference between all three conditions. Supervisory control had least control activity between obstacles ($M = 5.23$, $STD = 1.86$) than the other two conditions ($p<0.01$). HSC further induced slightly more control activity between obstacles ($M = 11.88$, $STD = 1.76$, $p<0.01$) than manual control ($M = 9.05$, $STD = 1.37$).

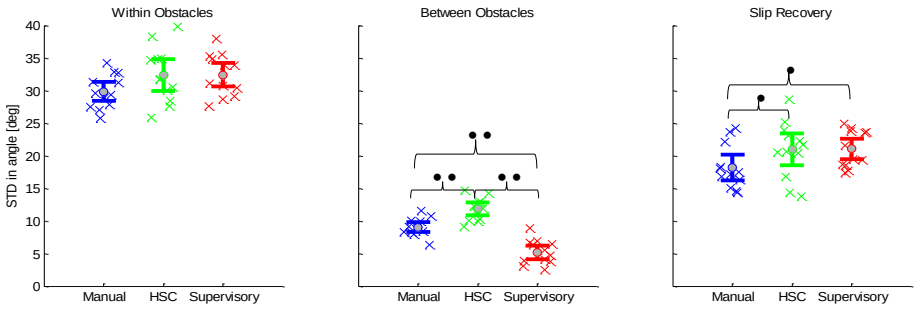

Figure 12. STD of the difference between left and right turning angles, categorized by task module, experimental conditions. *Left*: within obstacles. *Middle*: between obstacles. *Right*: slip recovery. Significance on the main effect is marked regardless of which handle it is. '●' ,'● ●' means a significance with $p<0.05$ and $p<0.01$, respectively.

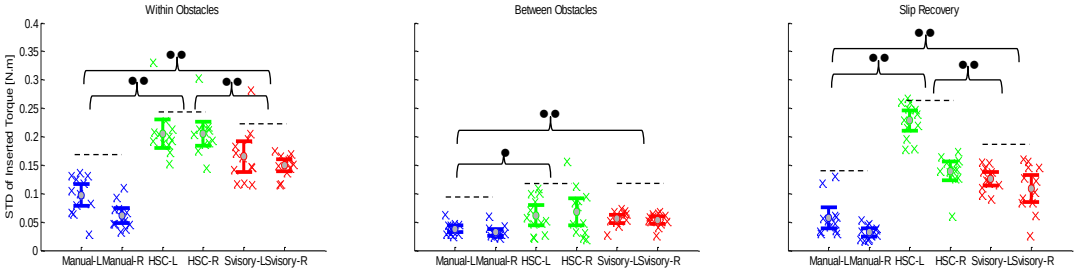

Figure 13. STD of each subject generated torque, categorized by task module, experimental conditions and left-or-right hand. *Left*: within obstacles. *Middle*: between obstacles. *Right*: slip recovery. Significance on the main effect is marked regardless of which handle it is. '●' ,'● ●' means a significance with $p<0.05$ and $p<0.01$, respectively.

Moreover during slip recovery, a statistical difference was also found for control activity, ($F(2,22) = 4.70$, $p=0.02$). HSC ($M=20.95$, $STD=4.31$,$p<0.05$) and Supervisory control ($M=21.07$, $STD=2.82$, $p<0.05$) both resulted into higher control activity than manual control ($M=18.19$,$STD=3.41$) for control activity during slip recovery, according to post-hoc multiple comparisons. But the difference between HSC and supervisory control was not significant during slip recovery.

Since subjects were asked to grab the handles throughout the experiment, they could conform to the guidance in HSC. Therefore the subjects might still have a high variation on the turning angles of the handles due to the guidance force, but instead did not concentrate on the steering. However if the subjects conformed to the guidance, they directly generated less force on the handles. Thus the torque inserted onto the handle is an alternative metric to measure subjects' physical workload (figure 13). Figure 13 depicts the standard deviation inserted torques on both handles in three experimental conditions, categorized by task module, where handle was taken as a factor and a two-way repeated ANOVA was calculated. The ANOVA revealed that within obstacles, assist condition had a strong effect in within obstacle regardless of which handle it was ($F(2,22) = 89.74$, $p<0.01$). Post-hoc gave significant difference between all three conditions ($p<0.01$). The assist conditions also brought a significant difference during normal operation between obstacles ($F(2,22) = 6.60$, $p<0.01$). Specifically, HSC had a difference compared to manual control ($p=0.04$), supervisory control also caused significantly higher torque variation than manual control ($p<0.01$). The main effect by assist condition continued in slip recovery ($F(2,22)=152.09$, $p<0.01$), where during supervisory control the STD of torques was significantly higher than during manual control ($p<0.01$), and the STD of torques during HSC was also higher than both during manual and supervisory control ($p<0.01$). Left-or-right handle, as a factor, only showed a significant effect within obstacles ($F(1,11)=10.55$, $p<0.01$) and slip recovery ($F(1,11)=30.80$, $p<0.01$). The effect of handle in slip recovery is reasonable since the slip event occurred during a left turn, so that subjects needed to steer the left track much more often than the right track.

4 Discussion

Manual Control

The level of automation increases stepwise from manual control to supervisory control, with HSC in between. As hypothesized, in manual control subjects had the lowest performance in path tracking between obstacles. While some subjects were able to perform the secondary task well regardless of the control condition, others had the lowest response accuracy with manual control. Ap-

parently subjects could not manage to perform both the primary task and the secondary task very well at the same time throughout the experiment. This discrepancy could be more severe in long term tasks. However as long as the subjects were fully involved in the primary steering task in manual condition, they kept a relatively higher vigilance towards the unexpected events than the two assist conditions. Although the difference of hit ratio was not significant, subjects did have less lateral deviation during slip under manual condition than the supervisory conditions.

Haptic Shared Control

The improvement in path tracking between obstacles was evident in HSC compared to manual control since the steering was partially completed by the guidance. HSC also helped to improve secondary task performance for those subjects who performed poorly with manual control. However HSC didn't exhibit the same level of tracking accuracy as full automation in the normal operation tasks between obstacles. This indicates that the operator did not completely conform to the guidance in HSC, even without the presence of obstacles. This phenomenon has also been reported in other experiments [32], [36]. This man-machine mismatch may be induced by the difference between the operator's preferred trajectory and the recommended trajectory used to design the guidance. Different subjects may have had different understandings of the vehicle's position with respect to the optimal path. In addition, human's 'satisficing instead of optimizing' maneuver could also play a role in incurring the mismatch [37]. Operators usually tend not to continuously pursue the most accurate tracking as long as the lateral deviation is acceptable, while the guidance in HSC always tries to minimize the tracking error. Concerning the control efforts, even during normal path tracking between obstacles, when abrupt maneuvers were not necessary to avoid obstacles, HSC induced a higher variation of difference between the two turning angles than manual control. This implies that the guidance in HSC tended to use more aggressive corrections than subjects did with manual control. Subjects' generated torque was also more variable than the other two conditions between obstacles, which is another illustration of the subjects' different level of acceptance towards the guidance. Some trusted and conformed to the guidance while others still fight with the haptic force between obstacles. Therefore a constant level of guidance could not bring the best assistance to each individual operator. One possible solution is to customize the parameters in rendering guidance forces according to each operator's preference.

Similar to the hypotheses, though HSC has a higher level of automation than manual control, it did not necessarily result in worse performance during the unexpected events. Despite the fact that HSC induced more collisions than the other two conditions, a large number of the collisions in HSC belongs to the type II collision, where subjects didn't have enough distance to steer the vehicle away from the obstacle. This was caused by method the simulator used to present the obstacle. Under the HSC condition, subjects performed certain obedience to the guidance between obstacles, which resulted into a relatively lower vehicle speed than both manual and supervisory control (figure 10-b). According to (1.1), there was less distance between the vehicle and obstacle in HSC when the obstacle appeared. Although the subject's mean reaction time was not significantly increased in HSC, the same reaction time was not sufficient to avoid the obstacle. Nevertheless, the guidance applied to the joystick within obstacles was faulty to the operator, as it still tried to navigate the vehicle back to the optimal path. Even though the stiffness of the virtual spring of the guidance had been tuned before the experiment to make the joystick stiff enough to reject undesired movement of steering and still compliant enough to be overcome by the operator, it sometimes might still cause problem for some subjects' intervention (e.g. made them hesitate to intervene), regarding several subjects' mean reaction time in HSC were much higher than the rest (figure 9-c). Similarly, HSC also led to the highest variation of torque during both obstacle avoidance and slip recovery, since the operator needed more physical effort to overcome the faulty guidance force. A more proactive haptic guidance could be achieved by on-line mitigating or even intelligently switching off the stiffness of the virtual spring according to human's intervention during the man-machine conflicts.

Supervisory Control

With the highest level of automation among the three conditions, supervisory control had a significantly higher path tracking performance than both manual control and HSC. When the vehicle traversed between obstacles, subjects totally relied on the automation. Despite the large variation in the secondary task performance due to inter-subject differences in prioritization of the tracking and secondary task, supervisory control still had a statistically significant improvement in response accuracy between obstacles, compared to manual control. Subjects' mental workload was relieved at least during these periods. However this superiority was not found when compared to HSC. Similarly, the reduced variation of difference between turning angles in supervisory control between obstacles is also reasonable since for the most of time between obstacles the vehicle was controlled by the automation system and subjects only responded to the secondary task.

For the performance during unexpected events, both the mean reaction time towards the secondary task within obstacles and maximum deviation in the slip event were statistically larger than that during manual control. In this experiment, operators intervention in the supervisory condition was designed to be quick and intuitive (figure 4-b), and thus is unlikely the cause of subjects' delayed reaction to these unexpected events. This revealed that the operator had significantly less system vigilance in supervisory control than manual control. Therefore the slightly improved response accuracy in the secondary task between obstacles under supervisory control sacrificed the operator's vigilance in the primary path tracking

task. Operators may have become complacent in the primary path tracking task under supervisory control, and switched their concentration to the secondary task. Since the obstacles presented in this experiment were much more frequent (about once per 90 seconds) than what will likely happen in reality, the degradation of vigilance under supervisory control may be further exacerbated when less frequent intervention is needed.

In addition, unlike normal path tracking between obstacles, the necessary transition procedure which switches the control authority in supervisory control increased the physical efforts during unexpected events. The operator in supervisory control tended to generate more torques onto these two handles than in manual control during all three task modules (figure 13). Because the subject was steering the joystick as a virtual spring in both manual and supervisory control, this increase in torque was most likely caused by the subjects' sudden intervention during the experiment. Even though subjects were informed that they could regain the control authority once they decrease either side of the speed input below a tolerance of 0.6m/s (figure4-b), subjects often abruptly reduced the handle far below the necessary tolerance. In addition to the increased torque due to the initial intervention, subjects might have become tenser once they detected the emergency and subconsciously generated higher torque in supervisory control. As a conjecture, subjects physically had more co-contraction in their neuromuscular system under supervisory control due to the higher mental nervousness. Thus the supervisory control could only reduce the control effort during the normal path tracking between obstacles, but caused more control effort when encountering unexpected events.

5 Conclusion

This study investigated the benefits of two support systems, HSC and supervisory control, for controlling a subsea crawler. The support systems were evaluated on operators' performance and workload for a tracking task, accompanied by sudden object avoidance and a simultaneous secondary task. For the experimental conditions studied, it can be concluded that compared to manual control:

- The performance of path tracking between obstacles was improved for both support systems, and HSC also reduced the length spent in avoiding the obstacle.
- The operator's physical control effort increased during obstacle avoidance and slip recovery with both support systems. Control activity increased for HSC while decreased for supervisory control during normal operation between obstacles.
- No substantial improvement were found for the secondary task for both support conditions, though all subjects had a slight improvement in the response accuracy only between obstacles in supervisory control, compared to manual control.
- Supervisory control significantly reduced operators' vigilance towards unexpected events, as larger maximum lateral deviation in the slip event was observed.

The results from this short-term experiment allude that supervisory control could bring the highest level of performance while appreciably reducing the operator's control effort for such a slow dynamic system, but may still induce the side-effects of automation when unexpected circumstances are encountered. HSC both improves the performance while still maintaining the operator's vigilance, especially in slip events, compared to supervisory control. This highlights HSC as a promising solution for long term operation tasks, such as deep sea mining. However it was found that the subjects didn't completely trust the guidance such that HSC did not deliver the same level of assistance in task performance as supervisory control. The faulty guidance, as the guidance was not aware of the obstacles nor the slip, implemented deliberately during unexpected events also increased the operator's control efforts. Future studies may focus on an improved design of haptic guidance and further improvement of the human's acceptance of HSC for teleoperated underwater machines.

References

[1] S. Ishiguro, Y. Yamauchi, H. Odaka, and S. Akiyama, "Development of Mining Element Engineering Test Machine for Operating in Seafloor Hydrothermal Deposits," *Mitsubishi Heavy Ind. Tech. Rev.*, vol. 50, no. 2, pp. 21–26, 2013.

[2] T. Parenteau, P. Espinasse, A. Benbia, and B. Ngim, "Subsea mining field development concept using a subsea crushing and feeding unit .," in *OTC*, 2013.

[3] B. Waquet, T. Mines, D. Faulds, P. Slingsby, A. Benbia, and M. M. D. Mineral, "Understanding the Effects of Deep-Sea Conditions on Seafloor Massive Sulfide Deposits Crushing Process," in *OTC*, 2011.

[4] S. Hong, H. W. Kim, and J. Choi, "Transient Dynamic Analysis of Tracked Vehicles on Extremely Soft Cohesive Soil," in *ISOPE*, 2002, pp. 100–107.

[5] N. Morgan, D. Cathie, J. Pyrah, and J. Steward, "Tracked Subsea Trencher Mobility and Operation in Soft Clays," in *The Seventeenth International Offshore and Polar Engineering Conference*, 2007, pp. 1366–1373.

[6] Y. Dai, S. Liu, L. Li, and Y. Li, "Development of a fast simulation model for dynamic analysis of the 1000 m deep ocean mining system," *World J. Model. Simul.*, vol. 6, no. 2, pp. 83–96, 2010.

[7] J. Y. Wong, *Terramechancis and Off-road Vehicle Engineering*. 2010.

[8] J. Y. Wong, "Development of high-mobility tracked vehicles for over snow operations," *J. Terramechanics*, vol. 46, no. 4, pp. 141–155, Aug. 2009.

[9] M. G. Bekker, *Off-the-road Locomotion: Research and Development in Terramechanics*. Ann Arbor, Michigan: The University of Michigan Press, 1960.

[10] Y. Dai and S. Liu, "An integrated dynamic model of ocean mining system and fast simulation of its longitudinal reciprocating motion," *China Ocean Eng.*, vol. 27, no. 2, pp. 231–244, Apr. 2013.

[11] G. Conte and A. Serrani, "Modelling and Simulation of Underwater Vehicles," in *International Symposium on Computer-Aided Control System Design*, 1996, pp. 62–67.

[12] C. Lee, H. Kim, S. Hong, and S. Kim, "A Study on the Driving Performance of a Tracked Vehicle on an Inclined Plane according to the Position of Buoyancy," in *The Ninth ISOPE Ocean Mining Symposium*, 2011, pp. 104–109.

[13] M. Ahmadi, V. Polotski, and R. Hurteau, "Path Tracking Control of Tracked Vehicles," in *International Conference on Robotics & Automation*, 2000, no. April, pp. 2938–2943.

[14] S. Hong, J.-S. Choi, H.-W. Kim, M.-C. Won, S.-C. Shin, J.-S. Rhee, and H. Park, "A path tracking control algorithm for underwater mining vehicles," *J. Mech. Sci. Technol.*, vol. 23, no. 8, pp. 2030–2037, Apr. 2010.

[15] J. S. Chung and T. Qi, "Smart Seafloor Mining Vehicle : Simulation with Successive Learning Track-Keeping Control," *Int. J. Offshore Polar Eng.*, vol. 10, no. 3, pp. 182–186, 2000.

[16] T. B. Sheridan, "Adaptive Automation, Level of Automation, Allocation Authority, Supervisory Control and Adaptive Control: Distinctions and Modes of Apaptation," *IEEE Trans. Syst. Man Cybern. A Syst. Humans*, vol. 41, no. 4, pp. 662–667, 2011.

[17] T. B. Sheridan, *Telerobotics, Automation, and Human Supervisory Control*. Cambridge, MA: The MIT Press, 1992.

[18] T.B.Sheridan, *Humans adn automation: system design and research issues.*, vol. 3. New York, 2002.

[19] R. Parasuraman, "Human and Automation: Use, Misuse, Disuse, Abuse," *Hum. Factors*, vol. 39, no. 2, pp. 230–253, 1997.

[20] D. a. Abbink, M. Mulder, and E. R. Boer, "Haptic shared control: smoothly shifting control authority?," *Cogn. Technol. Work*, vol. 14, no. 1, pp. 19–28, Nov. 2011.

[21] W. Griffin, "SHARED CONTROL FOR DEXTEROUS TELEMANIPULATION WITH HAPTIC FEEDBACK," 2003.

[22] T. Sheridan and W. Verplank, "Human and Computer Control of Undersea Teleoperators, Technical Report, Office of Naval Research," 1978.

[23] D. A. Abbink, "Neuromuscular Analysis of Haptic Gas Pedal Feedback during Car Following, Doctorate Thesis," Delft, the Netherlands, 2006.

[24] D. a Abbink, M. Mulder, F. C. T. van der Helm, M. Mulder, and E. R. Boer, "Measuring neuromuscular control dynamics during car following with continuous haptic feedback.," *IEEE Trans. Syst. Man. Cybern. B. Cybern.*, vol. 41, no. 5, pp. 1239–49, Oct. 2011.

[25] P. Griffiths and R. B. Gillespie, "Sharing Control Between Human and Automation Using Haptic Interface : Primary and Secondary Task Performance Benefits," *Hum. Factors*, vol. 47, no. 3, pp. 574–590, 2005.

[26] F. Mars, D. Mathieu, and J.-M. Hoc, "Analysis of human-machine cooperation when driving with different degrees of haptic shared control," *IEEE Trans. Haptics*, vol. 1412, no. c, pp. 1–1, 2014.

[27] M. Mulder, D. a. Abbink, and E. R. Boer, "Sharing Control With Haptics: Seamless Driver Support From Manual to Automatic Control," *Hum. Factors J. Hum. Factors Ergon. Soc.*, vol. 54, no. 5, pp. 786–798, May 2012.

[28] H. Boessenkool, D. a. Abbink, C. J. M. Heemskerk, and F. C. T. van der Helm, "Haptic shared control improves tele-operated task performance towards performance in direct control," *2011 IEEE World Haptics Conf.*, pp. 433–438, Jun. 2011.

[29] T. M. Lam, H. W. Boschloo, M. Mulder, and M. M. van Paassen, "Artificial Force Field for Haptic Feedback in UAV Teleoperation," *IEEE Trans. Syst. Man, Cybern. - Part A Syst. Humans*, vol. 39, no. 6, pp. 1316–1330, Nov. 2009.

[30] R. J. Kuiper, J. C. L. Frumau, and S. A. Miedema, "Influence of the Hyperbaric Effect on Apparent Material Strength of Fully Saturated Porous Rock for Low Strain Rates," in *Offshore Technology Conference*, 2013.

[31] F. Flemisch, J. Kelsch, and C. Loeper, "COOPERATIVE CONTROL AND ACTIVE INTERFACES FOR VEHICLE ASSISTANCE AND AUTOMATION," in *FISITA world automotive congress*, 2008, no. 2.

[32] P. Griffiths and R. B. Gillespie, "Shared control between human and machine: haptic display of automation during manual control of vehicle heading," *12th Int. Symp. Haptic Interfaces Virtual Environ. Teleoperator Syst. 2004.*, pp. 358–366, 2004.

[33] M. Mulder and D. a. Abbink, "Correct and faulty driver support from shared haptic control during evasive maneuvers," *2011 IEEE Int. Conf. Syst. Man, Cybern.*, pp. 1057–1062, Oct. 2011.

[34] F.A.Muckler and R.W.Obermayer, *Control system lags and man-machine system performance*. National Aeronautics and Space Administration, 1964.

[35] D. a. Abbink and M. Mulder, "Exploring the Dimensions of Haptic Feedback Support in Manual Control," *J. Comput. Inf. Sci. Eng.*, vol. 9, no. 1, p. 011006, 2009.

[36] P. Marayong and A. M. Okamura, "Speed-Accuracy Characteristics of Human-Machine Cooperative Manipulation Using Virtual Fixtures With Variable Admittance," *Hum. Factors J. Hum. Factors Ergon. Soc.*, vol. 46, no. 3, pp. 518–532, 2004.

[37] J. C. F. de Winter and D. Dodou, "Preparing drivers for dangerous situations: A critical reflection on continuous shared control," *2011 IEEE Int. Conf. Syst. Man, Cybern.*, pp. 1050–1056, Oct. 2011.

Appendices belonging to the Master's thesis:

Haptic Shared Control in Deep Sea Mining – Enhancing Teleoperation of a Subsea Crawler

K.Wang

Content

Appendix I – Experiment Setup

The experiment setting used in this study contains both hardware and software configurations. A complete appearance of the set-up is shown in figure 1.1.

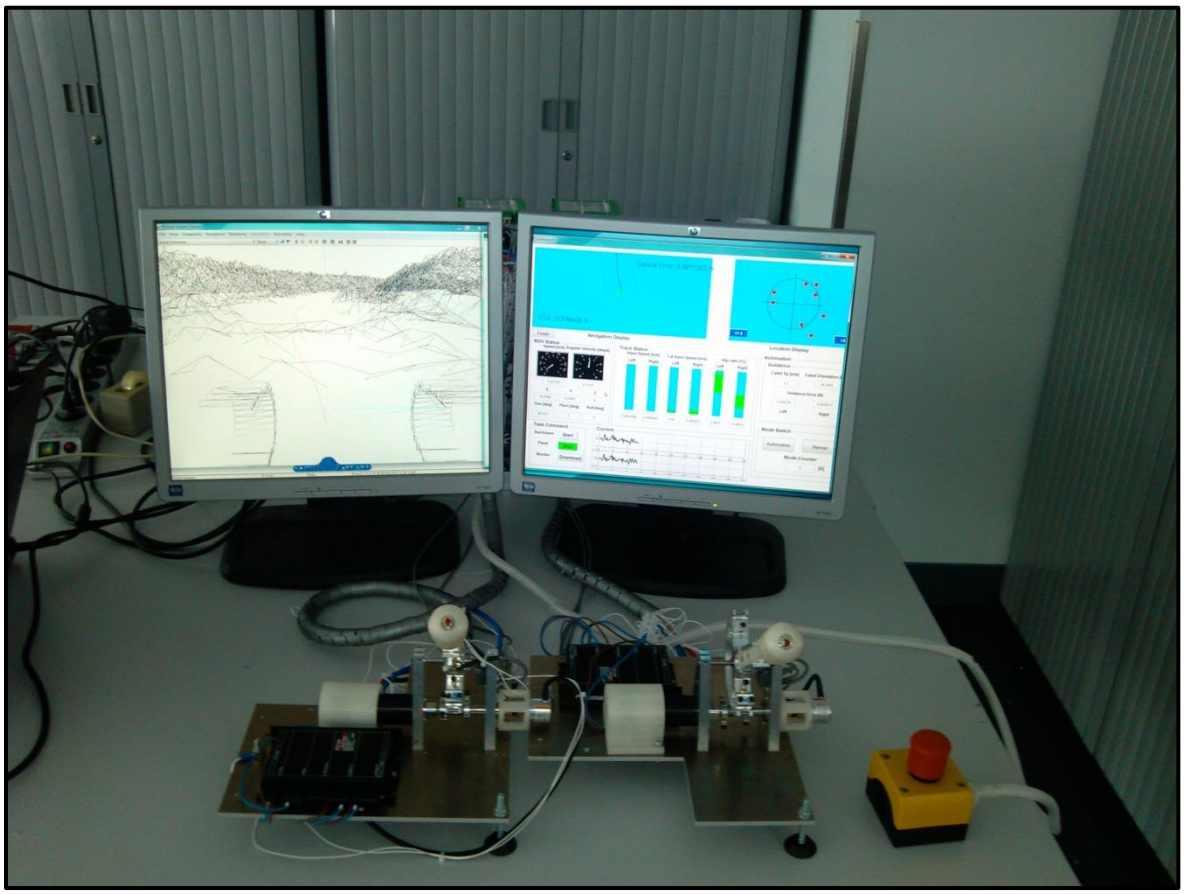

Figure 1.1. An over view of the whole experiment setup. Main parts include a couple of joysticks, two screens, real time computer (behind the two screens) and an emergency button.

The hardware contains a couple of self-built single degree of freedom rotary handles, acting as joysticks. These two handles were mainly constructed by Leroy Boerefijn and Ward Heij from the department of Mechanical Engineering in 2013 for their experiment of one degree of freedom hard contact teleoperation task. As shown in figure 1.2, one entire joystick system is integrated onto a platform. It consists of a 3D printed knob for the operator to grab. The knob is attached to the handle by 2 M5 bolted joints. The metal handle is connected to two trapezoid substrates by a shaft in between. These two trapezoid substrates are mounted to the platform. A maxon RE30 DC motor is also mounted to one of the substrates with a front flange. The motor is shielded by a 3D printed shell. On the opposite substrate the encoder is also mounted to the shaft.

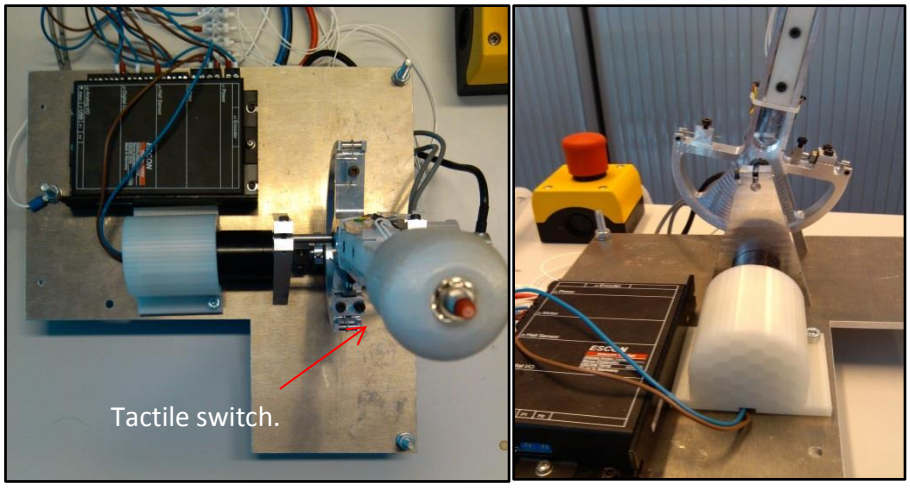

Figure 1.2 Overview of the joystick. *Left:* Top view of the whole integrated platform. *Right:* The connection between the handle and the platform.

An ESCON 70/10 amplifier is used to adjust the output current to the DC motor. The transmission between the handle and the motor is achieved by Capstan drives with a transmission ratio of i=1/10. The Capstan drive connects two rotary bodies by a wound steel cable (Φ=0.8mm). The transmission ratio is realized by set the radius of the circular part of the handle at 50mm and the radius of the capstan drum at 5mm. Two separate steel cables are used to actually connect the Capstan drum with the handle drum. For each steel cable, one side of it is fixated by screw on the lock, and the other side on the handle drum. The DC motor's shaft does not directly fit the Capstan drum, so that a separate Capstan shaft is made and connected to the motor's shaft with a double lock. One of the lock is tightly clamped with the motor's shaft by two M3 bolts (figure 1.3).

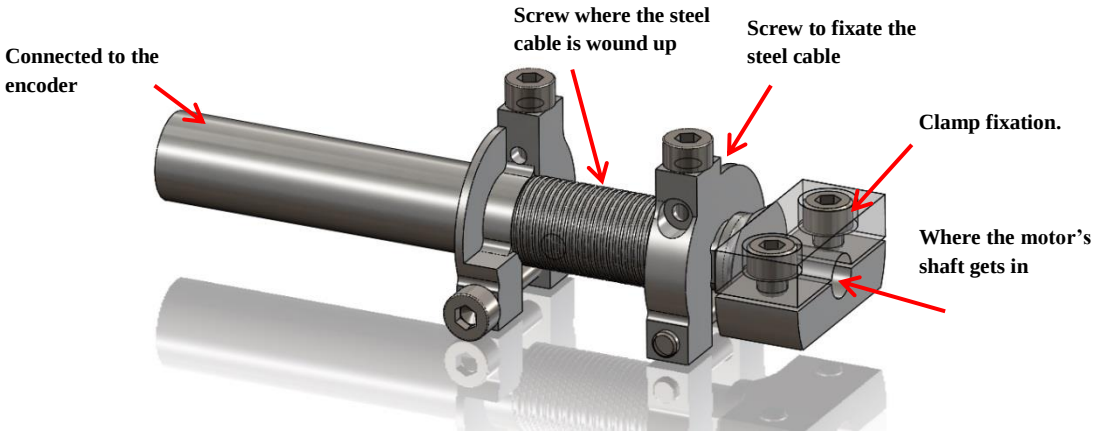

Figure 1.3. CAD drawing of the Capstan mechanism, adapted from Boerefijn and Heij's .

Four 1-DY13-6/350 strain gauges (figure 1.4) are attached to one handle and are connected in Wheatstone bridge manner to maximize the measuring accuracy. The output from the strain gauges is in millivolt, which is linear to the handle's deflection.

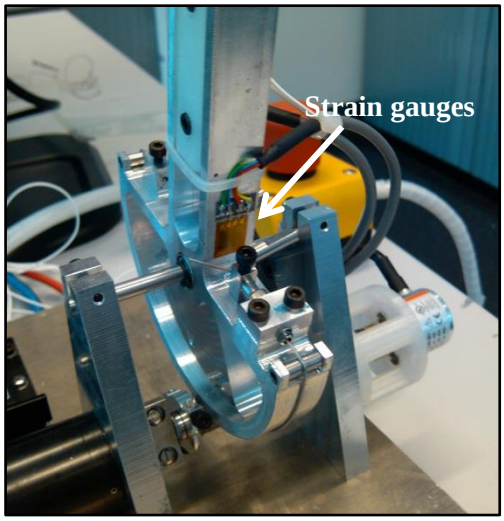

Figure 1.4. Strain gauges attached to the side of the handle.

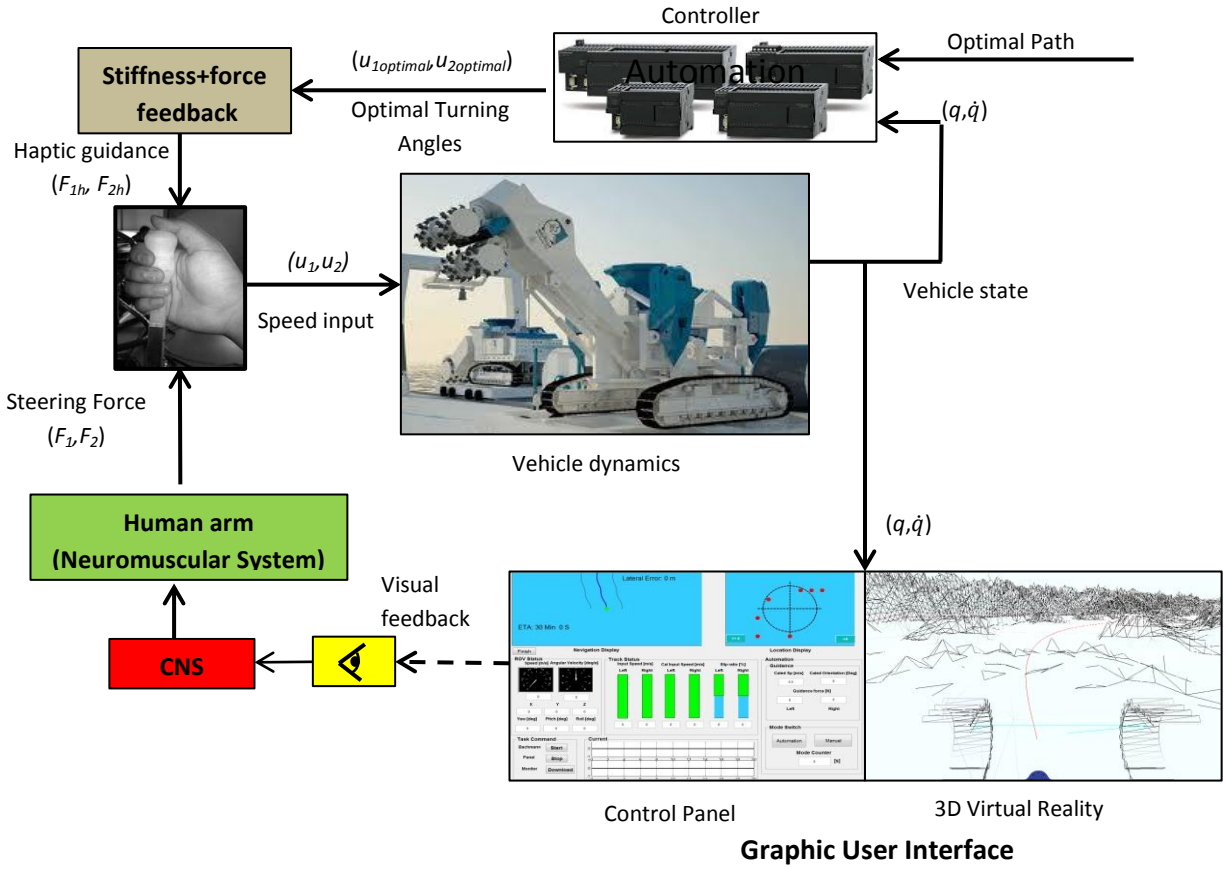

Figure 1.5. Overview of the control loop for HSC in this experiment. The central vehicle dynamics module calculates the theoretical updated vehicle's states $(q, \dot{q})$ based on vehicle's last time status and the speed inputs from these two joysticks. The controller computes the desired speed inputs by integrating the vehicle status with the global map information. The haptic guidance block then receives the desired speed inputs and renders the guidance forces according to stiffness and force feedback. Meanwhile the vehicle status is integrated by the GUI programme and represented through these two screens. The operator also is aware of the vehicle working situation though the visual information and controls the joysticks with his/her judgement.

An overview of the whole control loop for haptic shared control is shown in figure 1.5. The vehicle dynamic model contains a mathematical model of the simulated vehicle. Single body dynamics modelling instead of multibody dynamics modelling was used to ensure the computation speed for real time simulation (Kim et al., 2005), which integrates the soil-track interaction adapted from previous studies in terramechanics (Wong, 2010). The controller block receives the simulated vehicle status, and calculates the desired speed inputs for the vehicle with reference from the predefined optimal path. A haptic rendering block mentioned in section 1.1 calculates the required guidance forces according to the force plus stiffness feedback mechanism (Abbink & Mulder, 2009). The simulated vehicle status is also acquired by the self-written graphic user interface (GUI) program, which further converts the vehicle's working status into different types visual information, projected onto two screens. The operator should be able to interpret the vehicle's state such as the relative position with respect to the optimal path from the information delivered in GUI, and generate the control commands to the system through the joysticks. In manual control, the circuit between the controller and the vehicle dynamics is cut off such that the operator takes full responsibility of the vehicle movement. In supervisory control, a switch will be placed between the joystick and the vehicle dynamic model, once connected, the vehicle will be controlled by an internal loop where the desired control inputs calculated by the controller is sent directly to the vehicle dynamic model. The operator regains the control authority if the switch is disconnected. The haptic rendering is disabled in both manual control and supervisory control.

1.1 Design of haptic guidance

The vehicle dynamics block and the control algorithm for path tracking used in controller block are explained in details in appendix IV. The approach to render the haptic guidance is mainly adapted from previous study in caring driving (Abbink & Mulder, 2009), where the stiffness feedback could bring even higher improvement to the control performance than pure force feedback. Additional stiffness feedback could also avoid the instability problem in pure force feedback.

In manual control, the joystick has a self-centering stiffness K_0 with neural position at zero point to prevent erroneous input by accidental touch. Hence the operator feels the joystick as a virtual linear spring during manual operation. The similar virtual spring applies in supervisory control when the operator intervenes in the control loop and regains manual control mode. The only difference is that the neural position in supervisory control is shifted to full throttle during automatic control.

In HSC, force feedback is applied to the joystick to alter the equilibrium point from initial zero point to optimal turning angle θ_{opt} as calculated by the controller. Thus in an ideal case in force feedback, the operator should conform to the system and continuously seek for the shifting neutral position while the intercept of the shifted force-position characteristic on force axis will be the guidance force applied to the haptic interface. Apart from the shifting optimal

steering angle θ_{opt}, an additional stiffness feedback was applied to increase the stiffness based on the absolute lateral deviation e(t). Therefore more resistance force will be provided when operator steers away from the optimal steering angle. This combination of feedback forces are depicted in figure 1.6.

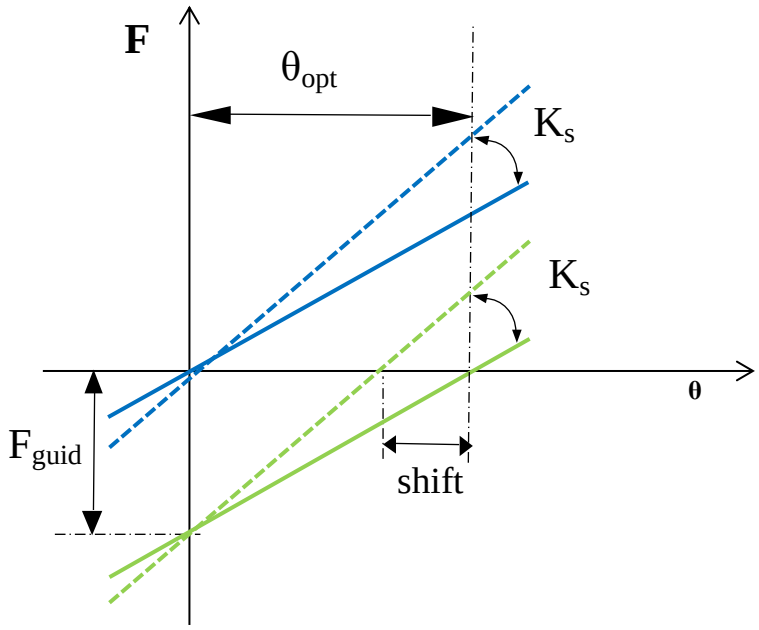

Figure 1.6. Illustration of stiffness and force feedback design. Blue solid force-angle line represents the centering stiffness (virtual spring) of the handle in manual control. The green solid line depicts the force feedback where the neutral point of former virtual spring is shifted to the optimal angle. The blue dashed line denotes the stiffness feedback, in which the former centering stiffness is increased by Ks according to the lateral deviation. The green dashed line gives the final force-angle relationship when both force and stiffness feedbacks are implemented.

$$F_{HSC} = K_0 \cdot \left(\theta_{steer} - \theta_{opt}\right) + c_s \left|e(t)\right| \cdot \left(\theta_{steer} - \theta_{opt}\right) \tag{1.1}$$

To establish the control algorithm for the crawler, a reference speed needs to be set. Here we set a constant reference speed at 0.8m/s for HSC design so that an extra speed range of 0.2m/s was left for operator's improvisation. In supervisory control the reference speed is set at 1m/s.

1.2 Graphic User Interface

The graphic user interface was constructed by using GUI toolbox in MATLAB®. The GUI program can both acquire the simulated data from and change module variables in the real time computers. The GUI program mainly generates two types of outcomes, one displays the 3D virtual reality environment and the other shows the integrated control panel.

Because this simulator aims to reproduce the actual scenario in future deep sea mining, yet the large water depth will absorb all natural lighting. Similarly any artificial lighting can also be assimilated easily by surrounding sea waters. Thus the operator will not receive enough

information from the traditional underwater video camera. A typical solution is to construct a virtual reality based on the data from bathymetry. Therefore one of the screens from the simulator renders a 3D virtual reality of the vehicle's working environment. It simulates a viewpoint set at the centre of the vehicle (figure 1.7). The prescribed optimal path is highlighted with a red curve showing at the middle of a seabed valley. The scenario in this study reproduces a subsea crawler to transit from one mining field to another. The terrain variation is also rendered by unsmooth meshes shown in front of the vehicle. The vehicle is assumed to be equipped with a local sensing system, to validate the actual terrain situation with previous investigation (e.g. multibeam pre-scan). Since the seabed environment is ever-changing, some parts of the terrain inevitably will be different in actual operation. Thus the operator's ability to avoid unexpected obstacles becomes an issue when investigating the best support for the operator. Therefore repeated sudden popped up obstacles are included and shown as an abrupt collapse of the meshes, representing a ditch on the terrain. Once the obstacle is shown, it remains visible.

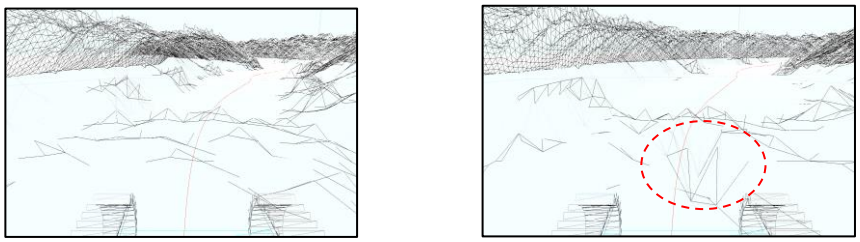

Figure 1.7. 3D representation through the viewpoint in virtual reality. Left: steering the vehicle in normal operation between obstacles. The subject aims to follow the red optimal path. Right: One of the 12 obstacle avoidances. Within the red highlighted circle is the ditch which the subject is supposed to get rid of. The subject needs to distinguish such a ditch from other normal terrain variations.

It is because the simulated subsea crawler is controlled by skid steering in this study, the vehicle speed is coupled with the heading angle. Hence if the obstacle is rendered according to the distance between the obstacle and the vehicle, subjects might run into the obstacle with completely different vehicle speed, which results into different difficulty of obstacle avoidance for each operator. If the distance when the obstacle pops up would be equal, it will be much harder for operators who drive faster to avoid the obstacle. Thus in this study the simulator calculates the moment to present the obstacle in the 3D virtual reality based on the vehicle speed.

$$L_{dist} = ttc \times v' \tag{1.2}$$

Where ***ttc*** stands for time to collide, ***v'*** is the vehicle's heading speed with respect to the obstacle center. In this experiment we set ***ttc*** at 7 seconds, and once the simulator detects the distance between vehicle center and obstacle edge falls into this pre-view range $\boldsymbol{L_{dist}}$, the obstacle will be presented on the screen. A schematic illustration of this judgement in the GUI program is shown in figure 1.8.

Besides the 3D virtual reality, the GUI program outputs a virtual control panel on another screen, as depicted in figure 1.9. This control panel aims to present additional information about the vehicle status along with the secondary task. On upper left part of the control panel an overview of the vehicle position in global coordinate, where the real time lateral deviation of the vehicle with respect to the optimal path and estimated time of arrival (ETA). The secondary task is presented on the upper right side of the panel. Eight red dot markers are shown around a dashed cross reference, and the operator is asked to recognize the number of red markers within the dashed circle. This task mimics the representation of underwater sonar system. There are two indicators in this display; each locates on one side of the sub-screen. The left side of the indicator will be enabled once the operator presses the left switch on the joystick. The vehicle's heading speed, rotating speed along with the global position is shown in the ROV status block. The tracks' status and their slip ratios are illustrated with a series of bar plots. The left couple of bar plots depict the actual speed inputs from the joysticks. The middle two represent the desired speed inputs calculated by the controller, and the right two for the real time slip ratio on the corresponding track. The calculated desired vehicle's heading speed; heading angle and the guidance force rendered on the joystick are shown in the guidance block on the right side. The mode switch block visually informs the operator of which status the control system is in during supervisory control. The '*automation*' indicator will be enabled once the system is fully controlled by the internal control loop and leaves the operator to a supervisory role. During human's intervention, the '*manual*' indicator will be enabled. The '*current*' block simulates randomized seawater current speed on longitudinal and lateral direction with respect to the vehicle. The experiment leader can start and stop the simulation in the task command block. After each subject completes a trial for each experimental condition, the collected experimental data can be copied from the memory of the Bachmann real time computer to the local memory in the personal computer by pressing the download button. A character string *'... file copied*' will be shown in the command window of MATLAB if the file is successfully downloaded. A more intuitive description of the whole control panel can be found in appendix V.

It is assumed that for the most of the time during the normal steering operation, the operator will only focus on the 3D virtual reality and the secondary task display on the control panel. However the rest of the supplementary information delivered on the control panel could help the operator to judge the vehicle status in special scenarios, such as avoiding obstacles and recovering from the slip event. The indications in '*mode switch*' block are also important to make the operator affirmative of the control authority in supervisory control.

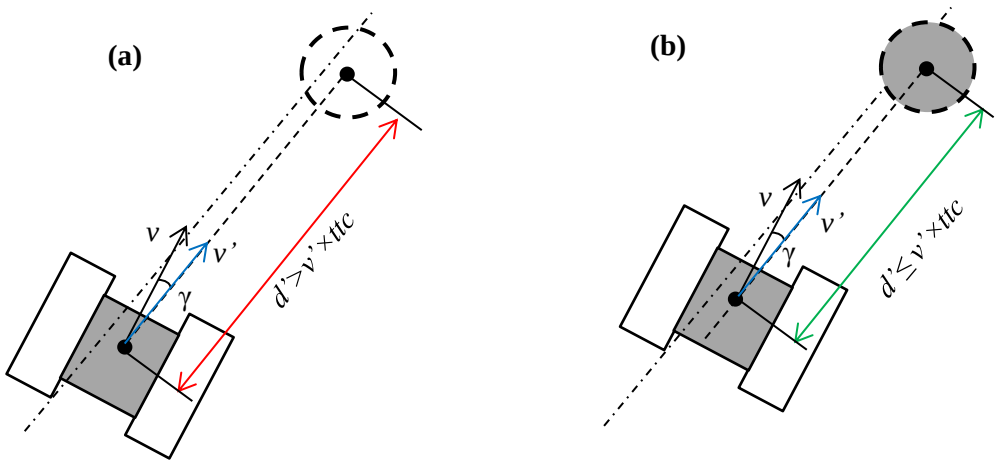

Figure 1.8. Illustration of the method the simulator used to calculate the pre-view distance so as to determine the moment when the obstacle is presented to the operator. (a) Vehicle's local sensor hasn't detected the obstacle because the distance between the vehicle and the obstacle is larger than the prescribed preview range. Therefore the obstacle is invisible. (b) The obstacle falls in the preview range so that the obstacle is visible on the screen.

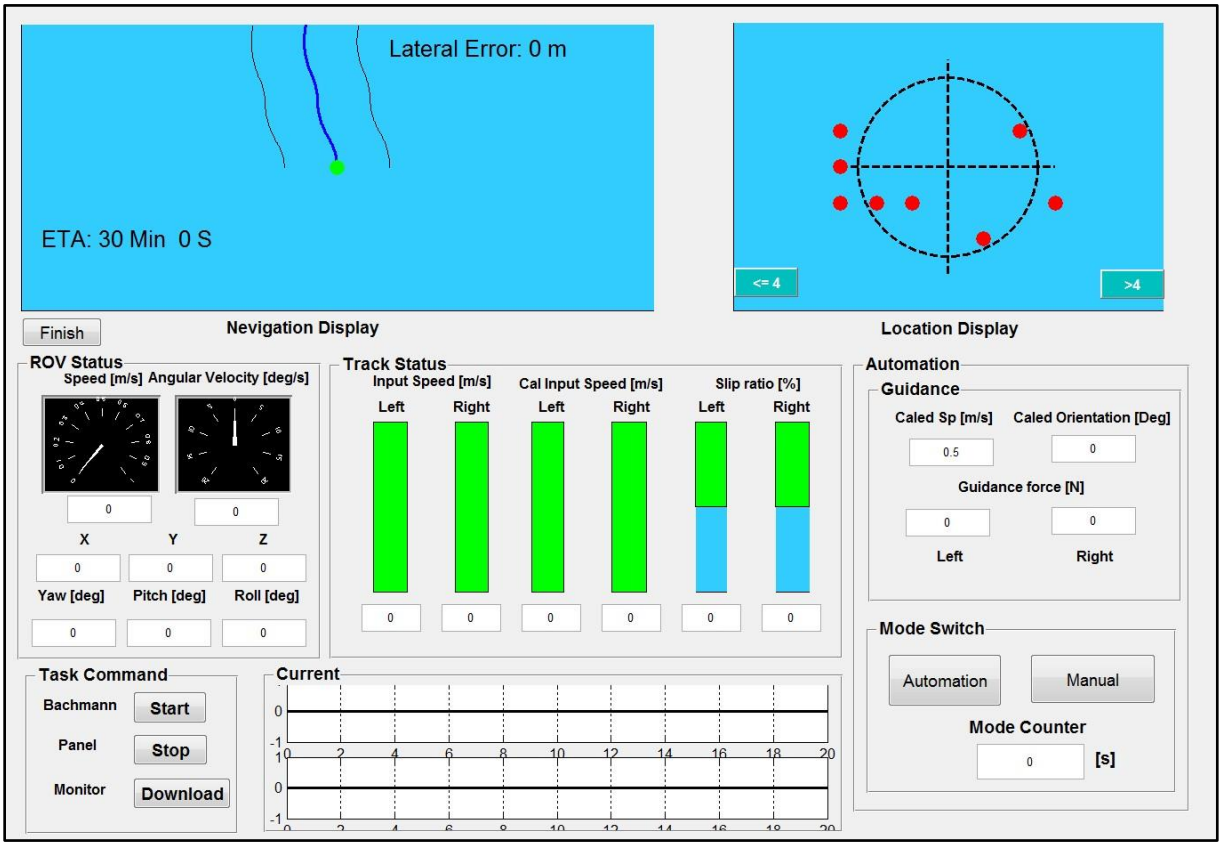

Figure 1.9. A screen shot of the control panel. The control panel not only provides supplementary information for the vehicle status from the 3D virtual reality, but also displays the secondary task to test the operator's mental workload.

Appendix II – Data Analysis

The raw data collected from the experiment includes two parts: '*ROVLOG*' contains a matrix with 32 rows of data sets with an update frequency of 500Hz, '*Dashboard*' contains information about the obstacles, the correct answer and the testing time of the secondary task, etc. Subjects' identity is abbreviated as '*S1, S2*', etc. For example, '*ROVLOGS1Manual*' represents the data of 1st subject's performance in manual control. Each row in file '*ROVLOG*' is:

1: Real time vector logged during the experiment [s].
2~3: Calculated optimal turning angles, on left and right handle respectively [rad].
4~5: Actual turning angles of these two handles [rad].
6~8: Vehicle's position on x, y and z global coordinates [m].
9~11: Vehicle's speed on x, y and z global coordinates [m/s].
12~14: Vehicle's pitch, roll and yaw angles [rad].
15~17: Vehicle's angular speed on pitch, roll and yaw angles [rad].
18: Data from odometer [m].
19: Vehicle's local heading speed [m/s].
20: Heading angle on optimal path [rad].
21: Vehicle's lateral error [m].
22: Traversed distance with respect to the prescribed optimal path [m].
23~24: Strain on both left and right strain gauge [V].
25~26: Power on left and right motor [V].
27~28: Subject's response towards the secondary task.
29~30: Speed of the handle inputs [rad/s].
31: Time point indicates whether supervisory control is enabled.
32: Time point where the slip event is triggered [s].

In order to better compare the effects of two assisting conditions on the operator under different task modules, we partitioned the whole data set into three parts, namely:

1. ***Within obstacles***: it starts once each obstacle shows up on the screen, and ends when the lateral error recovers within ±0.6m with respect to the centerline.
2. ***Between obstacles***: the duration when the vehicle traverses between each obstacle.
3. ***Slip recovery***: it starts when the slip event is triggered and lasts till to the end of the trial.

Figure 2.1 illustrates the partition between two between obstacles modules and one within obstacle modules. The simulator records the moment when the obstacle is shown on the screen (left red dot in figure 2.1). The script used for data analysis detects the first moment when the vehicle recovers back into the tolerance. Therefore the distance in between these two moments becomes the corresponding within obstacle module. However in slip event, there is no visual cue on the screen and the operator needs to identify the slip event from the

abnormal vehicle outcome, either with or without guidance, and intervene in the control system. The guidance cannot handle the slip event all by itself. There is no obstacle in slip event in order to prevent the interaction effect.

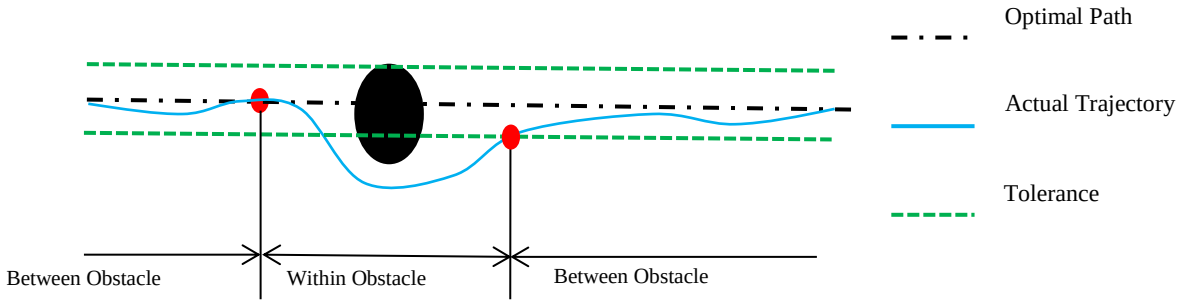

Figure 2.1. Illustration of demarcation between within obstacle and between obstacles.

The optimal path contains the five different curvatures whose reciprocals range within {20 25 30 35 40 [m]}. Negative and positive curvatures represent left and right turns respectively. Straight segments have curvature at 0 [m]. The slip is triggered at the end of the path where a left turn is required. An overview of the optimal path is shown in figure 2.2. This track is used in each condition for each subject.

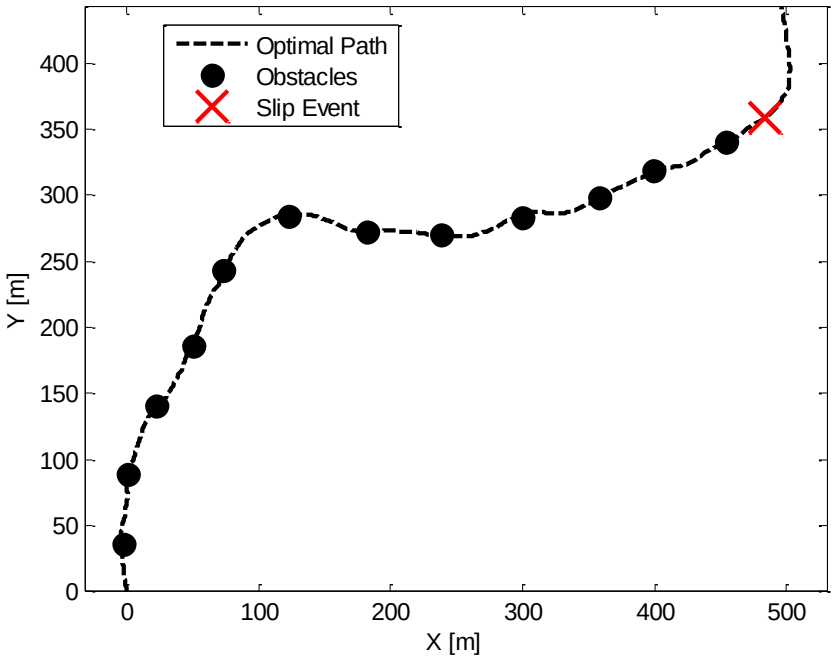

Figure 2.2. Overview of the map used in this experiment. Black circles denote the locations of each obstacles, and dashed black curve is the position of optimal path. Red cross indicates the place where the slip is triggered.

2.1 Actual Trajectory

Each subject's performance of obstacle avoidance within each obstacle under three experiment conditions is shown in figure 2.3. Subjects' identities are marked with different colors. If the distance between obstacle center and vehicle center falls into 3m, the collision is incurred.

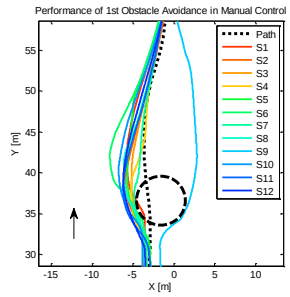

(1-a)

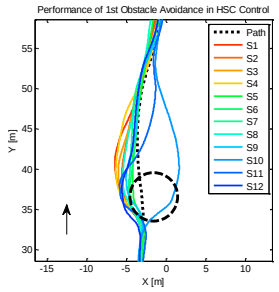

(1-b)

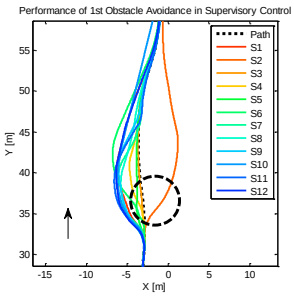

(1-c)

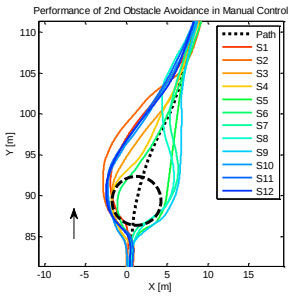

(2-a)

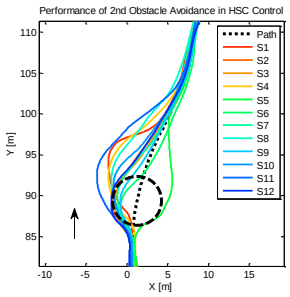

(2-b)

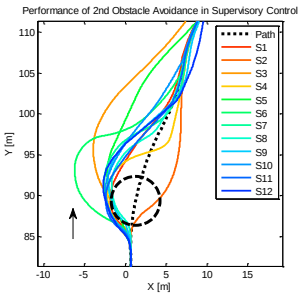

(2-c)

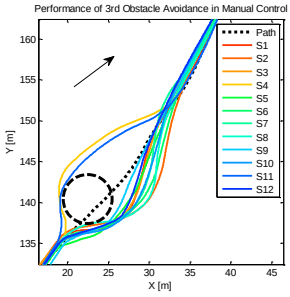

(3-a)

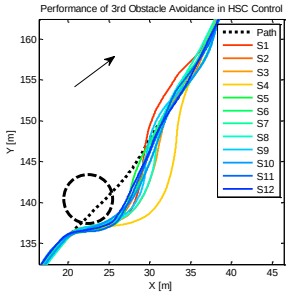

(3-b)

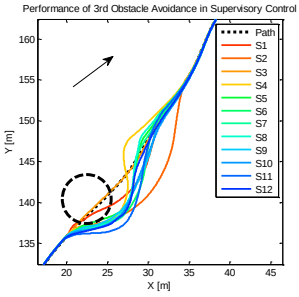

(3-c)

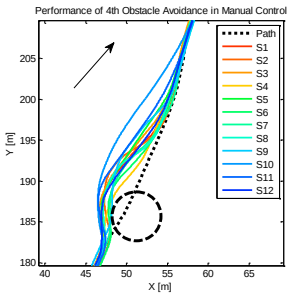

(4-a)

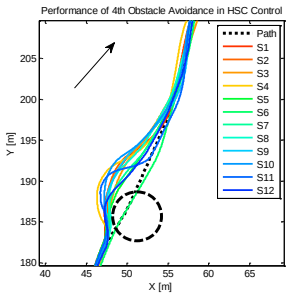

(4-b)

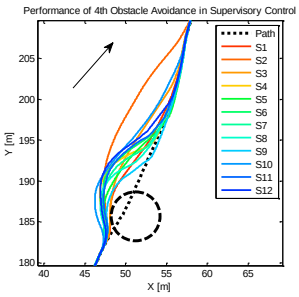

(4-c)

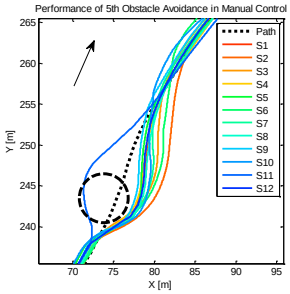

(5-a)

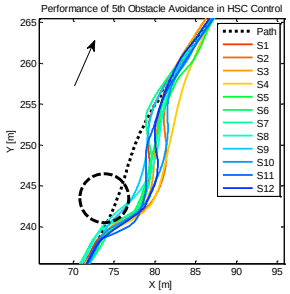

(5-b)

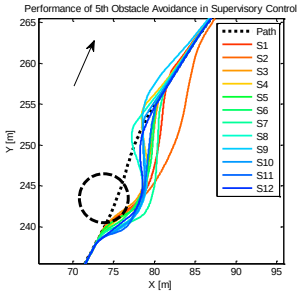

(5-c)

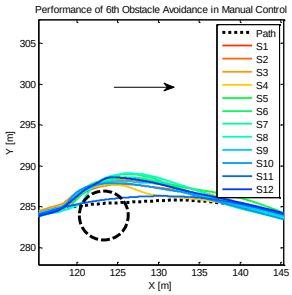

(6-a)

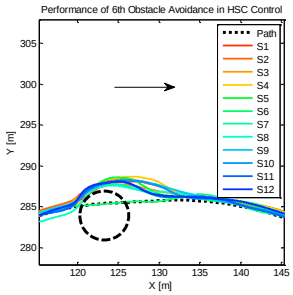

(6-b)

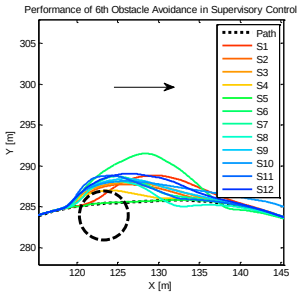

(6-c)

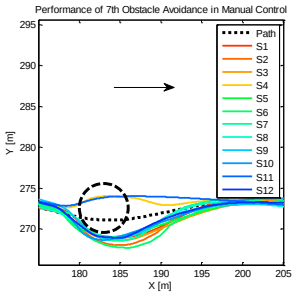

(7-a)

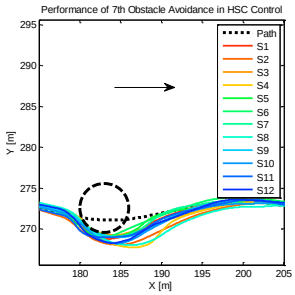

(7-b)

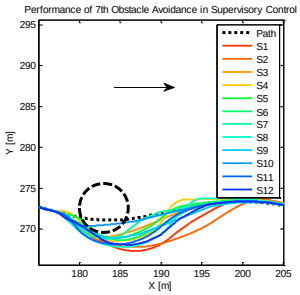

(7-c)

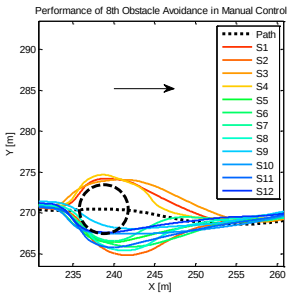

(8-a)

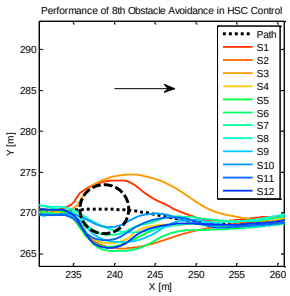

(8-b)

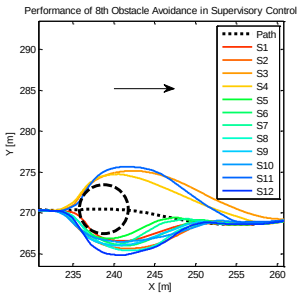

(8-c)

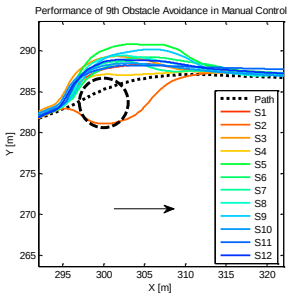

(9-a)

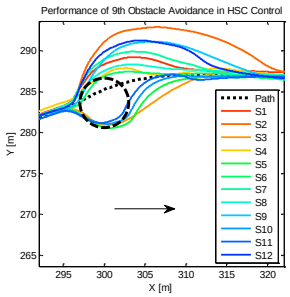

(9-b)

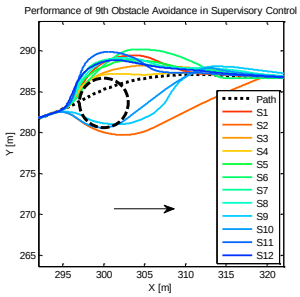

(9-c)

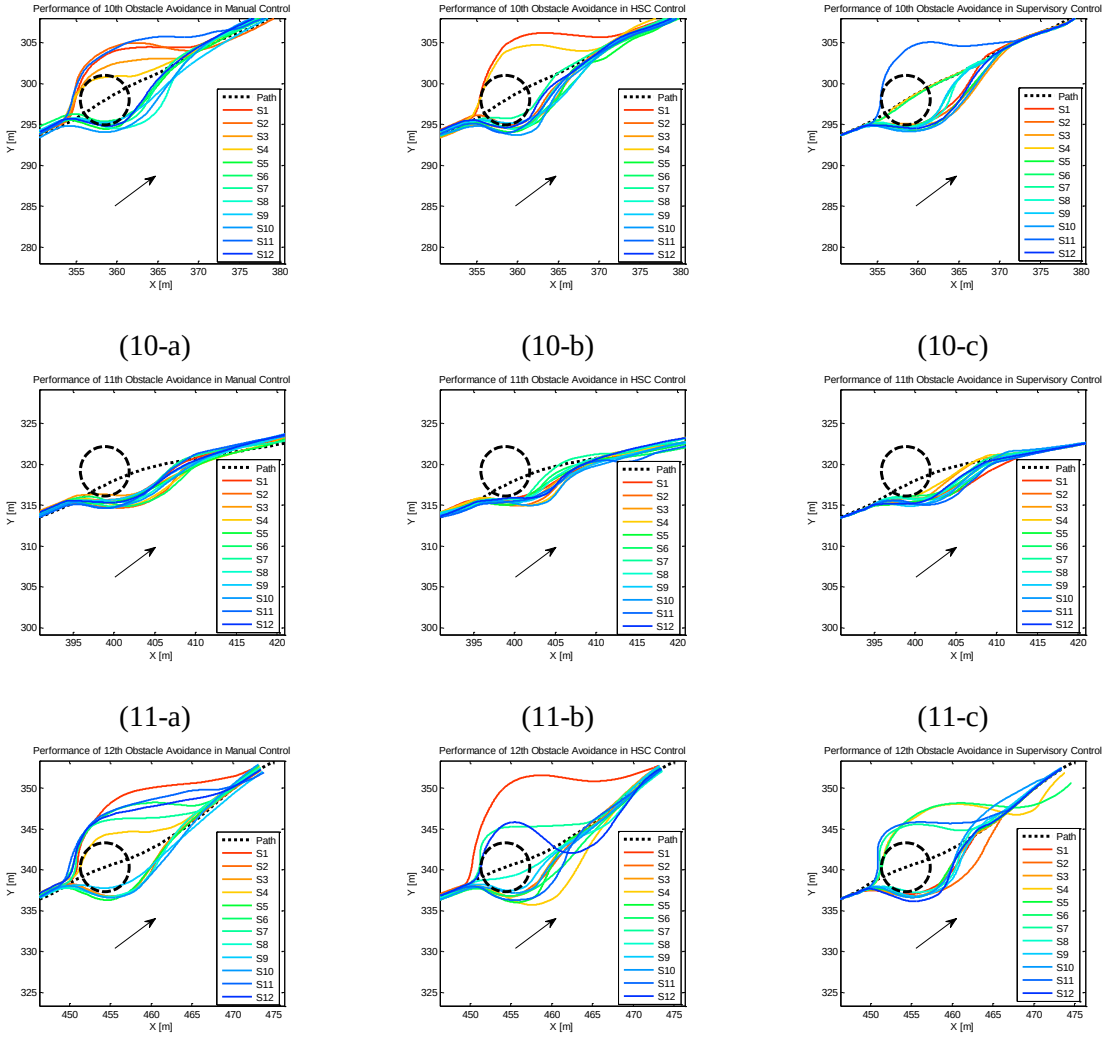

(10-a) (10-b) (10-c)

(11-a) (11-b) (11-c)

(12-a) (12-b) (12-c)

Figure 2.3. Performance of obstacle avoidance in obstacle 1~12. Three columns of subplots illustrate different obstacle avoidance between 12 subjects in manual control, HSC, and supervisory control, respectively.

2.2 Within Subjects Comparison

The raw path tracking and obstacle avoidance only give a straight impression on the differences between three experiment conditions. To objectively evaluate the effects between conditions, we should look further into different metrics. These metrics are categorized between performance and control effort.

Performance:

1. Lateral deviation between obstacles;
2. Number of collisions;
3. Mean reaction time in detecting the obstacles;
4. Distance traversed in obstacle avoidance;

5. Maximal absolute lateral error in slip recovery;

Control effort

1. Response accuracy in secondary task;
2. Reaction time in secondary task;
3. STD of the difference between two rotary handles.
4. STD of the torque generated by the operator
5. Reversal rate on each handle.
6. Subjects' answers from the questionnaire.

One way repeated measures ANOVA was used for most of the metrics to determine the statistical difference between experiment conditions and $p<0.05$ was taken as a measure of significance. The maximal deviation in slip recovery was tested by one way independent ANOVA since we are only interested in each subject's first time reaction towards the slip event. Another exception is the torque on each handle, where left-or-right hand was regarded as a factor and a two way repeated measures ANOVA was calculated to minimize the type I error.

2.2.1 Performance - Lateral Deviation

The lateral deviation is the most straightforward metric to evaluate the operator's performance in lane keeping between obstacles, where negative deviation indicates that the vehicle's position is deviated to the left side of the optimal path. Root mean square (RMS) is a common statistical measure of the magnitude of a varying quantity, especially suitable when the variable has both positive and negative values. Therefore the root mean square of vehicle's lateral error between obstacles was calculated and shown in figure 2.4-a (i.e. data in obstacle avoidance and slip recovery are excluded). Each subject's individual performance is marked with individual cross marks, the group mean with the colored circle and the spread with an error bar depicting the 95% confidence interval of the group mean.

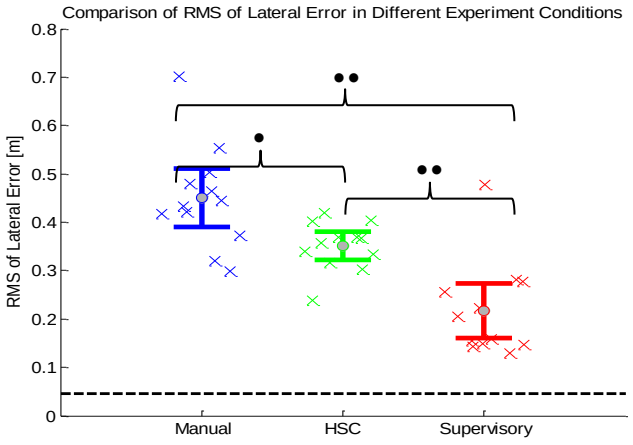

(a)

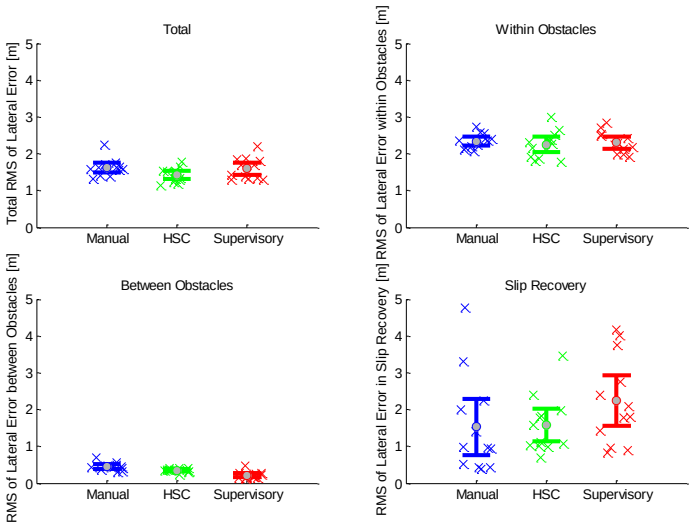

(b)

Figure 2.4. (a) Comparison of root mean square (RMS) of lateral errors between obstacles in three different experiment conditions with respect to the optimal path. The black horizontal dashed line represents the hypothetical RMS value when the system is run by full automation throughout the experiment. '○' , '●' ,'● ●' means a significance with p<0.1, p<0.05 and p<0.01, respectively. (b) Overview of the RMS of the lateral error in different task modules between experiment conditions. *Top-left*: in total. *Top-right*: within obstacles. *Bottom-left*: between obstacles. *Bottom-right*: slip recovery.

	Manual		HSC		Supervisory	
RMS of Lateral Error [m]	$\overline{X}$	S	$\overline{X}$	S	$\overline{X}$	S
	0.452	0.107	0.352	0.050	0.217	0.099

(a)

Test	$\Delta\overline{X}$ [m]	p value
Manual-HSC	**-0.100**	**p<0.05**
HSC-Supervisory	**-0.135**	**p<0.01**
Manual-Supervisory	**-0.235**	**p<0.01**

(b)

Table 2.1. Performance of lateral error in three experiment conditions. (a) group means and standard deviation. (b) multiple comparisons between three conditions.

The mean and standard deviation of the metric RMS is summarized in table 2.1. No statistically significant difference was found for the lateral deviation within obstacles and in slip recovery (figure 2.4-b). However for the lateral deviation between obstacles, one way ANOVA indicated a significant difference between conditions ($F(2, 22) = 7.11$, $p<0.01$) and post hoc test also revealed significant difference between all three conditions. Specifically HSC decreased the RMS of lateral deviation by 22% from manual control while supervisory control reduced by 52% compared to manual control. In supervisory control the subjects may still insist on manual intervention while the vehicle has already gotten back to the centerline after obstacle avoidance (figure 2.5). Thus the system was still controlled by human for some time when the vehicle's position was recognized as between obstacles already. Hence the performance of supervisory control was not exactly the same as full automation. Although both HSC and supervisory control prevails manual control in lateral deviation, there still exists some difference between lateral error

in HSC and that in full automation between obstacles. This indicates that there existed a phenomenon where the operator did not completely conform to the guidance in HSC.

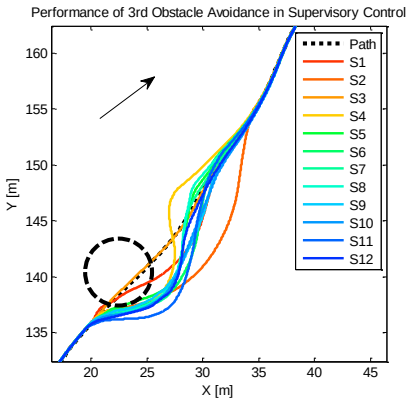

Figure 2.5. A plot depicts the obstacle avoidance in supervisory control, where subject 4 still remained in manual intervention after got back to the optimal path, to compensate for the overshoot.

2.2.2 Performance – Number of collisions

During each completed trial, the operator was presented with 12 obstalces distributed along the optimal path, but not necessarily on the center of the optimal path. The collision is regarded to occur once the distance between vehicle center and obstacle center falls into 3m. But since the vehicle speed was used to calculate the moment when simulator presents the obstacle to the operator, different subjects may have unconstant initial condition when the obstacle shown up. This may cause a biased comparison on the number of collision. The total number of collision conducted by each subject in three conditions are shown in figure 2.6.

Subject Identifier:

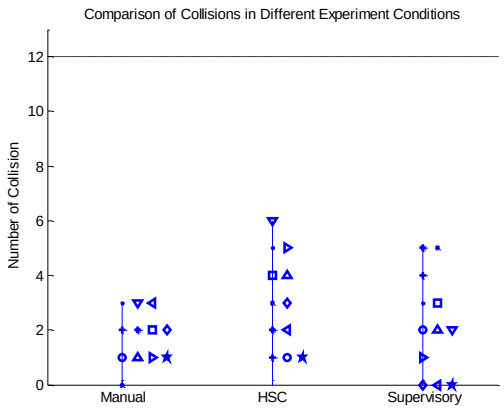

Figure 2.6. Theoretical collisions according to the raw data, where each subject's performance is marked with different identifier. Full automation will result into 12 collisions (100% collision), which is illustrated by black dashed line on top of the plot.

According to the results, 12 subjects totally ran into 21 collisions (14.6% hit ratio) in manual control, 37 in HSC (25.7% hit ratio) and 27 in supervisory control (18.6% hit ratio). However using a one way repeated ANOVA no statistically significant difference was found between the three conditions. Because of the fact that the operator could control both the speed and heading angle of the vehicle, only the total number of collision maybe too ambiguous to detect the difference between conditions. Thus more metrics are needed to look the obstacle avoidance in details. Figure 2.7 illustrates vehicle's least distance with respect to the obstacle

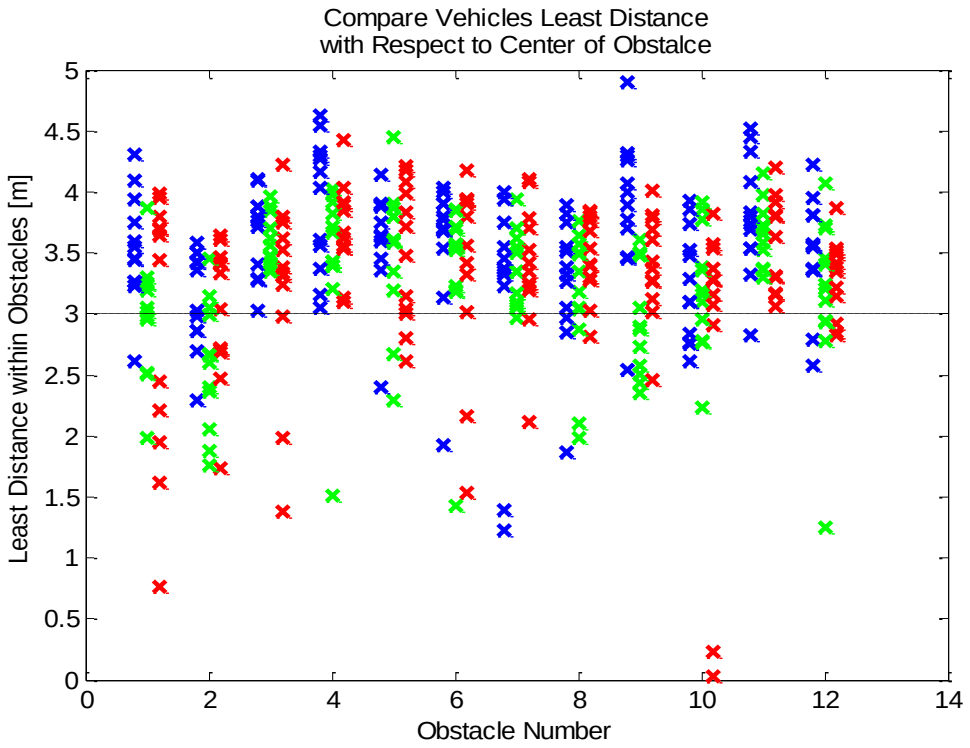

Figure 2.7. Overview of vehicle's least distance to the obstacle center in 12 obstacle avoidances. Performance in manual control is marked in blue, HSC in green and supervisory control in red. Dashed line at 3m represents the tolerance the simulator refers to define the collision.

center controlled by each subject in 12 obstacle avoidances. Similarly, these cross dots which fall below 3 m denote unsuccessful obstacle avoidances. Apparently there exist a distinct differences between some collisions. Some of the collisions occurred where the least distances were quite closest to 3m, while some others had least distances even closed to zero and therefore drove straight though the object with no avoidance maneuver at all. The averaged least distance across all 12 obstacles for each subject is shown in figure 2.8, displaying the group means along with its 95% confidence intervals.

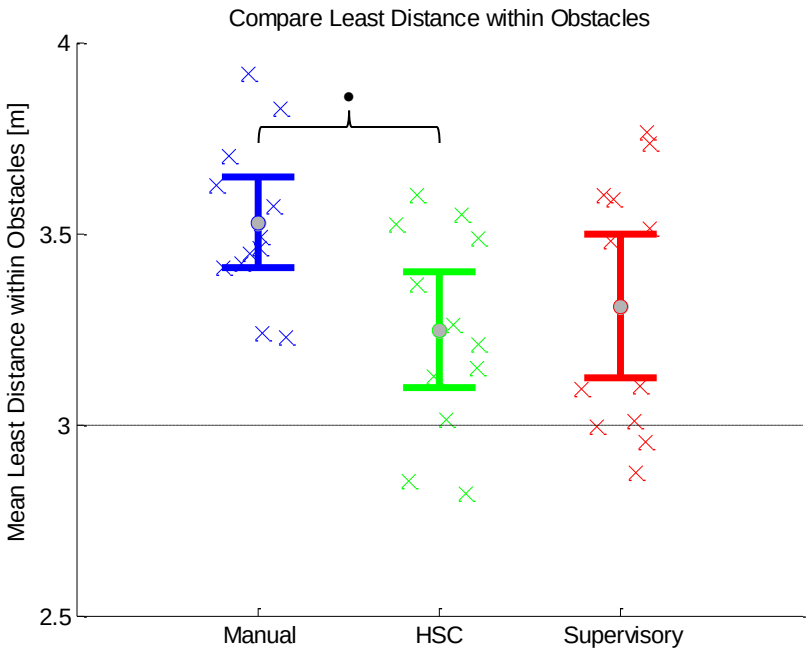

Figure 2.8. Vehicle's mean least distance towards obstacle center in three experiment conditions, averaged by 12 obstacle avoidances. The safety tolerance is 3m, represented by the black dashed line. '○' , '●' ,'● ●' means a significance with p<0.1, p<0.05 and p<0.01, respectively.

One way repeated ANOVA revealed a statistically significant difference between three conditions for the mean least distance ($F(2,22) = 4.21$, $p=0.028$) while post-hoc test pointed out sorely a significant difference between manual control and HSC ($p<0.05$). It seems subjects under HSC tended to steer the vehicle closer to the obstacle than in the other two conditions, but a pitfall is that subjects could have different difficulties in avoiding the obstacle under three conditions when facing the obstacles. The simulation system calculated the pre-view distance towards the obstacle in the simulation based on the speed of the vehicle (appendix I, figure 1.8):

$$d = v' \times ttc \tag{2.1}$$

Where ***v'*** is the relative local speed of vehicle with respect to the obstacle, and ***time to collide (ttc)*** is set to 7 seconds in the actual experiment. If we neglect the angle between vehicle heading direction and the segment from vehicle center to the obstacle center, the pre-view distance is then totally dominated by the vehicle speed. Therefore the subject will have a larger pre-view distance when driving faster. In order to testify whether this design bias is significant in this experiment, the vehicle's mean velocities when obstacles shown-up under three experiment conditions are exhibited in figure 2.9 and summarized in table 2.2. The results showed that the average speed of vehicle when obstacle shows-up was significantly affected by the experimental conditions. $F(1.1,12.03)=122.277$, $p<0.001$ (Mauchly's test indicated that the assumption of sphericity had been violated, $\chi^2(2)=17.66$, $p<0.05$, therefore the degrees of freedom were corrected using Greenhouse-Geisser estimated of sphericity ($\varepsilon= 0.55$)). Post hoc tests revealed significant differences between all three conditions (all multiple comparisons, $p<0.05$). We could tell from the data that each subject definitely had

individual preference on the vehicle speed, especially in manual control where the vehicle's speed was dominantly controlled by the subject. Some subjects were conservative on the vehicle even though they had been informed by the task description before the experiment that higher vehicle speed was preferred to complete the task (the ETA on the control pannel is also specially introduced to the subjects). Other subjects did drive the vehicle much faster, either because of the task description or their own aggressive driving maneuver. It is because of the fact that the recommended speed for haptic shared control is about 0.8 *m/s*, leaving some space for subject's improvisation, however subjects showed certain obedience towards the guidance force, so that the speed when obstacles shown-up on the screen in HSC is lower than in supervisory control and manual control. Averagely speaking, subjects in HSC drove 0.145m/s and 0.201m/s slower than manual and supervisory control, respectively. As we set the variable '***ttc***' to 7 seconds, this resulted into about *1m* and *1.4m* less pre-view distance for subjects to react in HSC than that in the other two conditions.

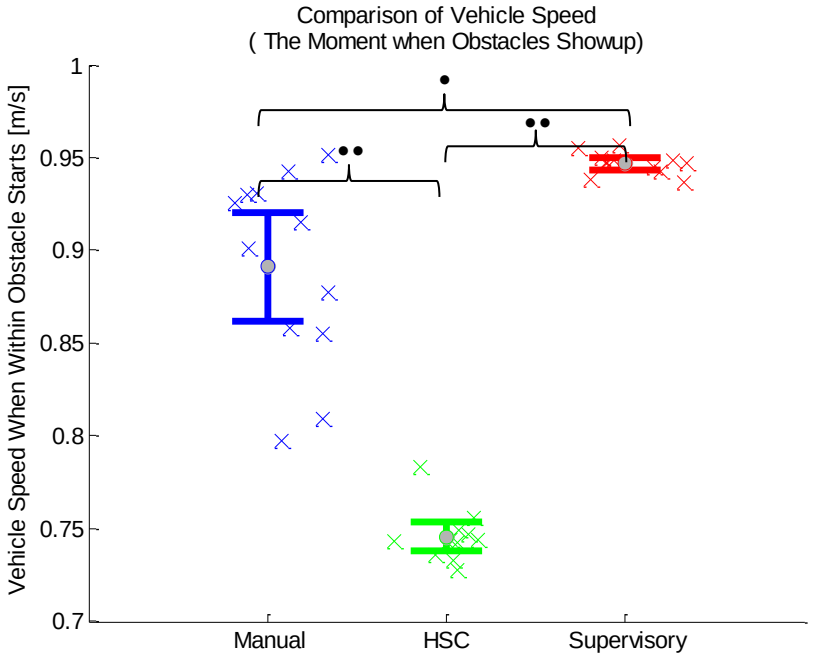

Figure 2.9. Vehicle's mean speed steered each subject when obstacles shown-up, the group mean is shown with 95% confidence interval. '○' , '●' ,'● ●' means a significance with p<0.1, p<0.05 and p<0.01, respectively.

	Manual		HSC		Supervisory	
Mean speed when obstacles show-up [m/s]	$\overline{X}$	S	$\overline{X}$	S	$\overline{X}$	S
	0.891	0.052	0.746	0.014	0.947	0.006

(a)

Test	$\Delta\overline{X}$ [m/s]	p value
Manual-HSC	**-0.145**	**P<0.001**
HSC-Supervisory	**+0.201**	**P<0.001**
Manual-Supervisory	**+0.056**	**P<0.05**

(b)

Table 2.2. (a) Group means and standard deviations of vehicle mean speeds. (b) Multiple comparisons between three experiment conditions.

2.2.3 Performance – Reaction time on the obstacles

Since subjects truly had a less pre-view distance (though with same reaction time) to detect the obstacle in HSC, human's reaction on avoiding obstacles need to be further elaborated. Therefore we categorize the obstacle avoidance into four different conditions:

1. Operator didn't detect the obstacle at all so that did not even react to the obstacle (***type I collision***).
2. Operator responded to the obstacle, but there was insufficient distance left, so that it was impossible for the operator to avoid the obstacle, even with maximum steering (***type II collision***).
3. Operator responded in time but still hit the obstacle while it was still possible to avoid it with maximum steering, because wrong steering maneuver was taken (***type III collision***).
4. Operator responded in time and successfully avoided the obstacle.

It is assumed that vehicle was supposed to have less distance towards the obstacle when type I occurred (data dots on the lower part in figure 2.7), than type III collisions and successful avoidances. And it is more accurate to compare the effects from assist conditions on the operator's vigilance on the obstacle for each type of collisions. Nevertheless, a sensitive metric is needed to identify whether the operator responds to the obstacle. If the subject did not respond to the obstacle at all (i.e. type I collision), the vehicle's trajectory was supposed to be closed to the optimal path (see figure 2.3). Here we found several collisions which most likely belong to type I collision (table 2.3):

Manual control	HSC	Supervisory control
S11Obs6	S6Obs4 S6Obs6	S3Obs1 S3Obs2 S5Obs6 S4Obs10 S6Obs10

Table 2.3. Collisions where the vehicle's trajectory was more closed to the optimal path than the other trajectories, selected by eyeballing. 'S*' represents the subject's identity and 'Obs*' stands for the number of the obstacle, e.g. 'S11Obs6' indicates the 11th subject's trajectory within the 6th obstacle.

The vehicle's heading angle is directly controlled by two speeds input from these two rotary handles. Thus the turning angles of these two handles become the most straightforward variables to identify the subject's awareness on the obstacle. The turning angles of two handles steered by the subjects under these circumstances (table 2.3) are showed in figure 2.10.

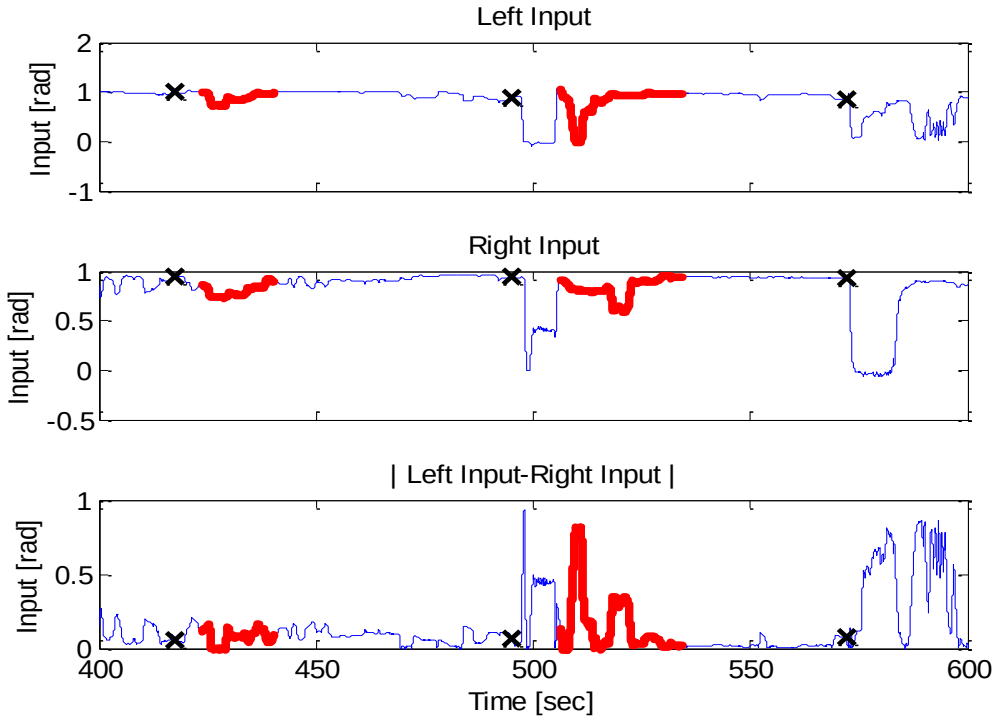

(a) Subject: 11, Obstacle:6~8

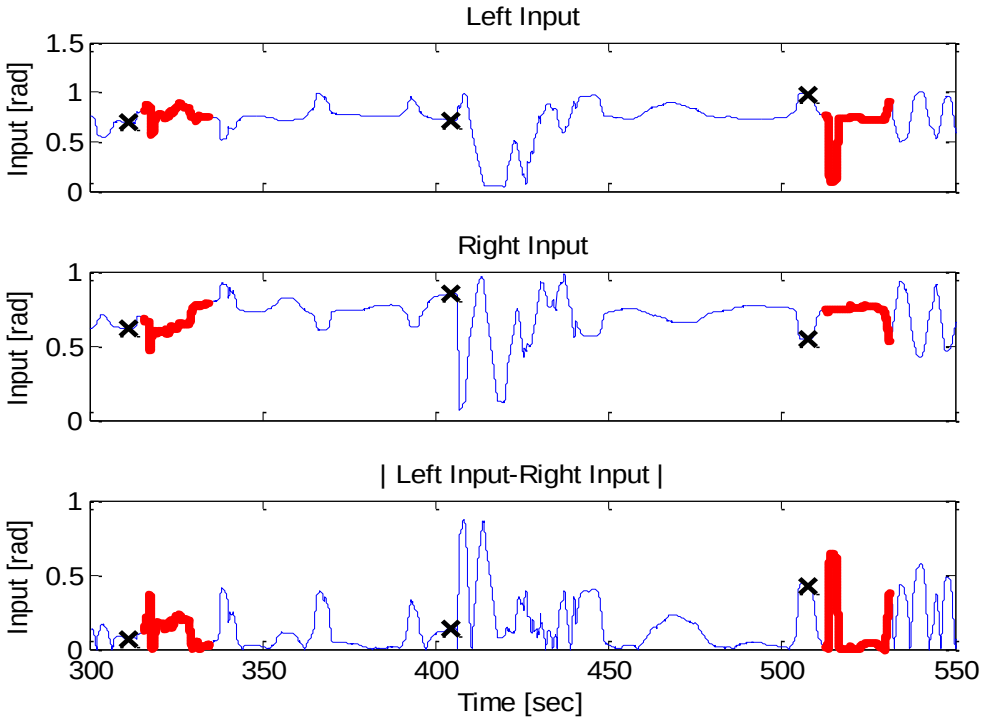

(b) Subject:6, Obstacle: 4~6

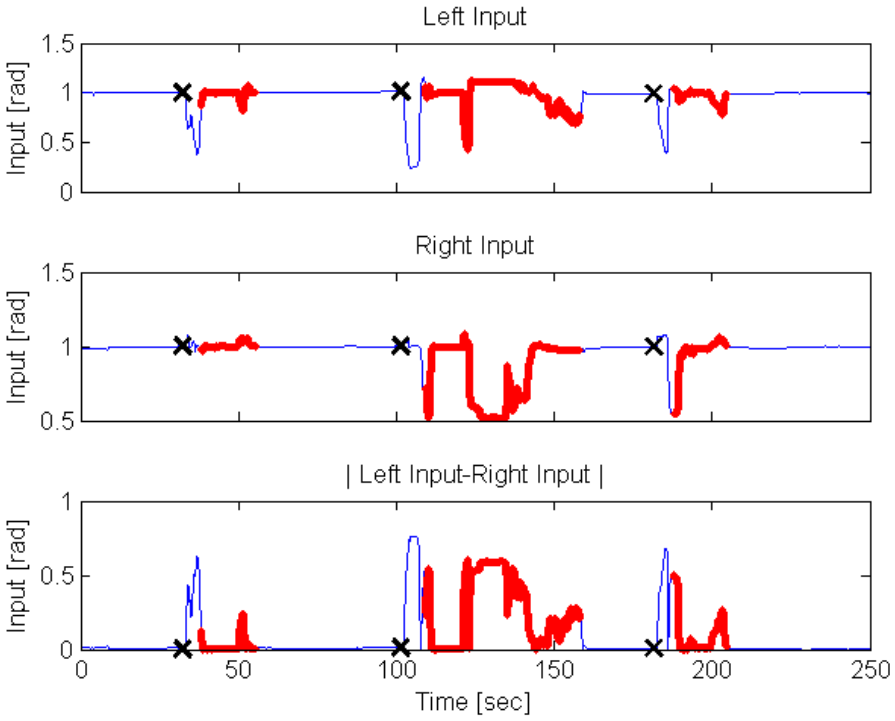

(c) Subject: 3, Obstacle: 1~3

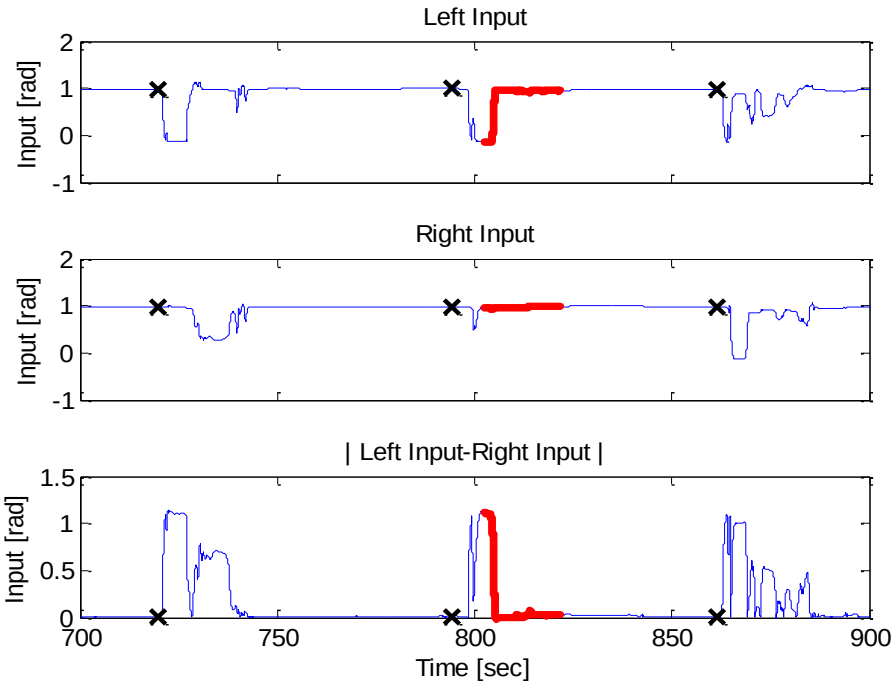

(d) Subject: 4, Obstacle: 9~11

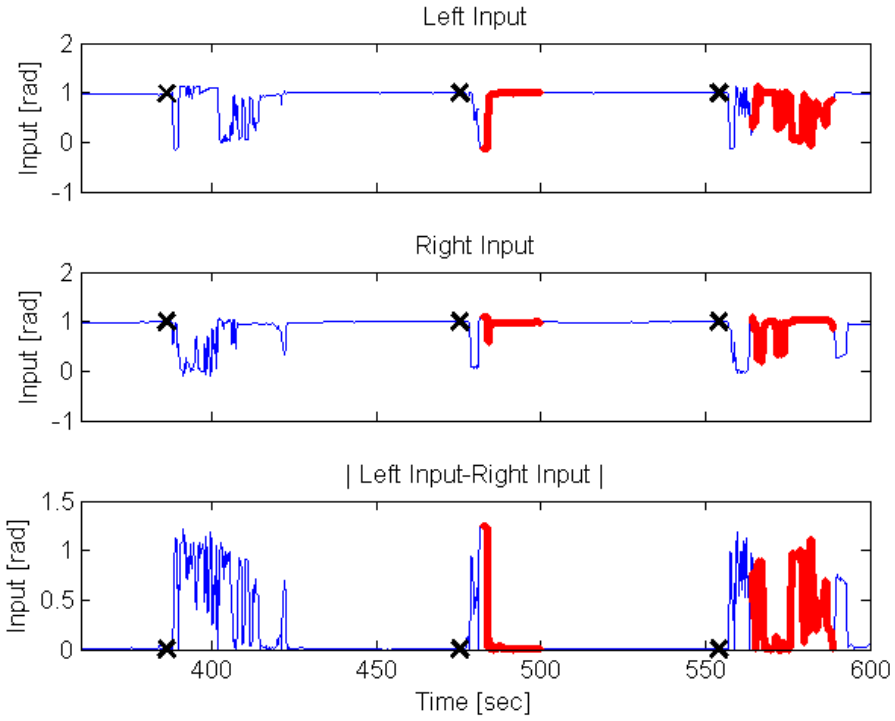

(e) Subject: 5, Obstacle: 5~7

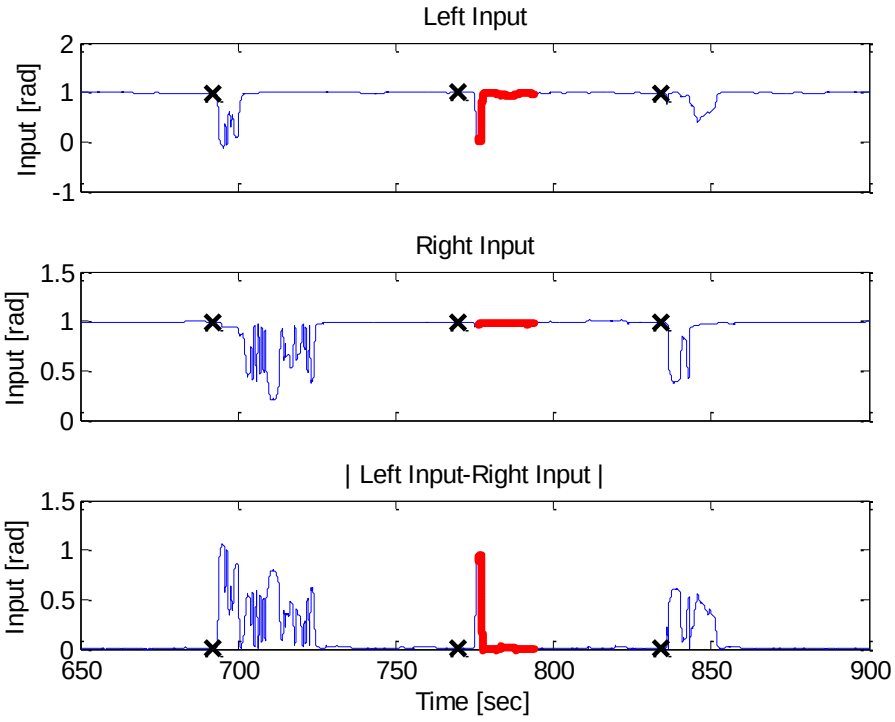

(f) Subject:6, Obstacle: 9~11.

Figure 2.10. Speed inputs in circumstances mention in table 2.3. Blue signal represents the actual speed input and red parts cover the duration from the moment collision occurred to the end of the corresponding obstacle avoidance (vehicle left the obstacle and recovered back to the optimal path). These black cross markers stand for the moment when the obstacle actually showed on the screen. The

upper subplot depicts the input speeds of the left handle. The middle subplot represents the input speeds on the right handle. The bottom subplot illustrates the absolute difference between left and right input speeds. (a). The 11th subject was avoiding 6th ~ 8th obstacles in manual control. Collisions occurred within the 6th and the 7th obstacles. (b). The 6th subject was avoiding 4th ~ 6th obstacles in HSC. Collisions occurred within both the 4th and the 6th obstacles. (c). The 3rd subject was avoiding 1st ~ 3rd obstacles in supervisory control. Collisions occurred within all three obstacles. (d). The 4th subject was avoiding 9th ~ 11th obstacles in supervisory control. Collisions only occurred within the 10th obstacles. (e). The 5th subject was avoiding 5th ~ 7th obstacles in supervisory control. Collisions occurred within both the 6th and the 7th obstacles. (f). The 6th subject was avoiding 9th ~ 11th obstacles in supervisory control. Collisions only occurred within the 10th obstacles.

In manual control, the 11th subject ran into collisions within both 6th and 7th obstacle and succeeded in avoiding the 8th obstacle. However the subject's speed manipulation was apparently different between 6th and 7th avoidance (figure 2.10-a). No significant decrease in either of these two speed inputs was found when the vehicle was in the 6th obstacle, while a distinct jitter was observed in the next avoidance. Therefore we proposed that the collision in 6th obstacle was caused by the subject's no response because of total ignorance (type I collision). But the subject clearly reacted to the 7th obstacle, though still ran into collision (either type II or type III collision). Some situation occurred for the 6th subject's performance in HSC from the 4th to 6th obstacle (figure 2.10-b). While the subject mistakenly ran into two collisions (4th and 6th obstacle), the later one (6th obstacle) have more significant reaction in the speed inputs. It is interesting to notice that even though the sudden decreases in speed input existed, these decreases overlaps fall into the red highlighted segments of the speed input signal. This means that the subject did respond to the obstacle when the vehicle had already collided to the obstacle and the simulator had paused. Thus these cases should also be attributed to type I collision. In supervisory control, the subject should first pull back at least one of the handle to seize the control authority from automation. Thus it is easier to identify whether the subject responded to the obstacle in supervisory control: at least one of the speed input should have an obvious decrease below 0.6. Otherwise the subject definitely didn't intervene in the system. It is observed from figure 2.10 (c), (d), (e), (f) that there always existed a clear sudden decrease in at least one side of the speed inputs before the red highlighted segments. This indicates the fact that all subjects clearly intervened in the control loop before the collision occurred.

Regarding the metric to identify whether the subject notice the obstacle or not, it is better to use the absolute difference between left and right speed inputs instead of the individual input speed. In some cases, subject preferred to only pull back the left handle while the others the opposite way. But we can tell from all subplots in figure 2.10, regardless of the experiment conditions, there were always a significant reaction on the absolute difference as long as the subject responded to the obstacle. Here we set 0.4 as a relatively fair tolerance to clarify the subject's intervention while get rid of the speeds variation during normal steering activities between obstacles (the tolerance 0.4 was chosen because it could detect the obvious change in turning angle, and also reject those normal jitters). Thus reaction time of the subject's intervention towards the obstacle becomes:

$$RT = \begin{cases} t_{\text{intervention}} - t_{\text{obstacle}} & ,if\ t_{\text{intervention}}\ exist \\ Inf & otherwise \end{cases} \tag{2.2}$$

$t_{\text{intervention}}$ stands for the very first moment during each obstacle avoidance when $\left|v_{left} - v_{right}\right| \geq 0.4,\ t_{\text{obstacle}} < t < t_{\text{collision}}$. v_{left} and v_{right} is the speed input on left and right side, respectively. $t_{obstacle}$ represents the moment when collision occurred.

Besides the type I collision, further categorization is needed to distinguish between type II and type III collisions. As the vehicle is steered by skid steering, a theoretical maximum steering angle can be simulated with the dynamic model used in this study. In figure 2.11, the

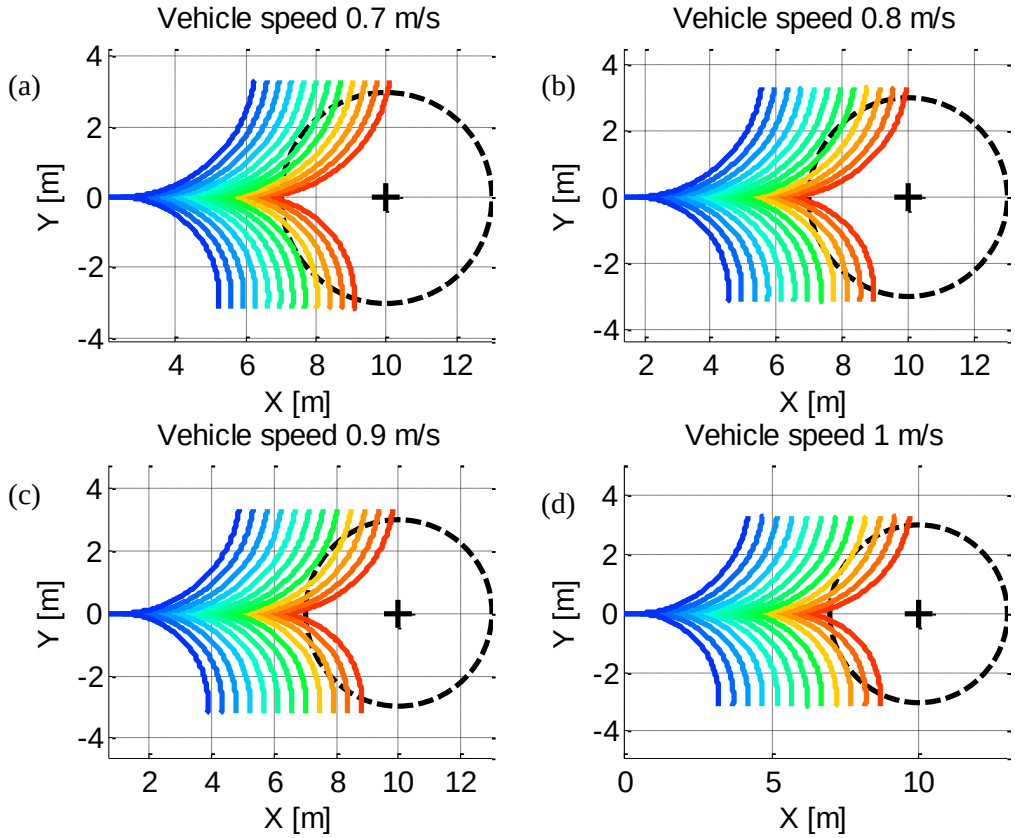

Figure 2.11. Ideal obstacle avoidance in different initial vehicle speed and different TTC (time to collide). In each subplot, left turning is driven under $v_l = 0.2\text{m/s}$ $v_r = 1\text{m/s}$, and right turning is driven under $v_l = 1\text{m/s}$ $v_r = 0.05\text{m/s}$. From left to right, each curve represents the trajectory with TTC averagely varies from 1.5s to 7s. Top Left: vehicle speed at 0.7m/s. Top right: vehicle speed at 0.8m/s. Bottom left: vehicle speed 0.9m/s. Bottom right: vehicle speed at 1m/s.

plots show vehicle's trajectory within two different steering maneuvers under several different initial vehicle speeds. Hypothetically the vehicle has an initial speed towards the center of the obstacle, and these left turns depict a modest steering, where maximum speed is generated on one side and 0.05m/s is driven on the other side. In contrast, those right turns represent a more aggressive avoidance, where maximum speed is inserted on one side and minimum on the

other side. The steering maneuver is theoretically the maximal avoidance the vehicle can perform. As illustrated in figure 2.11, with constant steering speeds on both tracks to avoid the obstacle, the hit ratio is noticeably influenced by the initial speed of the vehicle. With vehicle initial speed at 1m/s, it is possible to avoid the obstacle with TTC at least 2.5 seconds (3^{rd} right turning curve in bottom right subplot.). However, in the same circumstance, but with vehicle speed at 0.7m/s, at least 3.5 seconds is required to avoid the obstacle (5^{th} right turning curve from right to left, figure 2.11-a). This also testify the fact that the subject had more difficulty in avoiding the obstacle in HSC due to slower vehicle speed (figure 2.9). Here the trajectory of maximum steering with initial speed at 0.7m/s is used to distinguish type II and type III collisions. The difference between type II and type III collisions is illustrated in figure 2.12.

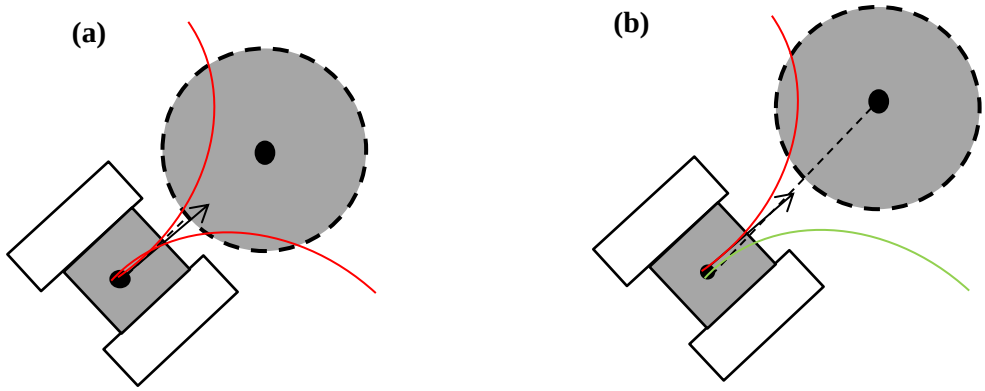

Figure 2.12. Illustration of the difference between type II and type III collisions. The colored curves represent the maximum steering the vehicle can perform. (a) type II collision depicts the moment when the subject responded to the obstacle, while maximum steering on both direction could not avoid the obstacle. (b) Type III collision indicates the moment when the subject responded to the obstacle, and at least the maximum steering could still avoid the obstacle.

In this way the total collisions shown in figure 2.6 was categorized into three types of collisions, displayed in figure 2.13.

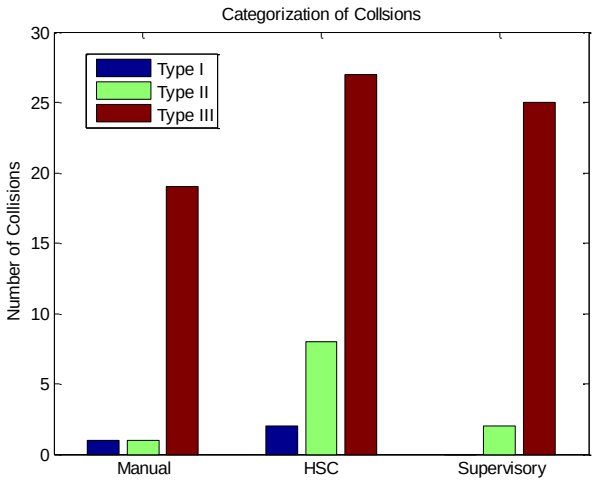

Figure 2.13. The number of three different types of collisions in each experiment condition.

Collision categorization in each experiment conditions is summarized in table 2.4. Type I collision occurred once in manual control and twice in HSC. Specifically, the 11th subject had type I collision within 6th obstacle in manual control, and the 6th subject ran into type I collision within the 4th and the 6th obstacle in HSC. This result collides with the speed inputs shown in figure 2.10-a, b. Aside from type I collision, HSC ran into appreciably more type II collisions than the other two conditions.

	Manual	HSC	Supervisory
Type I	1	2	0
Type II	1	8	2
Type III	19	27	25

Table 2.4. Summary of collision types in three experiment conditions.

Regardless of the reaction time in type I collision (which is infinite), the reaction time in type II and type III collisions are gathered in figure 2.14.

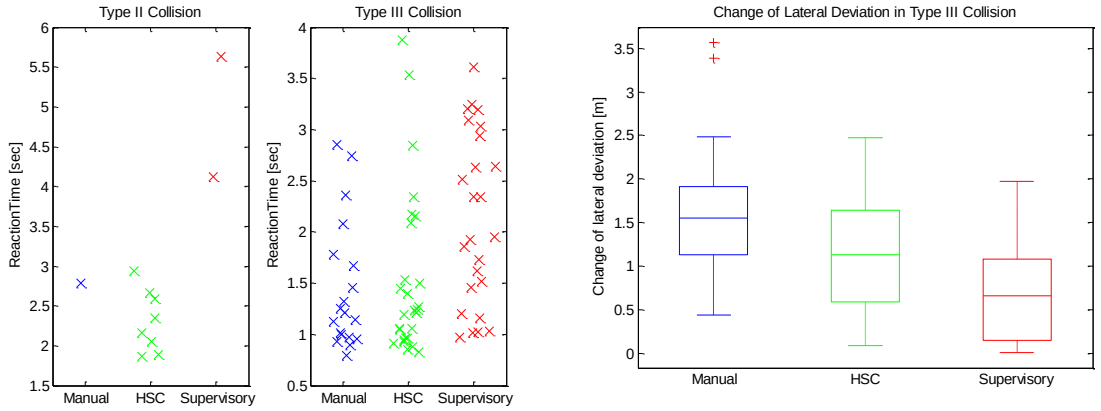

Figure 2.14. *Left:* Summary of subjects' reaction time in type II and type III collisions. *Right:* The vehicle's absolute change of lateral deviation in type III collision. It calculates from the moment the obstacle popped up on the screen to the moment the collision occurred.

We can tell from the figure that though type II collisions occurred, subjects still had a relatively low reaction time (<3 s) compared to supervisory control (>4 s). It was ambiguous to calculate the statistical significance for each type of collision, since each group has different number of data points, plus the fact that some subjects actually contributed more collisions than the others. But it's interesting to mention that when solely comparing the deviation changes for type III collisions (figure 2.14-right), we found a noticeable difference (not statistically) between conditions. The absolute change of lateral deviation, between the moments the obstacle popped up to the moment type III collision occurred, reflects the effort the subject made to avoid the obstacle. When neglecting the subject identity, Manual control had the highest change in lateral deviation (M =1.650, STD=0.818 [m]), HSC the second (M =1.136, STD=0.673 [m]) and supervisory control with least changes (M =0.692, STD=0.603 [m]) in average.

As a result, the mean reaction time, averaged by 12 obstacle avoidances, was calculated for each subject in three experiment conditions (type I collision excluded). The comparison is

shown in figure 2.15. One way repeated ANOVA showed a significant difference between conditions ($F(2,22) = 5.15$, $p<0.01$). Post hoc test found a significant difference supervisory control and manual control ($p<0.01$). Averagely speaking, supervisory control improves the reaction time towards obstacle by **22%** compared to manual control, though the collision ratio is not significantly increased. No statistically significant difference was found when compared HSC with either of the other two conditions.

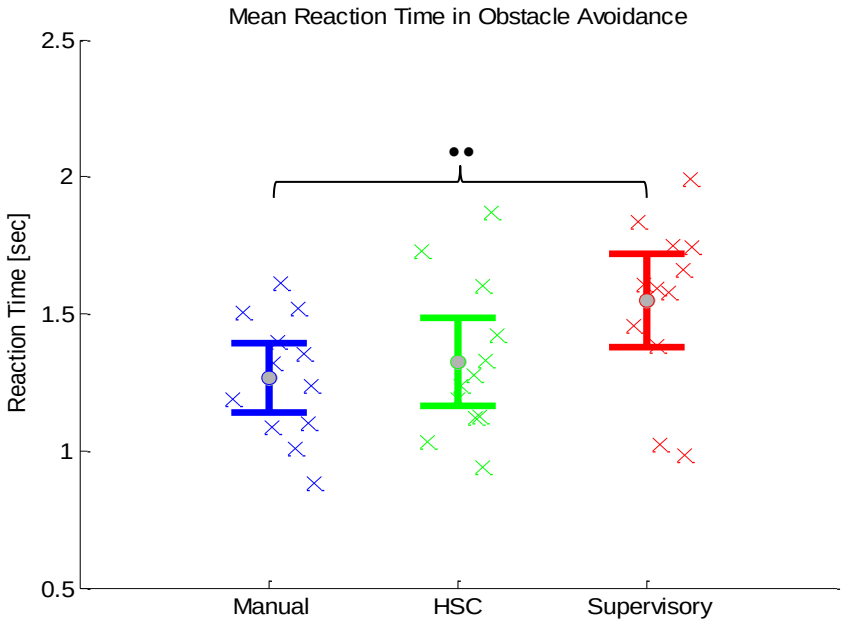

Figure 2.15. Comparison of each subject's mean reaction time towards the obstacle in three experiment conditions, averaged by 12 obstacle avoidances (type I collisions were excluded if any). '○' , '●' ,'● ●' means a significance with $p<0.1$, $p<0.05$ and $p<0.01$, respectively.

	Manual [s]	**HSC [s]**	**Supervisory [s]**
1	1.32	1.28	1.61
2	1.09	1.13	1.59
3	1.01	1.12	1.46
4	1.40	1.33	1.84
5	1.24	1.24	1.58
6	1.61	1.60	1.99
7	1.36	1.19	1.66
8	1.19	1.42	1.38
9	1.52	1.73	1.74
10	0.88	1.87	1.02
11	1.51	1.03	1.75
12	1.10	0.94	0.99
Mean	**1.27**	**1.32**	**1.55**
STD	**0.22**	**0.28**	**0.30**

Table 2.5. Summary of each subject's reaction time in three experiment condition, with group mean and stand deviation.

Therefore it can be concluded that subjects in supervisory control consumed more reaction time towards the obstacle than manual control. Even though subjects totally ran into more collisions in HSC, a noticeable number of times were biased by the experiment design, which resulted into type II collisions. At last, HSC did not significantly increase subjects' reaction time in obstacle avoidance.

2.2.4 Performance – Distance traversed in obstacle avoidance

The subject's steering maneuver may also be altered by the assisted conditions. Since the guidance always tried to guide the vehicle back to the centerline regardless of the obstacle, it could help the subject to recover to the optimal path if the subjects conformed to the guidance after the avoidance. In supervisory control, it is necessary for the vehicle to be back to the optimal path within the tolerance (±0.6m) in order to let the automation retrieve the control authority. This experiment setting could stimulate the subject to recover back to the optimal path quicker so as to return the steering task back to the automation. With collisions excluded, the mean distance traversed in obstacle avoidance of each subject is shown in figure 2.16 and table 2.6, where both group mean and 95% confidence interval are also displayed.

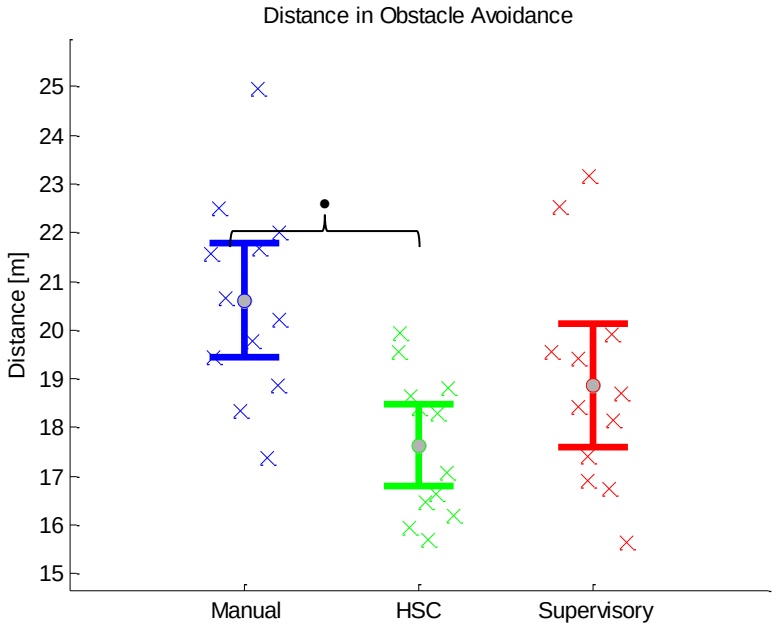

Figure 2.16. Each subject's mean traversed length with respect to the optimal path, averaged by all successful obstacle avoidances. '○' , '●' ,'● ●' means a significance with p<0.1, p<0.05 and p<0.01, respectively.

	Manual		HSC		Supervisory	
Distance in obstacle avoidance [m]	$\overline{X}$	S	$\overline{X}$	S	$\overline{X}$	S
	20.614	2.076	17.651	1.489	18.878	2.245

Test	$\Delta\overline{X}$ [m]	p value
Manual-HSC	**-2.963**	**0.02**
HSC-Supervisory	**+1.227**	**0.248**
Manual-Supervisory	**-1.736**	**0.120**

Table 2.6. summary of the mean distance traversed during obstacle avoidance by each subject. The upper table shows the group mean and standard deviation, the bottom table gives multiple comparisons between conditions.

The results showed that the distance traversed by vehicle within obstacle avoidance was significantly affected by the experiment conditions, $F(2,22)=7.39$, $p<0.01$. Post hoc tests revealed a significant difference between HSC and Manual control conditions ($p<0.05$), but not between other comparisons. Therefore in HSC, the subjects can return to the optimal path with less length with respect to the optimal path. Subject's steering maneuver was significantly adapted in HSC during the recovery period after the obstacle avoidance.

2.2.5 Performance – Lateral deviation in slip recovery

The reliability of the subject's system awareness is tested by introducing a slip event at the end of the each trial for every subject. That is to say, the slip event was presented to each subject in all three conditions. A collection of all subjects' steering performance during slip recovery is shown in figure 2.17, where HSC had a bit less amplitude from eyeballing.

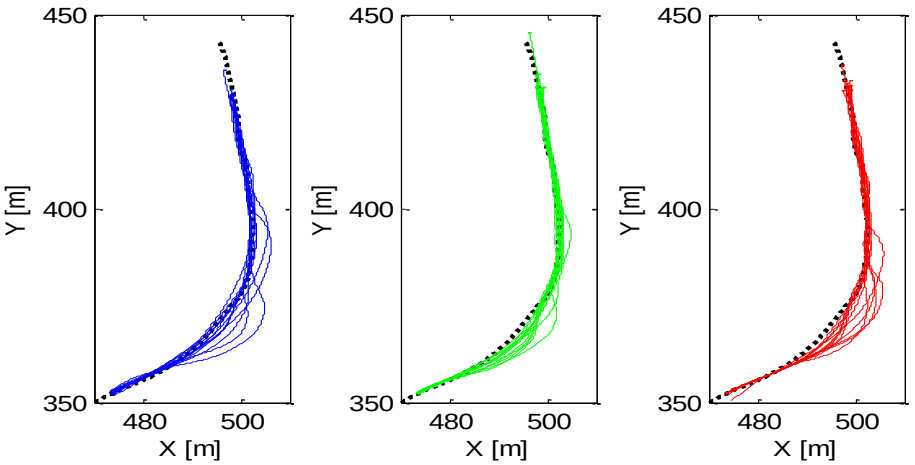

Figure 2.17. Performance of lane keeping in slip recovery module. Blue: manual control, green: HSC, red: supervisory control. The black dashed curve represents the prescribed optimal path.

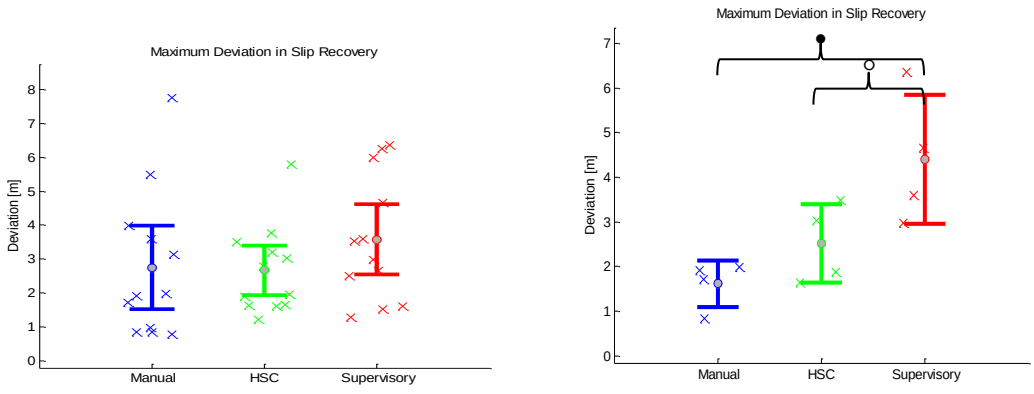

(a) (b)

Figure 2.18. Maximum absolute lateral deviation from each subject's performance during slip recovery. (a) A collection of subjects' maximum lateral error in all three conditions. (b) The maximum lateral error from each subject's steering when they encountered the slip for the first time. '○' , '●' ,'● ●' means a significance with $p<0.1$, $p<0.05$ and $p<0.01$, respectively.

The optimal path requires a left turn at the place where the slip was triggered. All subjects eventually succeeded in returning to the optimal path. However their maximal lateral error was noticeably different. The maximal lateral deviation is the metric that can be immediately influenced by the subject's awareness of the slip event. The longer the subject took to respond to the slip event, the larger of the maximum lateral error. Here the absolute value of maximum lateral error was used to avoid negative values, in case some subjects might restore the lane keeping from the slip event on the left side of the path. However since each subject was tested with a slip event three times, once per experimental conditions, they could have expectation on the slip event in the latter two trials. The subject could prepare for the slip event if they expected it, which would result into much less deviation before the vehicle converges to the optimal path again. As expected, if each subject's performance of the slip event in all three conditions were taken into account, no effects on the experimental conditions could be found (figure 2.18-a). Thus in order to minimize this expectation effect, each subject's performance at the first time the slip was triggered was separately selected for comparison (figure 2.18-b). Therefore there were only four subjects for each group. Nevertheless, one way independent ANOVA indicated a significant difference between conditions in the maximum absolute lateral error, $F(2,9)=7.429$, $p<0.05$). Post hoc test revealed that supervisory control induced significantly higher maximum lateral error than manual control ($p<0.05$). HSC had a closed-to-significance difference to supervisory control ($p=0.089$). No statistically significant difference was found between HSC and manual control. Larger subject volume is needed to determine whether the operator will have a less lateral deviation in HSC than in supervisory control, which is likely to happen from the results in this experiment.

2.2.6 Performance – Accuracy in secondary task

Besides the actual need of secondary task in deep sea operation, the subject's accuracy in responding to the secondary task is an indirect approach to evaluate his/her mental workload in performing the primary steering task. Figure 2.19 shows each subject's accuracy in different task modules, and a summary of accuracies in secondary task is listed in table 2.7 and 2.8.

Subject identifier: 

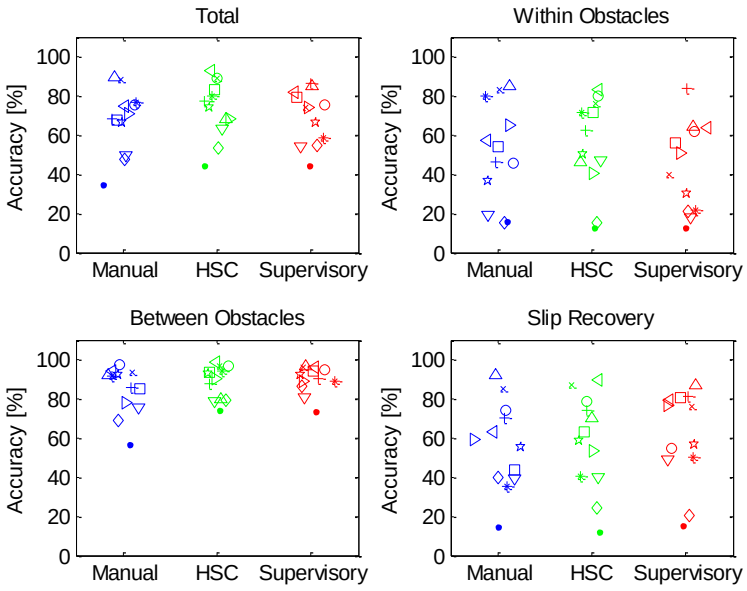

Figure 2.19. Overview of accuracy distributions of subjects' performance in answering secondary task (correlation between primary and secondary task.). *Top-left*: in total. *Top-right*: within obstacles. *Bottom-left*: between obstacles. *Bottom-right*: slip recovery.

	Manual				**HSC**				**Supervisory**			
	Total	Within	Between	Slip	Total	Within	Between	Slip	Total	Within	Between	Slip
S1	68.5	46.1	85.7	70.0	77.4	62.7	87.7	73.9	86.3	83.8	90.1	81.3
S2	75.7	45.5	97.2	74.4	88.8	80.2	96.9	78.6	75.2	61.5	94.9	54.5
S3	76.8	79.8	91.2	35.2	80.1	71.7	94.4	40.5	58.3	22.0	89.1	50.0
S4	34.7	16.2	56.6	14.3	44.5	12.5	74.4	12.2	44.6	12.5	73.4	15.2
S5	88.1	82.9	93.4	85.3	88.9	76.3	96.5	86.8	73.8	39.8	95.9	76.2
S6	67.4	54.3	85.4	43.5	82.9	71.4	93.8	63.0	79.0	55.7	94.4	80.6
S7	47.7	15.2	68.8	39.5	53.3	15.1	79.2	24.4	54.9	21.3	86.5	20.4
S8	89.8	84.8	92.2	92.3	68.0	46.5	80.1	70.5	85.1	64.3	96.6	87.2
S9	49.3	19.0	75.6	38.9	63.3	47.0	78.7	40.0	53.9	17.8	80.6	48.6
S10	70.7	65.3	77.8	59.4	68.4	40.4	90.4	53.7	73.8	50.6	88.7	76.5
S11	74.9	57.1	94.2	63.3	92.9	83.2	98.9	89.8	81.8	63.9	96.4	78.9
S12	66.4	36.5	92.2	55.3	74.4	50.0	92.9	58.5	66.5	30.1	91.9	56.8

Table 2.7. Each subject's response accuracy in the secondary task, distinguished by experiment conditions and task modules, unit [%]. Yellow highlighted identity numbers represent subjects whose accuracies in manual control between obstacles were less than 90%.

	Manual		HSC		Supervisory	
Accuracy of secondary task [%]	$\overline{X}$	S	$\overline{X}$	S	$\overline{X}$	S
	84.17	12.00	88.67	8.53	89.92	7.05

Test	$\Delta\overline{X}$ [%]	p value
Manual-HSC	**+4.5**	**0.16**
HSC-Supervisory	**+1.3**	**1**
Manual-Supervisory	**+5.8**	**p<0.05**

Table 2.8. Summary of subjects' accuracies in secondary task between obstacles. *Top*: group means and standard deviation, *Bottom*: multiple comparisons between conditions and their significance.

The results showed that the accuracy of the secondary task between obstacles was significantly affected by the experiment conditions, $F(2,22)=5.046$, $p<0.05$, but not for within obstacles and slip recovery. Post hoc tests revealed a significant difference between supervisory and manual control between obstacles ($p<0.05$), albeit between other comparisons. However, taking the 4th subject as an example, it seems HSC and supervisory control can improve these subjects who responded badly to the secondary task in manual control. Moreover for the subjects who already had satisfactory accuracies in manual control, the treatment did not decrease the performance according to statistics. To take a step further, Here we selected the subjects whose responses were less satisfactory in manual control (specifically, accuracy <90%), and did another statistical analysis only with these subjects' data. In fact, subjects with identity number *1,4,6,7,9,10,* had less accuracies than 90% in manual control (highlighted subjects in table 2.7). In this case, both supervisory control and HSC had a significant higher accuracy than manual control (table 2.8). Averagely HSC improved the accuracy by 9.1% while supervisory control brought 10.6% improvement. Therefore it is possible that these two assist conditions could bring more benefits to subjects who need improvements in secondary tasks, while others could maintain their accuracies under assist conditions.

	Manual		HSC		Supervisory	
Accuracy of secondary task [%]	$\bar{x}$	s	$\bar{x}$	s	$\bar{x}$	s
	74.98	11.02	84.03	7.66	85.60	7.52

Test	$\Delta\bar{x}$ [%]	p value
Manual-HSC	**+9.1**	**p<0.05**
HSC-Supervisory	**+1.5**	**0.847**
Manual-Supervisory	**+10.6**	**p<0.05**

Table 2.9. Further comparison with specially selected subjects, who had less accuracy in manual control between obstacles. The table is arranged in the same manner as table 2.8.

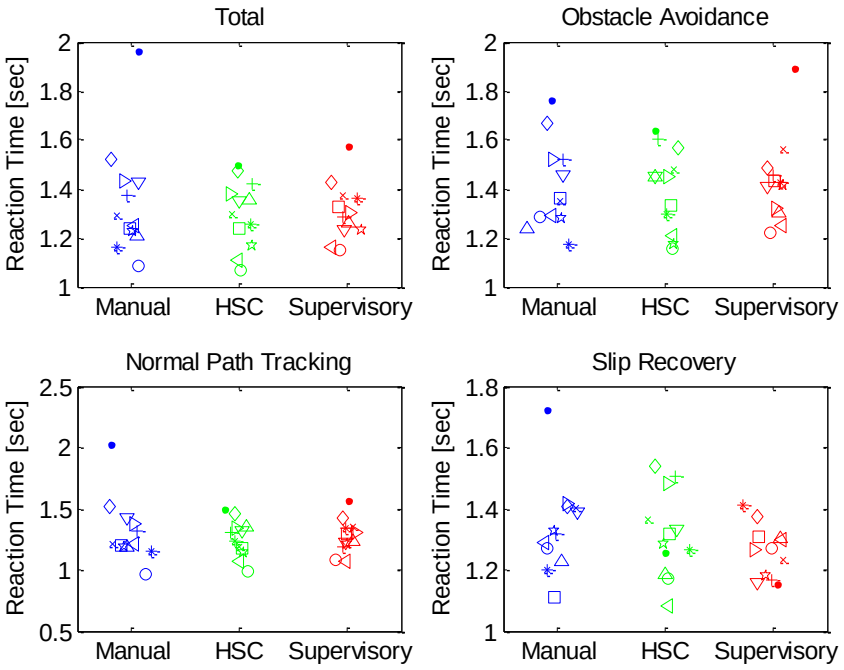

Figure 2.20. Overview of each subject's reaction time towards the secondary task, categorized by task modules and experiment conditions.

Figure 2.20 showed each subject's mean reaction time in different task modules. However no significant difference was found in any of the comparisons. Actually the reduction of reaction time introduced by haptic shared control to the secondary task in a similar study of car driving was also not substantial (Griffiths & Gillespie, 2005). It was difficult to regulate all subjects' vigilance and strength in responding to the secondary task the same level. Some subjects had a high and constant level of accuracy with low reaction time across three conditions (e.g. 2nd subject, marked by '○' in figure 2.19, 2.20), while some subjects' performances were much more influenced by the assist conditions (e.g. 4th subject, marked by '•' in figure 2.19, 2.20). Thus their performances of the secondary task varied significantly, and severely affected by individual differences. However it is noticeable that in most of the cases, HSC and supervisory control can improve subjects' response accuracies of secondary task during between obstacles modules, and maintain the performances from those who already have relatively higher accuracies in manual control.

2.2.7 Additional Metrics

Mean Vehicle Speed

Figure 2.21 illustrates the simulated mean vehicle's heading speed in different task modules. Although vehicle speeds in manual and supervisory control had much higher variation between subjects than HSC, it is still obvious that the subject's preference vehicle speed under manual control is quite closed to the vehicle speed in supervisory control. Subjects tended to agree with the heading speed dominated by the guidance and not to accelerate in HSC. This

obedience resulted into a significantly slower vehicle speed in HSC both between obstacles and within obstacles, compared to the other two conditions (table 2.10). However this difference vanished in slip recovery.

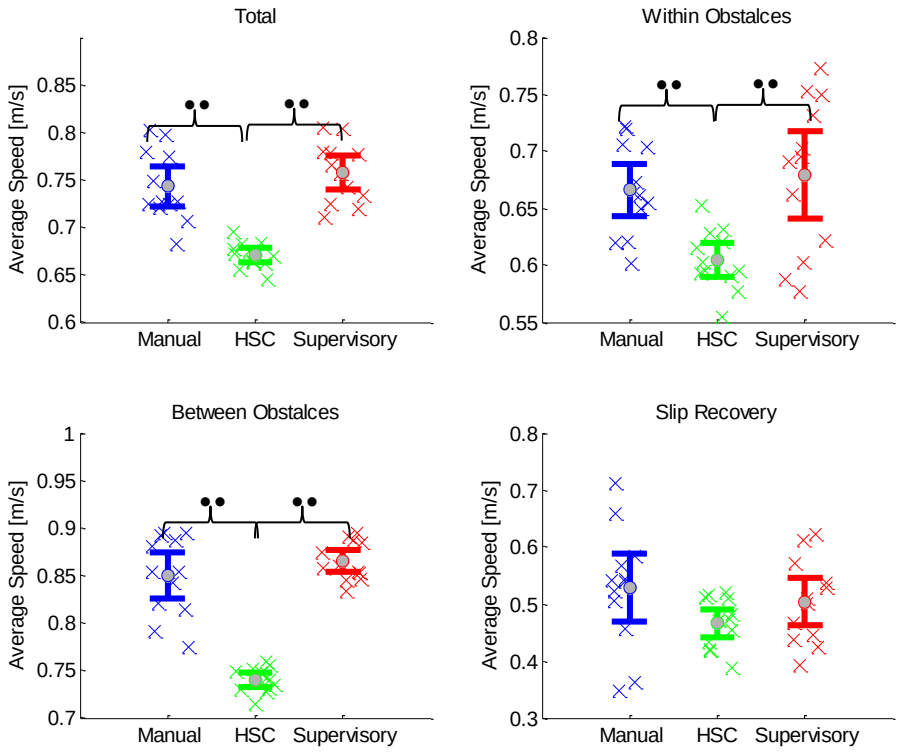

Figure 2.21. Average Speed during different task modules. '●' ,'● ●' means a significance with p<0.1, p<0.05 and p<0.01, respectively.

	Manual		HSC		Supervisory	
Average speed [m/s]	$\bar{X}$	S	$\bar{X}$	S	$\bar{X}$	S
Total	0.743	0.038	0.670	0.014	0.758	0.032
Within Obstacle	0.666	0.040	0.605	0.027	0.679	0.068
Between Obstacle	0.850	0.042	0.740	0.013	0.865	0.021
Slip recovery	0.528	0.105	0.467	0.044	0.504	0.074

Test pairs	Total		Within Obstacle		Between Obstacle		Slip Recovery	
	$\Delta\bar{X}$ [m/s]	p value	$\Delta\bar{X}$ [m/s]	p value	$\Delta\bar{X}$ [m/s]	p value	$\Delta\bar{X}$ [m/s]	p value
Manual-HSC	-0.073	p<0.01	-0.061	p<0.01	-0.110	p<0.01	-0.061	0.393
HSC-Supervisory	+0.088	p<0.01	+0.074	p<0.01	+0.125	p<0.01	+0.038	0.429
Manual-Supervisory	+0.015	0.832	+0.013	-	+0.015	-	-0.024	-

Table 2.10. Summary of vehicle's mean heading speed, categorized by experiment conditions and task modules. *Top*: group means and standard deviation. *Bottom*: multiple comparisons and their significances.

Total Time Spent

As the subject had been informed from the task description that the whole steering task was time-optimal before the actual experiment, the times spent to complete the whole path in each experiment condition are shown in figure 2.22, with group means and 95% of confidence interval. One way repeated ANOVA discovered a significant difference between conditions, ($F(2,22) = 10.19$, $p<0.01$). More specific, subjects spent more time in HSC than manual control ($p<0.01$) and supervisory control ($p=0.033$), according to the post hoc tests. This result collides with the aforementioned comparison of vehicle speed. Since the simulated vehicle ran much slower in HSC than the other two conditions, it required more time to complete the whole task. Moreover, regardless of the collision types, HSC induced more collisions than the other two conditions (figure 2.6), which brought longer time penalty in the actual experiment.

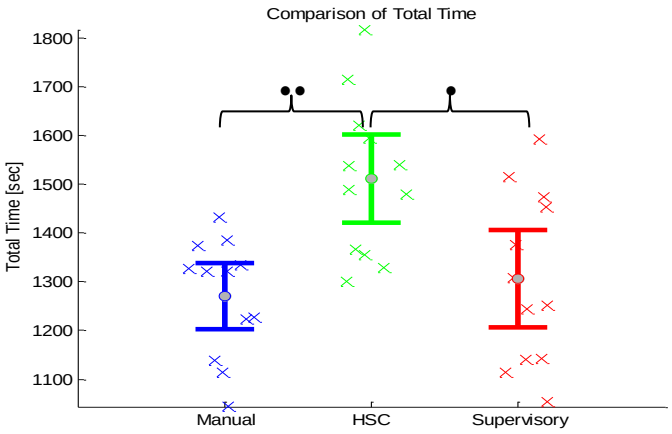

Figure 2.22. Total time spent to complete the whole optimal path in each experiment condition. '○', '●','● ●' means a significance with $p<0.1$, $p<0.05$ and $p<0.01$, respectively.

2.2.8 Control Effort – STD of the angle difference

The subject controlled the simulated vehicle speed through these two rotary handles. Thus their control efforts directly influenced the variation of the turning angles of these two 'joysticks'. The higher of the variation, the more steering activities the subject performed during the experiment. Since there were two handles, the standard deviation of each handle's turning angle was calculated separately (figure 2.23-a,b). Before calculating, the raw data of the turning angles collected from the real time computer had been filtered by a non-causal low-pass filter at a cut-off frequency of 10 Hz. One way repeated ANOVA found significant difference between conditions between obstacle and in slip recovery, but not within obstacles. The results from multiple comparisons are shown in table 2.11. The subject had significantly less STD in turning angles than the other two conditions between obstacles ($p<0.01$). Conversely, in slip recovery, at least on the left handle, the subject had significantly more variations of turning angle in supervisory control than the other two ($p<0.01$). In addition, as the simulated vehicle heading angle is adjusted by the relative absolute difference between the

speed of left and right track, the difference between the left and right handles directly exhibits the subject's steering activity. Hence the standard deviation of the difference between left and right turning angles was also calculated for comparison (figure 2.23-c).

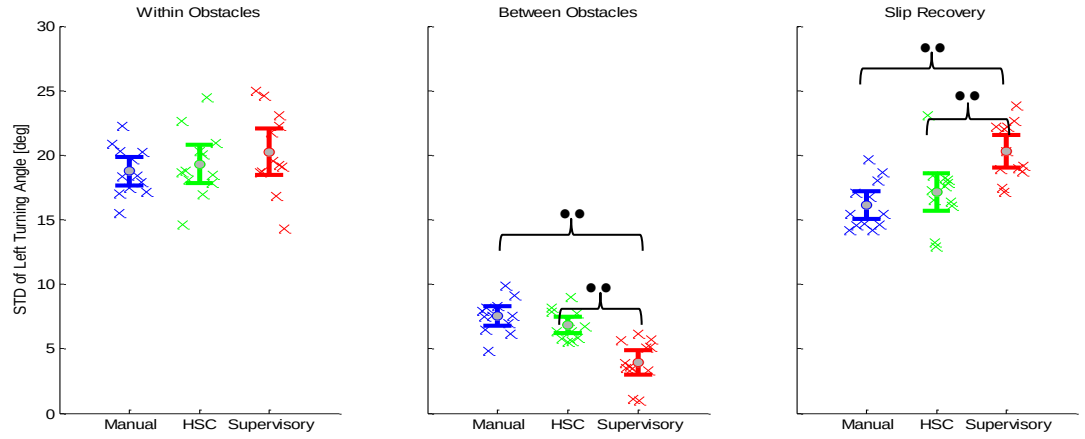

(a)

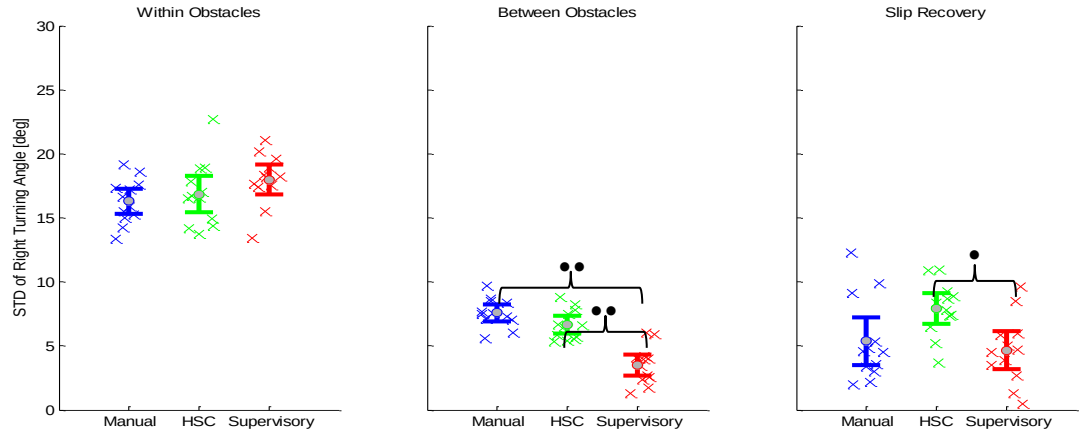

(b)

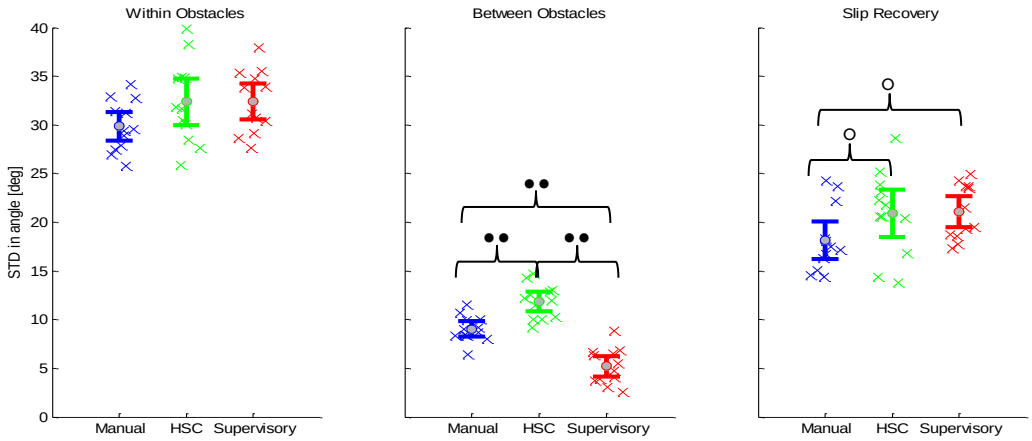

(c)

Figure 2.23. Standard deviation of the controlled turning angles by each subject, categorized by task modules and experiment conditions. The group means and 95% of confidence interval are also shown. In each plot, the left subplot depicts the situation within obstacles, the middle subplot for between obstacles, and slip recovery in the right subplot. (a) STD of the turning angle on the left handle. (b) STD of the turning angle on the right handle. (c) STD of the difference between left and right handle. '○' , '●' ,'● ●' means a significance with p<0.1, p<0.05 and p<0.01, respectively.

	Manual		HSC		Supervisory	
STD [m/s]	$\overline{x}$	s	$\overline{x}$	s	$\overline{x}$	s
Within Obstacle(L/R)	18.76/16.31	1.93/1.76	19.33/16.86	2.60/2.53	20.25/17.99	3.18/2.04
Between Obstacle(L/R)	7.53/7.58	1.34/1.13	6.84/6.66	1.14/1.19	3.96/3.52	1.69/1.49
Slip recovery(L/R)	16.12/5.39	1.89/3.27	17.14/7.91	2.60/2.12	20.30/4.66	2.20/2.65

Test pairs	Within Obstacle		Between Obstacle		Slip Recovery	
	$\Delta\overline{x}$ [m/s]	p value	$\Delta\overline{x}$ [m/s]	p value	$\Delta\overline{x}$ [m/s]	p value
Manual-HSC(L)	0.552	-	-.689	0.837	1.026	0.309
Manual-HSC(R)	0.552	-	-.918	0.286	2.520	0.128
HSC-Supervisory(L)	0.922	0.983	-2.885	p<0.01	-3.162	p<0.01
HSC-Supervisory(R)	1.132	0.545	-3.145	p<0.01	-3.244	p<0.05
Manual-Supervisory(L)	1.482	0.439	-3.574	p<0.01	-4.188	p<0.01
Manual-Supervisory(R)	1.684	0.096	-4.063	p<0.01	-0.724	-

Table 2.11. Summary of the STD of turning angles on left and right handles. Top table shows the group mean and standard deviation in each task module. Bottom table gives the results from multiple comparisons.

For the difference in turning angles, no significant difference between conditions was found within obstacles (table 2.12). However one-way repeated ANOVA reported a significant main effect in two assist conditions between obstacles ($F(2,22=52.07)$, $p<0.01$). Post-hoc comparison of the three groups indicated strong difference between all three conditions. Most obviously Supervisory control had less STD of the angle difference between obstacles (M = 5.23, Std = 1.86) than both manual control and HSC ($p<0.01$ for both cases). HSC further induced a bit more variation (M = 11.88, Std = 1.76, $p<0.01$) than manual control (M = 9.05, Std = 1.37). Moreover during slip recovery, a statistical difference was also found between conditions ($F(2,22) =4.70$, $p=0.02$). But according to post-hoc multiple comparisons, HSC (M = 20.95, Std = 4.31) and supervisory (M = 21.07, Std = 2.82) control both resulted into a slightly higher variation than manual control (M = 18.19, Std = 3.41), but not statistically significant, neither the difference between HSC and supervisory.

	Manual		HSC		Supervisory	
STD [deg]	$\overline{x}$	s	$\overline{x}$	s	$\overline{x}$	s
Within Obstacle	29.87	2.64	32.38	4.25	32.41	3.23
Between Obstacle	9.05	1.37	11.88	1.76	5.23	1.86
Slip recovery	18.19	3.41	20.95	4.31	21.07	2.82

Test pairs	Within Obstacle		Between Obstacle		Slip Recovery	
	$\Delta\overline{x}$ [m/s]	p value	$\Delta\overline{x}$ [m/s]	p value	$\Delta\overline{x}$ [m/s]	p value
Manual-HSC	2.52	0.125	2.83	p<0.01	2.76	0.091
HSC-Supervisory	0.03	-	-6.65	p<0.01	0.13	-
Manual-Supervisory	2.55	0.074	-3.82	p<0.01	2.88	0.074

Table 2.12. Summary of the STD of the difference between turning angles on left and right handles. Top table shows the group mean and standard deviation in each task module. Bottom table gives the results from multiple comparisons.

2.2.9 Control Effort – Steering Torque

Since subjects were asked to grab the handles throughout the experiment, they could conform to the guidance in HSC. Therefore the subjects might still have a high variation on the turning angles of the handles due to the guidance force, but did not concentrate on the steering instead. Thus the torque inserted onto the handle is a better metric to measure subjects' physical workload. Figure 2.24 depicts the standard deviation inserted torques on both handles in three experiment conditions, categorized by task module. Handle was taken as a factor and a two-way repeated ANOVA was calculated (table 2.13). The ANOVA revealed that within obstacles, assist condition had a strong effect in within obstacle regardless of which handle it was ($F(2,22) = 89.73$, $p<0.01$). Post-hoc gave significant difference between all three conditions ($p<0.01$). The assist conditions also brought a significant difference between obstacles ($F(2,22) = 6.60$, $p<0.01$). Specifically, HSC had a difference compared manual control ($p=0.04$), supervisory control also caused significantly higher torque variation than manual control ($p<0.01$). The main effect by assist condition continued in slip recovery ($F(2,22)=152.09$, $p<0.01$), where supervisory control was significantly higher than manual control ($p<0.01$), and HSC was even higher than both manual and supervisory control ($p<0.01$). Handle, as a factor, only showed a significant effect within obstacles ($F(1,11)=10.55$, $p<0.01$) and slip recovery ($F(1,11)=30.80$, $p<0.01$), along with a modest interaction with assist conditions within obstacle ($F(1.3,14.4)=5.70$, $p=0.024$) and an interaction in slip recovery ($F(2,22)=12.84$, $p<0.01$). Within subjects contrast indicated that the interaction was only significant when manual control was compared to HSC within obstacles ($F(1,11) = 20.25$, $p<0.01$), but extremely strong present in all three conditions during slip recovery($p<0.01$). The effect from handle is reasonable since the slip event occurred during a left turn, so that subjects needed to steer the left track much more often than the right track.

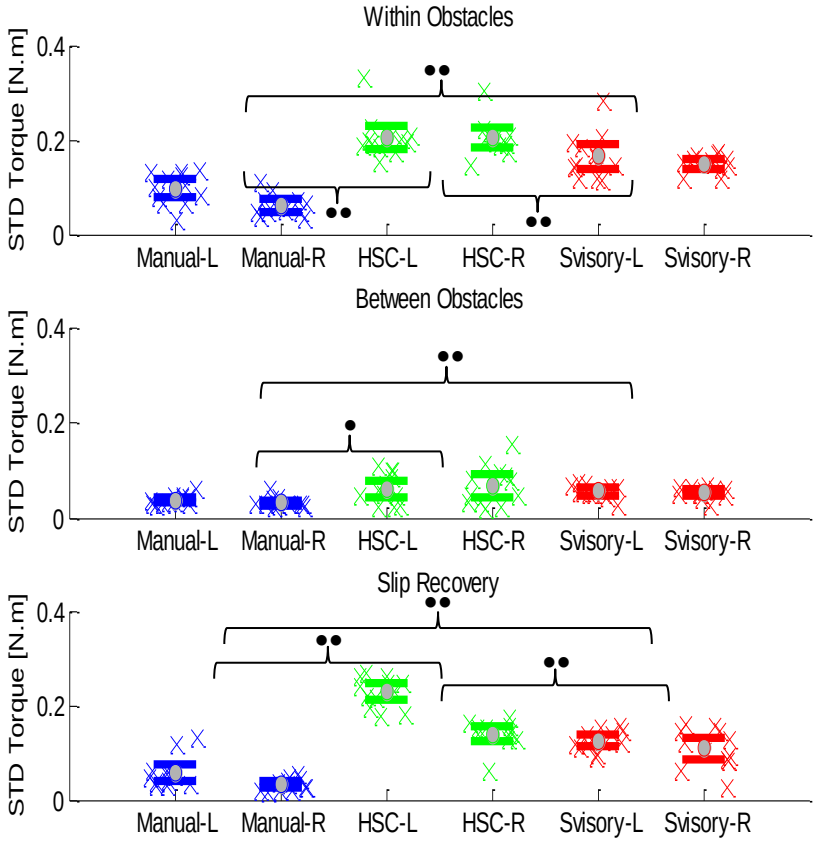

Figure 2.24. STD of each subject generated torque, categorized by task module, experiment conditions and left-or-right hand. *Top*: within obstacles. *Middle*: between obstacles. *Bottom*: slip recovery. Significance on the main effect is marked regardless of which handle it is. '○' , '●' ,'● ●' means a significance with p<0.1, p<0.05 and p<0.01, respectively.

	Manual		HSC		Supervisory	
STD [N.m]	$\bar{x}$	s	$\bar{x}$	s	$\bar{x}$	s
Within Obstacle	0.097/0.061	0.034/0.023	0.205/0.206	0.044/0.038	0.165/0.150	0.048/0.019
Between Obstacle	0.038/0.032	0.011/0.011	0.062/0.068	0.031/0.042	0.056/0.054	0.013/0.012
Slip recovery	0.058/0.032	0.033/0.013	0.228/0.140	0.031/0.029	0.126/0.109	0.021/0.042

Test pairs	Within Obstacle		Between Obstacle		Slip Recovery	
	$\Delta\bar{x}$ [N.m]	p value	$\Delta\bar{x}$ [N.m]	p value	$\Delta\bar{x}$ [N.m]	p value
Manual-HSC	0.126	p<0.01	0.030	0.04	0.139	p<0.01
HSC-Supervisory	-0.048	p<0.01	-0.010	0.67	-0.067	p<0.01
Manual-Supervisory	0.078	p<0.01	0.020	p<0.01	0.073	p<0.01

Table 2.13. Summary of the STD of the difference between turning angles on left and right handles. Top table shows the group mean and standard deviation in each task module. Bottom table gives the results from multiple comparisons.

2.2.10 Control Effort – Reversal rate

The reversal rate depicts the frequency of reversal of the handle, steered by the subject. The turning angles of these two handles were filtered by a non-causal low pass filter with cut-off frequency at 10 Hz, while only turning angle differences more than 5 °are taken into account (figure 2.25).

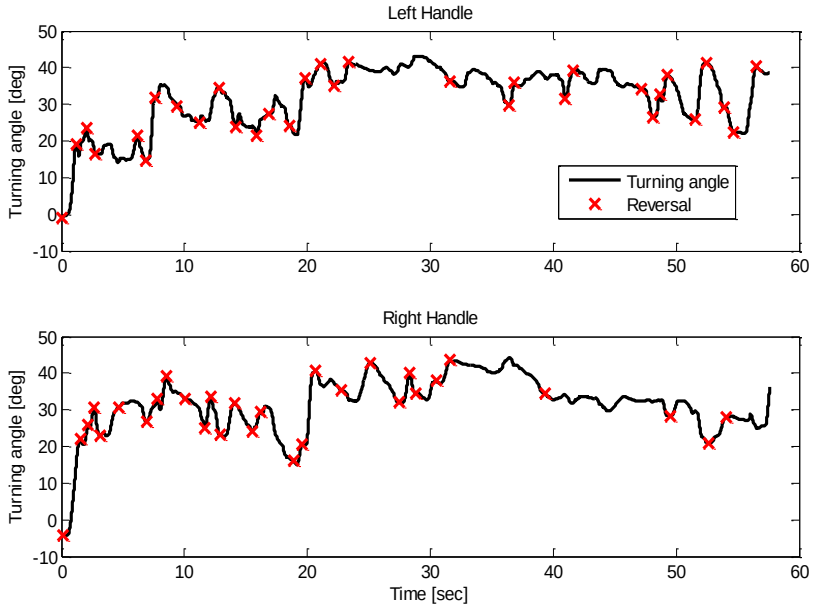

Figure 2.25. An example on how the reversal was calculated. This figure shows the turning angles of these two handles before the first obstacle, steered by the 1st subject. *Top*: Left handle. *Bottom*: Right handle. Black curves represent the filtered turning angles and these red-cross markers stand for the moment when the reversal accounted.

Figure 2.26 shows the reversal rate on both handles, and table 2.14 summarizes the group statistics.

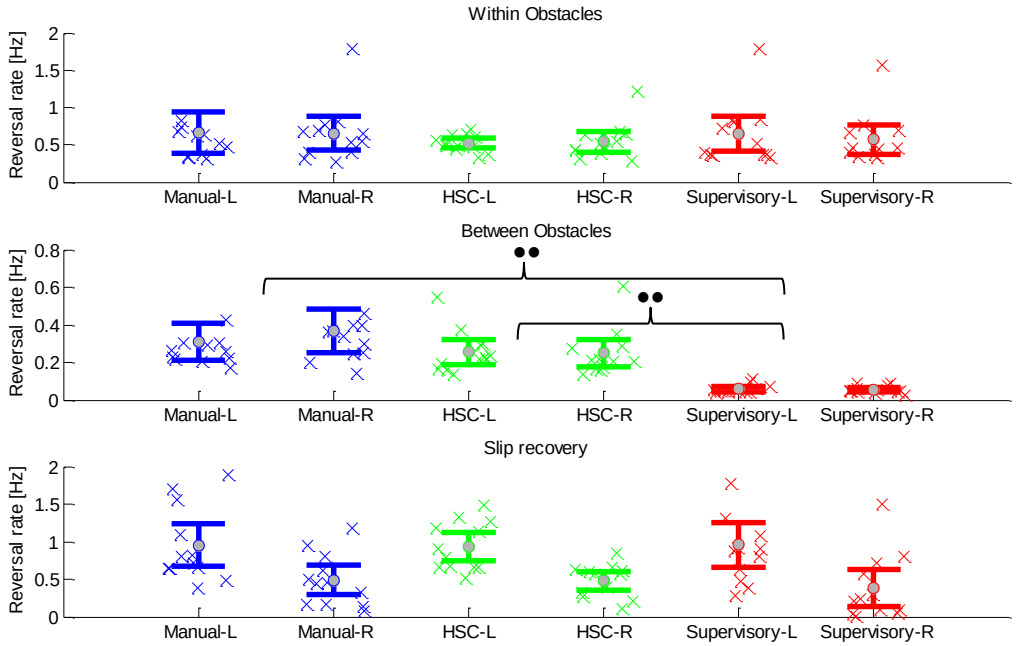

Figure 2.26. Each subject's reversal rate per unit of time on both handles, categorized by task module, experiment conditions and left-or-right hand. The group means are shown with 95% of confidence interval. *Top*: Within obstacles. *Middle*: Between obstacles. *Bottom*: Slip recovery. Significance on the main effect is marked regardless of which handle it is. '○' , '●' ,'● ●' means a significance with $p<0.1$, $p<0.05$ and $p<0.01$, respectively.

	Manual		HSC		Supervisory	
STD [Hz]	$\bar{x}$	s	$\bar{x}$	s	$\bar{x}$	s
Within Obstacle (L/R)	0.667/0.652	0.497/0.397	0.524/0.544	0.112/0.249	0.644/0.575	0.413/0.346
Between Obstacle(L/R)	0.310/0.367	0.173/0.202	0.255/0.250	0.113/0.128	0.060/0.056	0.024/0.022
Slip recovery(L/R)	0.950/0.486	0.499/0.346	0.937/0.484	0.326/0.218	0.957/0.384	0.535/0.443

Test pairs	Within Obstacle		Between Obstacle		Slip Recovery	
	$\Delta\bar{x}$ [Hz]	p value	$\Delta\bar{x}$ [Hz]	p value	$\Delta\bar{x}$ [Hz]	p value
Manual-HSC	-0.125	0.514	-0.086	0.526	-0.008	-
HSC-Supervisory	0.076	0.721	-0.195	p<0.01	-0.040	-
Manual-Supervisory	-0.050	0.826	-0.281	P<0.01	-0.048	-

Table 2.14. Summary of the reversal rate on left and right handles. Top table shows the group mean and standard deviation in each task module. Bottom table gives the results from multiple comparisons.

Similarly the left-or-right hand was taken as an additional factor and two ways repeated ANOVA was calculated. A significant difference was only found between conditions for the reversal rates between obstacles ($F(2,22)=15.16$, $p<0.01$). Post hoc test reported a significant difference between HSC and supervisory control ($p<0.01$), and between manual and supervisory control ($p<0.01$). No noticeable difference was found for the reversal rates within obstacles and during slip recovery.

To sum up the data analysis in control effort, regardless of the metric we chose, the difference between supervisory control and manual control was always evident when the simulated vehicle was between obstacles. Subjects conducted less steering activities, though with slightly more torques, on the master device in supervisory control than manual control when the lane keeping was the only task to perform. However supervisory control did cause more torques than manual control when the vehicle ran into unexpected events (i.e. obstacle, slip). This indicates that subjects felt more stressed by the unexpected events in supervisory control, and possibly more significant co-contraction was generated when the subject intervened in the control loop. What's more, HSC induced more physical effort to the subject than the other two conditions, especially within obstacles, and in slip recovery. The subject needed to confront with the faulty guidance during these periods, which directly resulted into much higher torques.

2.3 Subjective Evaluation

Besides the objective metrics to evaluate the subjects' performance and control efforts, a self-reported workload was obtained using the standard NASA TLX questionnaires in paper copies [1]. Each subject was asked to rate their subjective feelings in six different aspects: mental demand, physical demand, temporal demand, performance, effort and frustration. However a big limitation of the results from the NASA TLX questionnaire is that subject's subjective feeling cannot be distinguished between normal operation between obstacles and within obstacles. These results function more like a reflection on the subjects' general grading of the experimental conditions for the whole experiment contents. Actual NASA TLX Workload was subdivided into six measures in figure 2.27.

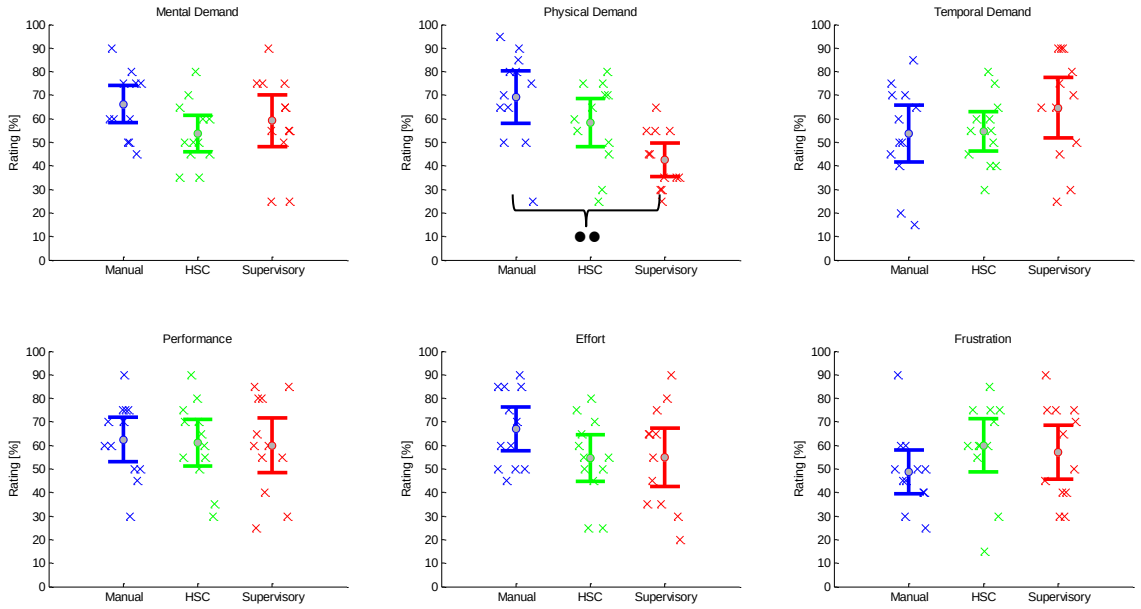

Figure 2.27. Self reported workload for the total experiment content, categorized by six measures (Blue: Manual control, Green: HSC, Red: Supervisory control). '○' , '●' ,'● ●' means a significance with $p<0.1$, $p<0.05$ and $p<0.01$, respectively.

One way repeated ANOVA only reported a significant difference between experimental conditions for physical demand, ($F(2,22)=5.95$, $p<0.01$). Sidak post hoc analysis revealed that the subjects felt more physical demand subjectively in manual control than in supervisory control ($p<0.01$), which collides with the conclusion from objective measurements. Aside from physical demand, subjects' rating in other five measures found no statistical difference, and some even had noticeably opposite rating preference (table 2.15). Taking the mental demand as an example, while majority rated HSC with less mental load than manual control, the 10th subject showed an opposite rating propensity. It is worthwhile to notice that the 10th subject also ran into the most number of collisions in HSC among all three conditions (figure 2.6). Similarly, for frustration, while the other subjects felt more frustrated in HSC, the 1st and 2nd subject exhibited appreciably less frustration with HSC than the other two conditions.

[1] The NASA TXL form can be obtained from:
http://humansystems.arc.nasa.gov/groups/tlx/downloads/TLXScale.pdf

Besides the individual difference, the main reason that causes these opposite rating preference was subject's self-weighting of their feelings between different task modules. Some emphasized their experience on the benefits brought from HSC and supervisory control during normal operation between obstacles, while the others' assessment of the assist conditions were more influenced by those side-effects from assist conditions during unexpected conditions.

	Mental Demand [%]			**Physical Demand [%]**			**Temporal Demand [%]**			**Effort [%]**			**Performance [%]**			**Frustration [%]**		
Subject	M	H	S	M	H	S	M	H	S	M	H	S	M	H	S	M	H	S
1	60	35	75	50	30	55	20	45	75	60	80	55	50	25	65	60	15	75
2	75	50	65	90	25	55	70	30	80	75	90	60	85	65	80	45	30	70
3	50	35	25	75	70	35	60	55	65	50	65	30	70	80	55	50	60	40
4	75	50	55	80	45	55	50	65	90	90	30	40	45	25	90	30	75	90
5	75	50	65	70	50	45	75	60	65	75	60	25	85	50	65	50	60	75
6	60	45	75	80	55	65	65	40	70	50	35	55	60	50	35	40	75	65
7	50	65	75	65	80	45	45	50	90	70	55	65	60	55	75	25	60	75
8	80	60	50	85	65	35	85	75	50	45	70	85	85	70	65	45	60	30
9	75	60	90	95	60	25	70	80	90	60	75	85	90	60	20	60	85	40
10	45	80	55	65	75	30	40	55	30	70	50	80	50	75	30	40	70	30
11	90	70	55	50	70	35	15	40	25	30	55	60	75	45	35	90	55	50
12	60	45	25	25	75	30	50	60	45	75	70	80	50	55	45	50	75	45

Table 2.15. Overview of all subject's subjective answers in task workload. Abbreviation: M: Manual control, H: Haptic shared control, S: supervisory control.

Appendix III -Modelling Specification

Since the current researches mainly focuses on tracked vehicles as the most popular option to implement deep sea mining, we hereby also choose to construct the dynamics of a tracked vehicle. The mathematical model used in this study to predict spatial motion of subsea crawler is developed from former research of terrestrial tracked vehicle in planar motion on level pavement and in non-level terrains (Kitano & Jyozaki, 1976; Murakami et al., 1992). As the performance of a tracked vehicle is principally determined by the normal and shear stress distribution at the track-terrain interface, the essential issue in mathematical modelling of motion of subsea tracked crawler consists of three parts: to discover the relationship between the track-soil interaction, design parameters of the miner and the control algorithm (Le, 1999).

3.1 Track-Soil Interaction and Vehicle Dynamics

The Tracked vehicle is assumed to be a rigid body moving in Euclidian 3-space, $\mathbf{R}^3$. Two rectilinear coordinates are introduced: a global reference coordinate $\mathbf{E}$=(X,Y,Z) and a body fixed local coordinate $\mathbf{e}$=(x,y,z), which usually locates at the mass centre of the vehicle. By implementing Tait-Bryan angles to represent the rotation sequence of the body, the transformation between body-fixed coordinate and global coordinate system is given as follow:

$$\{\mathbf{E}\} = [\mathrm{U}]\{\mathbf{e}\} \tag{3.1}$$

Where $\{\mathbf{e}\}=[\mathbf{e}_1,\mathbf{e}_2,\mathbf{e}_3]^T$, $\{\mathbf{E}\}=[\mathbf{E}_1,\mathbf{E}_2,\mathbf{E}_3]^T$, are the base unit vectors of local coordinate and global coordinate, respectively. Matrix [U] is a 3×3 transformation matrix that is obtained by **X-Y-Z** rotation sequence:

$$\begin{aligned}[\mathbf{U}] = \mathbf{R}_x\mathbf{R}_y\mathbf{R}_z &= \begin{bmatrix} 1 & 0 & 0 \\ 0 & \cos\theta_1 & -\sin\theta_1 \\ 0 & \sin\theta_1 & \cos\theta_1 \end{bmatrix} \bullet \begin{bmatrix} \cos\theta_2 & 0 & \sin\theta_2 \\ 0 & 1 & 0 \\ -\sin\theta_2 & 0 & \cos\theta_2 \end{bmatrix} \bullet \begin{bmatrix} \cos\theta_3 & -\sin\theta_3 & 0 \\ \sin\theta_3 & \cos\theta_3 & 0 \\ 0 & 0 & 1 \end{bmatrix} \\ &= \begin{bmatrix} c_2c_3 & -c_2s_3 & s_2 \\ c_1s_3+c_3s_1s_2 & c_1c_3-s_1s_2s_3 & -c_2s_1 \\ s_1s_3-c_1c_3s_2 & c_3s_1+c_1s_2s_3 & c_1c_2 \end{bmatrix}\end{aligned} \tag{3.2}$$

In which $\mathbf{c_i = \cos\theta_i}$, $\mathbf{s_i = \sin\theta_i}$ for simplicity. Similarly, the transformation matrix converts the global coordinate to local coordinate can be yielded as (Hong et al., 2002):

$$\mathbf{[U]^{-1}}=\mathbf{R_z^T R_y^T R_x^T} = \begin{bmatrix} c_2c_3 & c_1s_3+s_1s_2c_3 & s_1s_3-c_1s_2c_3 \\ -c_2c_3 & c_1c_3-s_1s_2s_3 & s_1c_3+c_1s_2s_3 \\ s_2 & -s_1c_2 & c_1c_2 \end{bmatrix} \tag{3.3}$$

The position of an arbitrary point with the body-fixed location $\mathbf{x}$ can be described as a summation of position of the origin of body fixed coordinate and its own position vector in body fixed coordinate as:

$$\mathbf{X}(t)=\mathbf{X}_c(t)+\mathbf{x} \tag{3.4}$$

Where $\mathbf{X_c}(t)$ is the position vector of local origin in the global coordinate system.

The velocity of an arbitrary point on the vehicle can be obtained by taking the time derivative of equation **1.4**. Since the position vector in local coordinate x is constant all the time if we assume the subsea crawler as a rigid body without deformation throughout the simulation, the time derivative of x is always equal to zero. Thus the velocity is given as:

$$\dot{\mathbf{X}}(t)=\dot{\mathbf{X}}_c(t)+\boldsymbol{\omega}\times\mathbf{x} \tag{3.5}$$

Where $\boldsymbol{\omega} = [\omega_1, \omega_2, \omega_3]^T$ represents the rotational velocity of the vehicle. The rotational velocity of the vehicle can be converted from the time derivative of the global Tait-Bryan angles.

$$\omega=\mathbf{T}\dot{\boldsymbol{\theta}}=\begin{bmatrix}0\\0\\\dot{\theta}_3\end{bmatrix}+R_z^T\begin{bmatrix}0\\\dot{\theta}_2\\0\end{bmatrix}+R_z^TR_y^T\begin{bmatrix}\dot{\theta}_1\\0\\0\end{bmatrix}=\begin{bmatrix}c_2c_3 & s_3 & 0\\-c_2s_3 & c_3 & 0\\s_2 & 0 & 1\end{bmatrix}\begin{bmatrix}\dot{\theta}_1\\\dot{\theta}_2\\\dot{\theta}_3\end{bmatrix} \tag{3.6}$$

The acceleration of an arbitrary point is then calculated similarly as:

$$\ddot{\mathbf{X}}(t)=A_c(t)+\dot{\omega}\times x+\omega\times(\omega\times x) \tag{3.7}$$

The acceleration vector of the mass center is:

$$\mathbf{A}_c(t)=\sum_{j=1}^{3}\dot{V}_j^C e_j+\boldsymbol{\omega}\times\sum_{j=1}^{3}V_j^C e_j \tag{3.8}$$

The rotational acceleration can be obtained by again taking the time derivative of equation **1.6** as:

$$\dot{\boldsymbol{\omega}}=\mathbf{T}\ddot{\boldsymbol{\theta}}+\mathbf{S}\dot{\boldsymbol{\theta}} \tag{3.9}$$

Where 3×3 matrix **S** is the derivative of transformation matrix **T** in equation **1.6**:

$$\mathbf{S}=\begin{bmatrix}-\dot{\theta}_2s_2c_3-\dot{\theta}_3c_2s_3 & \dot{\theta}_3c_3 & 0\\\dot{\theta}_2s_2s_3-\dot{\theta}_3c_2c_3 & -\dot{\theta}_3s_3 & 0\\\dot{\theta}_2c_2 & 0 & 0\end{bmatrix} \tag{3.10}$$

The slip-traction force relationship of tracked vehicles plays an important role in their mobility(Wong, 2010). The slip is essentially the relative speed between vehicle and the track. The slip velocity of an arbitrary point on the track is then expressed as:

$$\begin{aligned}\mathbf{V}_S^j(\mathbf{x},t)&=\mathbf{V}(\mathbf{x},t)-V_k^j e_1\\&=\mathbf{V}_C(\mathbf{x},t)+\boldsymbol{\omega}\times\mathbf{x}^j-V_k^j e_1\end{aligned} \tag{3.11}$$

where the superscript j represents one of tracks, 1 for left track and 2 for right track, respectively. $\boldsymbol{V_k}$ is the local speed of two tracks, which is driven by the sprockets locate at the front side of the vehicle. Thus $\boldsymbol{V_k}$ is usually calculated as product of the effective radius of the corresponding sprocket and its revolving speed. However in the man-machine experiment involved in this study, the teleoperator is supposed to manipulate such local speeds by two joystick handles. ***V(x,t)*** is the actual speed of the track expressed in local coordinate and $\boldsymbol{x^j}$ is the relative position of track with respect to the center of

subsea crawler. If the slip speed is determined, then the shear displacement for a track piece ***i*** locates at a distance **x** from the front side of the vehicle is given by:

$$s = \mathbf{V}_{si} t = \mathbf{V}_{si} \frac{x}{\mathbf{V}_t} = i_s x \tag{3.12}$$

Where i_s is called slip ratio, representing the ratio between slip speed and theoretical speed of the track.

Influencing forces exert on a subsea crawler during mining can be categorized into three different types:

1. Soil-track interaction (e.g. traction force, bulldozing resistance, compaction resistance)
2. Water-vehicle interaction (e.g. hydrodynamic resistance)
3. Other influencing forces (e.g. internal resistance, constraint forces)

Because of the fact that the influencing forces caused by soil-track interaction usually have much higher magnitudes than other forces, elaboration on soil-track interaction while making approximation on water resistance and internal resistance is preferred (Dai et al., 2010). The traction force, sometimes also called tractive effort (Wong, 2010), is the main force to drive the tracked vehicle forward. To calculate the traction force of a tracked vehicle, the shear stress generated on the track-soil interface need to be determined as traction force is integral of shear stress with respect to the track-soil contacting area. When a driving torque is applied to the sprocket, shearing action takes place on the surface between track and soil. The shear stress-displacement relationship in terramechanics associates the slip ratio to actual thrust on the vehicle. By equation 1.11 we can obtain the slip velocity vector in body fixed coordinate. However for the sake of simplicity, here we use a meshed element model to approximate the soil-track interaction, where the whole track is averagely partitioned into several segments in accordance with the number of roadwheels usually, as showed in Figure 1.

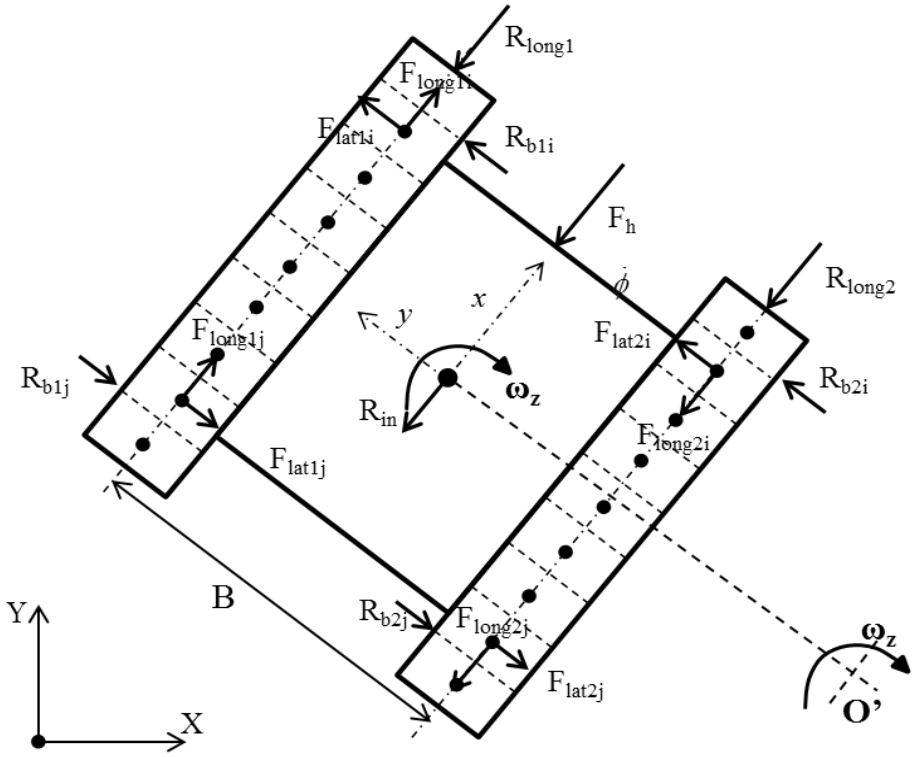

Figure 3.1. Force analysis of subsea crawler and meshed element model for track-soil interaction.

In figure 1, each segment of track generates traction force on both longitudinal and lateral direction, denoted by $\boldsymbol{F_{long1j}}$ and $\boldsymbol{F_{lat1j}}$ for left track as an example. $\boldsymbol{j}$ stands for the sequence of the partitioned track segment. Meanwhile resistances exert on the vehicle on both directions as well. Longitudinal resistance consists of compaction resistance and bulldozing resistance, summarized by $\boldsymbol{R_{long}}$. Lateral resistance is induced by relative lateral slip of each segmented track and is mostly bulldozing resistance, represented by $\boldsymbol{R_{b1j}}$ for $\boldsymbol{j^{th}}$ left track segment. Hydrodynamic force and internal resistance are labeled as $\boldsymbol{F_h}$ and $\boldsymbol{R_{in}}$ respectively. To keep the model simple and relatively controllable for further manipulation, we assume the center of mass overlays with the geometric center of the vehicle and both hydrodynamic force and internal resistance act directly on the center of vehicle, thus their moments are not taken into account. Furthermore the centrifugal force is neglected since the vehicle move at quite a low speed (around 1m/s) and the curvatures of working paths are relatively small, therefore causing low rotational accelerations.

In the following part, each force is explicitly explained for their analytical evaluation methods based on study of terramechanics (Wong, 2009).

Analytical expression of traction force on longitudinal direction when acting on ductile heavy clay soil:

$$F_{long_i} = \tau_{x_i} \Delta A = \left(c + p_{x_i} \tan\phi + C_d \left(1 - e^{-\mu \dot{s}}\right)\right)\left(1 - e^{-s/K}\right)\Delta A; \tag{3.13}$$

Where $\boldsymbol{c}$ is the cohesion pressure of soil and $\boldsymbol{\phi}$ is the angle of internal friction. $\boldsymbol{p_{xi}}$ is the normal pressure on the segmented track determined by vehicle weight and soil-track contacting area. $\boldsymbol{s}$ and $\dot{\boldsymbol{s}}$ represents the shear displacement and shear velocity respectively, which essentially are slip displacement and slip velocity. $\boldsymbol{C_d}$ and $\boldsymbol{\mu}$ are material constants. $\boldsymbol{K}$ is a measure of the magnitude of the shear displacement required for the development of the maximum shear stress (Janosi & Hanamoto, 1961), as depicted by type 'c' curve in figure 2.

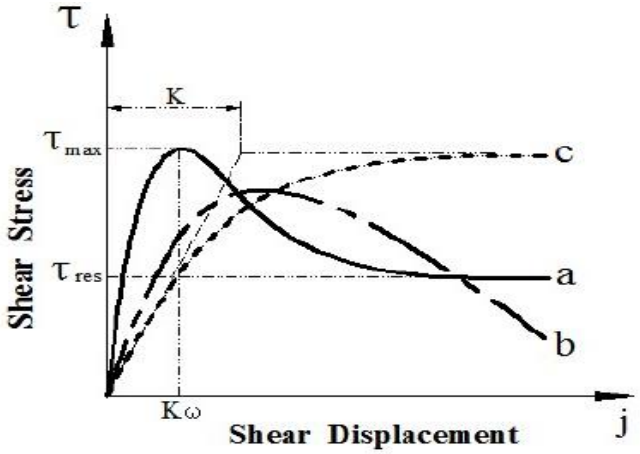

Figure 3.2. Categorized shear stress-shear displacement relationship in soil-track interaction. Type a represents brittle feature, which converges to a residual level after the maximum, usually exhibits in soft cohesive soil. Type b continuously decreases after the maximum, discovered in typical organic soil types. Type c denotes typical ductile soil property, where the curve converges gradually to the peak value (Wong, 2010).

For more brittle soil, such as weak sediments that could possibly present in future mining field, the traction force becomes as follows:

$$F_{long_i} = \tau_{x_i} \Delta A$$
$$= \left(c + p_{x_i} \tan\phi + C_d \left(1 - e^{-\mu \dot{s}}\right)\right) K_r \left\{1 + \left(\frac{1}{K_r(1 - \mathrm{e}^{-1})} - 1\right) e^{1 - s/K_\omega}\right\} \left(1 - e^{-s/K_\omega}\right) \Delta A; \quad (3.14)$$

where K_ω is the shear displacement where maximal shear stress occurs and K_γ is ratio between residue shear stress and maximum shear stress (figure 4). Traction force on lateral direction is similar to that on longitudinal direction, by only replacing the longitudinal slip speed and slip displacement with lateral counterparts.

Since sufficient tractive effort is a prerequisite for successful deep sea operation, we assume the grousers are added to the virtual vehicle to extend the traction capability. Maximal additional traction forces caused by presence of grousers are approximated empirically as:

$$\Delta F_{\max} = 2Lhc + \frac{W}{\pi} \tan\phi \left[\frac{h}{b} arc\cot\left(\frac{h}{b}\right)\right] \quad (3.15)$$

in which b and h are respectively the width and height of grouser. W is the vehicle weight and L is the instantaneous contacting length of the track.

In this manner the additional traction force in discretized track element for ductile and brittle soil are:

$$\Delta F_i = \left\{2\Delta x_i hc + \frac{W}{2n\pi} \tan\phi \left[\frac{h}{b} arc\cot\left(\frac{h}{b}\right)\right]\right\} \left(1 - e^{-s_{xi}/K}\right) \quad (3.16)$$

$$\Delta F_i = \left\{2\Delta x_i hc + \frac{W}{2n\pi} \tan\phi \left[\frac{h}{b} arc\cot\left(\frac{h}{b}\right)\right]\right\} K_r \left\{1 + \left(\frac{1}{K_r(1 - \mathrm{e}^{-1})} - 1\right) e^{1 - s/K_\omega}\right\} \left(1 - e^{-s/K_\omega}\right) \quad (3.17)$$

where $\Delta \mathbf{x_i}$ is the length of a partitioned track element and n is the number of roadwheels.

The normal pressure p_{xi} in equation 1.13 is also associated with vehicle sinkage and soil resistance. The distribution of normal pressure for tracked vehicle under static load can be characterized into different analytical models, such as uniform distribution, sinusoid distribution, linear increase and linear decrease, etc. (Wills, 1963). From the vehicle safety point of view, the uniformly distributed normal pressure is more stable for vehicle performance and can avoid severe sinkage, hence less track motion resistance, especially for pelagic soil which is generally much weaker than on-land soil types. Uniformly distributed normal pressure pattern can be achieved by closely distributed small size roadwheels and higher initial track tension (Wong, 2009). Therefore the uniform normal pressure is assumed for the simulation in this study. The normal pressure for a tracked vehicle then becomes:

$$p = \frac{W}{2bl} \quad (3.18)$$

By implementing Bekker's classic pressure-sinkage model we can calculate the sinkage depth as (Bekker, 1969):

$$z_s = \left(\frac{p}{k_c / b + k_\phi} \right)^{1/n} = \left(\frac{W / 2bl}{k_c / b + k_\phi} \right)^{1/n} \tag{3.19}$$

where $\boldsymbol{k_c}$ and $\boldsymbol{k_\phi}$ are modulus of soil cohesion and modulus of internal friction angle.

The work done in compacting the terrain to a depth of $\boldsymbol{z_s}$ with uniformly distributed normal pressure equals in magnitude with the work done by tow force along the contacting length of the track. Then combining with equation 1.17, the compaction force on both sides of the track will be:

$$\begin{aligned} R_{c_i} l &= bl \int_0^{z_s} p dz = bl(\mathrm{k_c}/\mathrm{b} + \mathrm{k}_\phi) \left(\frac{z_s^{n+1}}{n+1} \right) \\ R_{c_i} &= \frac{b(\mathrm{k_c}/\mathrm{b} + \mathrm{k}_\phi)}{n+1} \left(\frac{W / 2bl}{k_c / b + k_\phi} \right)^{(\mathrm{n}+1)/n} = \frac{1}{(\mathrm{n}+1)\,\mathrm{b}^{1/\mathrm{n}} (\mathrm{k_c}/\mathrm{b} + \mathrm{k}_\phi)^{1/\mathrm{n}}} \left(\frac{W}{2l} \right)^{(\mathrm{n}+1)/n} \end{aligned} \tag{3.20}$$

Besides the compaction force, there also exists bulldozing resistance since the vehicle's motion also pushes the soil in front of the vehicle. Bulldozing resistance is usually approximated empirically as:

$$R_{b_i} = b\left(0.67 c z K_c + 0.5 z^2 \gamma K_\gamma \right) \tag{3.21}$$

where $\boldsymbol{K_c}$ and $\boldsymbol{K_\gamma}$ are modulus of cohesion of soil deformation and modulus of density of soil deformation.

Asides from the soil track interaction, the internal resistance is induced by friction between mechanical components inside of the vehicle and empirically holds a linear relationship with the speed of the vehicle (Wong, 2001):

$$R_{in} = W(222 + 3\mathrm{V}) \tag{3.22}$$

Hydrodynamic resistance is composed of inertia force and form frag in relative flow field:

$$F_h = -\frac{1}{2} C_{drag} \rho_\omega A_m \left| v_\omega - v_m \right| \left(v_\omega - v_m \right) - C_m \rho_\omega V_m \left(\dot{v}_\omega - \dot{v}_m \right) \tag{3.23}$$

Where $\boldsymbol{\rho_w}$ is the mass density of seawater, $\boldsymbol{V_m}$ is the immersed volume of the vehicle, $\boldsymbol{v_w}$ is the local velocity of the current. $\boldsymbol{A_m}$ is the projection area of the vehicle, $\boldsymbol{C_{drag}}$ and $\boldsymbol{C_m}$ are drag coefficient and added mass, respectively. In the simulation is added mass is neglected.

Based on the Newton's second law, equation of motion becomes:

$$
\begin{aligned}
M\ddot{x} &= \sum_{i=1}^{N}(\mathrm{F}_{\mathrm{long}_{1i}} + \mathrm{F}_{\mathrm{long}_{2i}} + \Delta\mathrm{F}_{\mathrm{long}_{1i}} + \Delta\mathrm{F}_{\mathrm{long}_{2i}}) - (\mathrm{R}_{\mathrm{c}_1} + \mathrm{R}_{\mathrm{c}_2} + R_{long_{b1}} + R_{long_{b2}} + \mathrm{F}_{hlong} + R_{in}) \\
M\ddot{y} &= \sum_{i=1}^{N}(\mathrm{F}_{\mathrm{lat}_{1i}} + \mathrm{F}_{\mathrm{lat}_{2i}} + \mathrm{R}_{\mathrm{lat}_{b1}} + \mathrm{R}_{\mathrm{lat}_{b2}}) + \mathrm{F}_{\mathrm{hlat}} \\
I\ddot{\psi} &= \frac{B}{2}\sum_{i=1}^{N}(-\mathrm{F}_{\mathrm{long}_{1i}} + \mathrm{F}_{\mathrm{long}_{2i}} - \Delta\mathrm{F}_{\mathrm{long}_{1i}} + \Delta\mathrm{F}_{\mathrm{long}_{2i}}) - \frac{B}{2}(-\mathrm{R}_{\mathrm{c}_1} + \mathrm{R}_{\mathrm{c}_2} - R_{long_{b1}} + R_{long_{b2}}) \\
&\quad - \sum_{i=1}^{N}(\mathrm{x}_{\mathrm{c}} - \mathrm{x}_{\mathrm{i}})(\mathrm{F}_{\mathrm{lat}_{1i}} + \mathrm{Fl}_{\mathrm{at}_{2i}} + \mathrm{R}_{\mathrm{lat}_{b1}} + \mathrm{R}_{\mathrm{lat}_{b2}})
\end{aligned}
\tag{3.24}
$$

where subscript 1,2 represents left and right track and ***i*** is the number of track segments. ***N*** is the total number of track segments. $\boldsymbol{F_{long}}$ stands for the longitudinal traction force while $\boldsymbol{\Delta F_{long}}$ is additional traction force caused by grouser on the surface of the track. R_c is the compaction force and R_{longb} denotes the longitudinal bulldozing resistance. F_h is the longitudinal hydrodynamic resistance (water drag) and R_{in} is the internal resistance due to frictions from different mechanical parts.

Vehicle's motion on pitch and roll angles are neglected because a subsea crawler's weight will definitely cause sinkage to the soil so that the soil-track contacting interface is still nearly flat regardless of the topographic variation (figure 3.3).

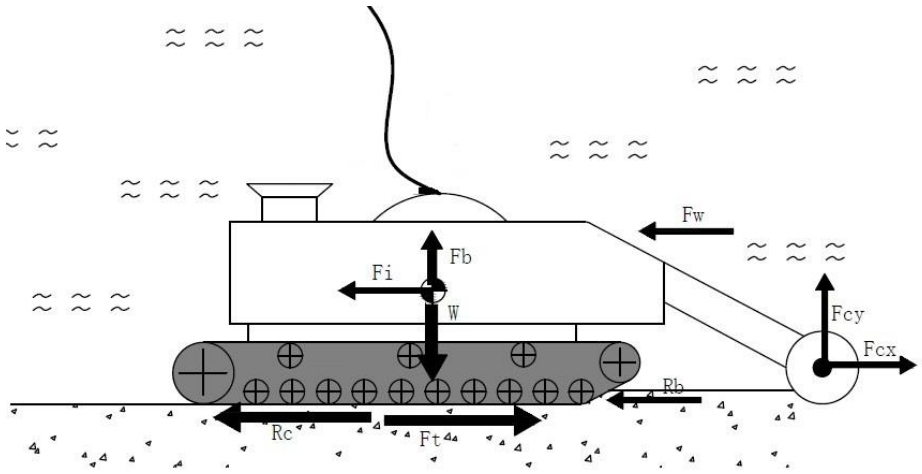

Figure 3.3. Force exerted on the subsea crawler.
Estimation of cutting force is excluded in this study to control the complexity of teleoperation.

The states of the vehicle is a vector $q = \begin{bmatrix} X & Y & Z & \dot{X} & \dot{Y} & \dot{Z} & \alpha & \beta & \gamma & w_x & w_y & w_z \end{bmatrix}^T$, consists of global position, global velocities, global heading angles and angular speeds. The dynamics is integrated by fixed step ode solver (Ode4 Runge-Kutta) in Simulink®. Based on aforementioned force analysis and knowledge in terramechanics, we can construct the dynamic model of a subsea crawler in Simulink®. The virtual vehicle model is mainly driven by forces from soil-track interaction, water drag and internal resistance (figure 4).

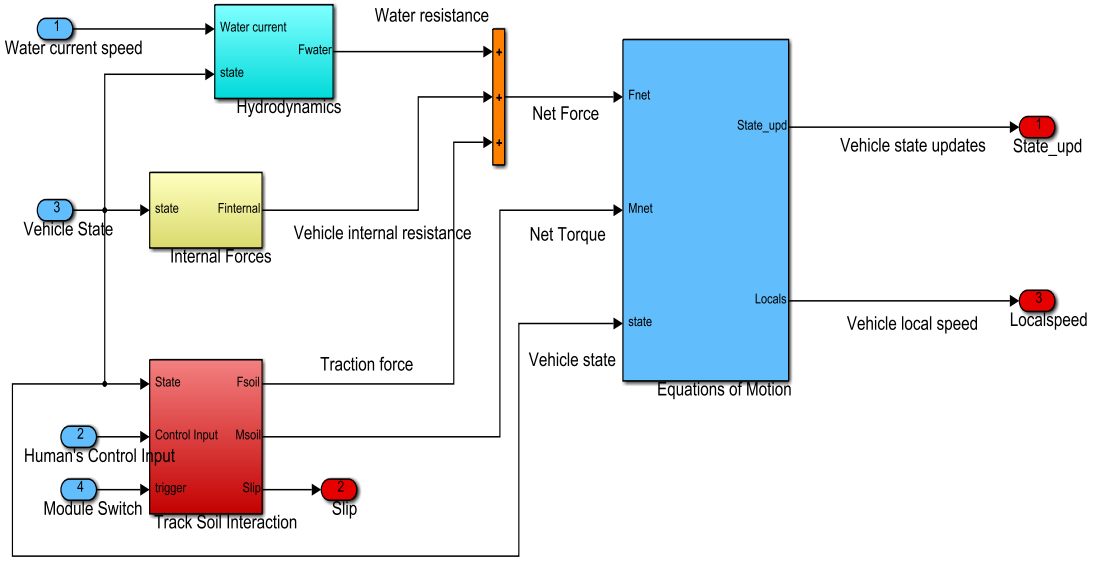

Figure 3.4. Overview of the Simulink model of vehicle dynamics.

3.2 Control Algorithm for Subsea Crawler

In unassisted manual control, the teleoperator can manipulate the rectilinear speed of left and right tracks through corresponding rotary cranks. The turning angle of each rotary crank is proportional to the speed of the track (figure 5). To control the space for the operator to improvise, we limited the speed input between 0.05 and 1m/s so that the vehicle cannot move back (to limit the operator's behavior for better comparison of the main effect). In this way we regulate the operator's steering maneuver to better compare their behavior under different experiment conditions.

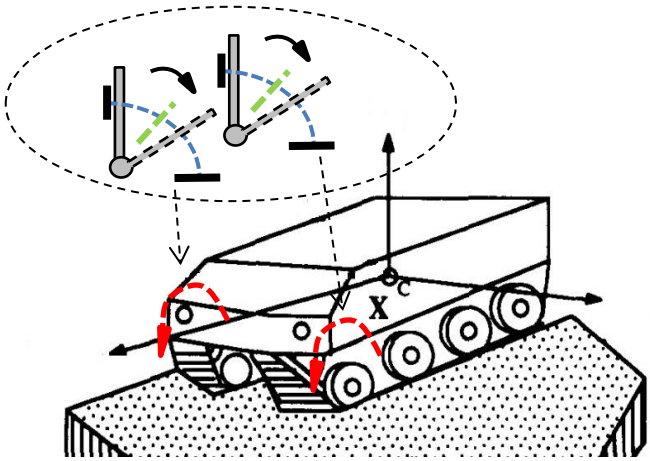

Figure 3.5. Teleoperator controls the turning angle of master crank to manipulate the speeds of corresponding track, to form a bi-manual control maneuver. The turning angle of each rotary crank is equal to the corresponding speed input.

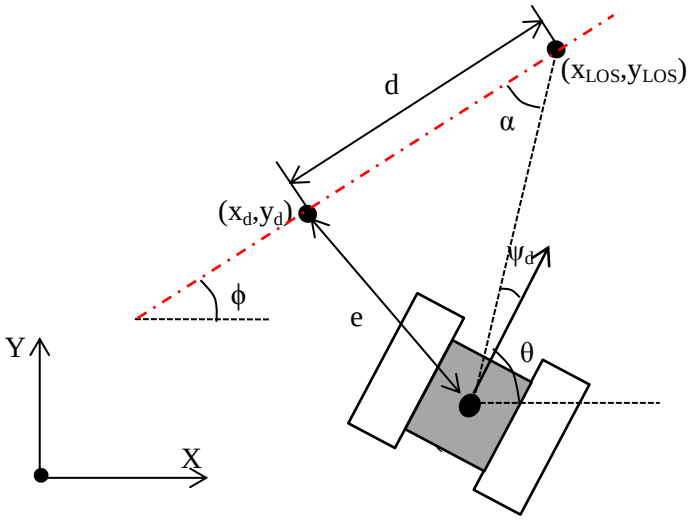

Figure 3.6. Schematic overview of controller design, lateral error *e* is the distance between vehicle center (x,y) and the nearest point on the trajectory (x_d,y_d). Heading angle error is depicted as ψ_d.

The desired vehicle velocity for a vehicle at point (x,y) is obtained with reference from the waypoint. The nearest point on the desired trajectory is named as (x_d,y_d). A newly defined parameter ***d*** represents a certain distance that is ahead of the closest point on the desired path. In this study ***d*** was set at 5 m. The desired heading angle points to the desired heading position (x_{Los}, y_{Los}), which locates at the

distance of ***d*** ahead from (x_d,y_d). Thus the angle error between actual vehicle heading angle and optimal heading angle is:

$$\begin{aligned} \psi_d &= \alpha + \phi - \theta \\ \alpha + \phi &= \text{atan}\left(\frac{y_{LOS} - y}{x_{LOS} - x}\right) \end{aligned} \tag{3.25}$$

Where ϕ is the orientation of desired path and θ is the instantaneous orientation of the vehicle. Since the subsea crawler is using skid steering mechanism, in which the vehicle could only steer the direction based on relative speed difference between left and right track. Thus we also need to define the desired speed for the optimal path. This is also realistic to define the desired speed for vehicle operation since the moving speed of the vehicle is influenced by the mineral recovery rate. Nevertheless, the optimization of path planning is not the main concern in this study, we only define the desired velocity at a constant speed v_d throughout the simulation. Then the speed error e_v and heading angle error e_ψ are defined as:

$$\begin{aligned} e_v &= v_d - v \\ e_\psi &= \psi_d - \psi \end{aligned} \tag{3.26}$$

Thus the main target for the controller is to minimize the closed loop of these two errors as:

$$\begin{aligned} \dot{e}_v + k_{vP} e_v + k_{vI} \int e_v dt = 0 \\ \ddot{e}_\psi + k_{\psi D} \dot{e}_\psi + k_{\psi P} e_\psi = 0 \end{aligned} \tag{3.27}$$

Because in usual deep sea mining operations, the subsea crawler has very slow speed and does not have to perform quick and sharp turning motion, the change of desired speed and heading angle $\dot{v}_d$ and $\ddot{\psi}_d$ can be neglected (Hong et al., 2010).

$$\begin{aligned} -\dot{v} + k_{vP} e_v + k_{vI} \int e_v dt = 0 \\ -\ddot{\psi} + k_{\psi D} \dot{e}_\psi + k_{\psi P} e_\psi = 0 \end{aligned} \tag{3.28}$$

For the design of controller, the lateral resistance in vehicle dynamics can also be negligible since we assume low yaw rate of the vehicle and the slave system does not need to perform sharp steering. Then we can simplify equation 1.24 into:

$$\begin{aligned} M\ddot{x} &= \bar{F}_R + \bar{F}_L \\ I\ddot{\psi} &= \bar{F}_R \frac{B}{2} - \bar{F}_L \frac{B}{2} \end{aligned} \tag{3.29}$$

Where $\bar{F}_L$ and $\bar{F}_R$ is the net track force on left and right track, including traction forces and all resisting forces. By combing equation 1.28 and 1.29 we yield:

$$\begin{aligned} \bar{F}_{Ld} + \bar{F}_{Rd} &= M\left(k_{vP} e_v + k_{vI} \int e_v dt\right) \triangleq \bar{F}_{d1} \\ \bar{F}_{Ld} - \bar{F}_{Rd} &= -\frac{I}{b}\left(k_{\psi D} \dot{e}_\psi + k_{\psi P} e_\psi\right) \triangleq \bar{F}_{d2} \end{aligned} \tag{3.30}$$

Thus the desired net traction force for left and right track becomes:

$$\begin{aligned} \bar{F}_{Ld} &= \frac{\bar{F}_{d1} + \bar{F}_{d2}}{2} \\ \bar{F}_{Rd} &= \frac{\bar{F}_{d1} - \bar{F}_{d2}}{2} \end{aligned} \tag{3.31}$$

If we can determine the mechanical properties of the soil layer and the slip-thrust relationship within the vehicle's soil-track interaction, we can obtain a nonlinear relationship between track slips and their net traction forces. This method is usually used in experimental study on mobility of tracked vehicle (Wu et al., 2008). In this way the controller calculates the desired slip ratio based on the optimal net traction force from 1.31. Thereafter with calculated slip ratio i_{Ld} and i_{Rd}, according to equation 1.12, the desired rectilinear speeds of two tracks become:

$$\begin{aligned} V_{L\mathrm{d}} &= \frac{\dot{x} - \dot{\psi} B / 2}{(1 - i_{Ld})} \\ V_{\mathrm{Rd}} &= \frac{\dot{x} + \dot{\psi} B / 2}{(1 - i_{Rd})} \end{aligned} \tag{3.32}$$

The aforementioned control algorithm is based on theoretical kinematic and dynamics of the tracked vehicle, thus additional correction is added to deal with potential model inaccuracy. Here we set a constant gain K_{ψ}, which acts as an extra proportional controller on the angle error. Thereby the calculated desired rectilinear speed of left and right track becomes:

$$\begin{aligned} V_{L\mathrm{d}} &= \frac{\dot{x} - \dot{\psi} B / 2}{(1 - i_{Ld})} - K_{\psi} e_{\psi} \\ V_{\mathrm{Rd}} &= \frac{\dot{x} + \dot{\psi} B / 2}{(1 - i_{Rd})} + K_{\psi} e_{\psi} \end{aligned} \tag{3.33}$$

3.3 Parameterization of the Numerical Model

There are quite a lot of studies with deep sea mining on polymetallic manganese nodules mainly because of the worldwide burst of research on deep sea mining in 1970s to 1980s (Dai et al., 2010; Hong et al., 2002), where the pelagic soil are generally regarded as 'brittle' type. Comparatively study on SMS mining is still in its infancy. But due to the general differences on ground condition and soil properties, the environment investigation on PMN cannot be generalized to study on SMS mining. Nevertheless it is usually thought that the SMS field is much stronger than that in PMN filed and exhibits ductile characteristic during shear deformation. The soil parameters used in the simulation for this study was chosen as ductile type of soil, while the information about the vehicle was mainly adapted from previous studies on the prototyping of deep sea mining machines.

3.3.1 Soil Properties

Since the in-situ soil samples are quite scarce, researchers usually choose to fabricate artificial soil samples which share similarities with pelagic soil for study. Unlike the weak bentonite soil used for simulating soil in PMN field (Choi, Hong, Kim, & Lee, 2003; Kim, Hong, & Choi, 2004; Li & Li,

2010), heavy clay and sandy loam are more similar to soil condition in SMS deposit, since the foundation of SMS deposit is similar to weathered rock. But in this study we only simulate ductile types of soil in the experiment. Thus with reference from past research on lab tracked vehicle testing (Wong, 2001, 2010), the soil parameters for virtual pelagic soil used in this study are listed in table 3.

Pressure-sinkage model	Modulus of cohesion of soil deformation	$\mathbf{k_c}$	10 [kN/m^{n+1}]
	Modulus of friction of soil deformation	$\mathbf{k_\phi}$	100 [kN/m^{n+2}]
	Soil deformation exponent	**ns**	0.2~1.0
Shear stress model	Soil cohesion	**c**	10 [kPa]
	Soil angle of internal friction	$\boldsymbol{\phi}$	6 [Deg]
	Shear deformation modulus	**K**	1.5~2.5 cm
	Material constant	$\mathbf{C_d}$	0
	Pelagic soil density	$\boldsymbol{\gamma}$	1200 [kg/m^3]
	Coefficient of soil density	$\mathbf{K_\gamma}$	1.0
Soil resistance model	Coefficient of soil cohesion	$\mathbf{K_c}$	2.0
	Coefficient of dynamic sinkage	$\mathbf{c_0}$	0.017
	Coefficient of dynamic sinkage	$\mathbf{c_1}$	1
Dynamic sinkage model	Coefficient of dynamic sinkage	$\mathbf{c_2}$	0.5
	Density of seawater near seafloor	$\boldsymbol{\rho_w}$	1030 [kg/m^3]
	Average seawater speed	$\mathbf{V_w}$	0~1 m/s
water resistance	Drag coefficient	$\mathbf{C_w}$	2~5

Table 3.1. Soil parameters used in this study (Hong et al., 2002).

3.3.2 Parameterization of the Virtual Vehicle

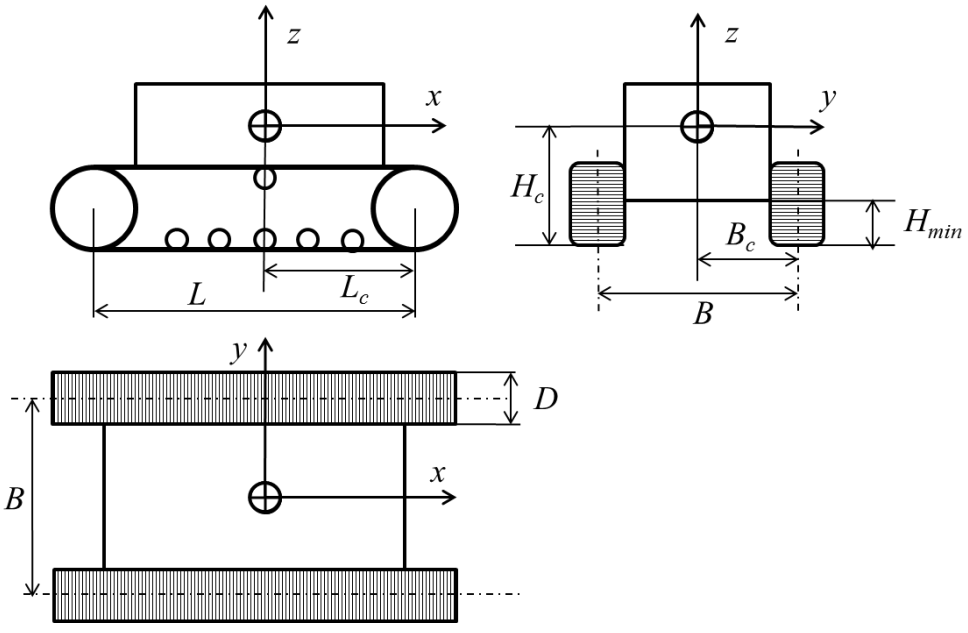

Figure 3.7. Vehicle model and body-fixed coordinate.

Track Length	**L**	6 m	Mass Center	$\mathbf{H_c}$	1.5 m
Track Width	**D**	0.6 m		$\mathbf{L_c}$	3 m
Thread Width	**B**	5 m		$\mathbf{B_c}$	2.5m
Vehicle Mass (in air)	**M**	30 ton	Moment of Inertia with respect to the mass center	$\mathbf{I_{xx}}$	$3.5E^4$ Kg/m^2
Projection Area	$\mathbf{A_p}$	15 m^2		$\mathbf{I_{yy}}$	$8\ E^4$ Kg/m^2
Chassis height	$\mathbf{H_{min}}$	0.5 m		$\mathbf{I_{zz}}$	$9\ E^4$ Kg/m^2

Table 3.2. Parameters of subsea miner used in this study, partially adapted from (Hong et al., 2002)

Sizes of the miner are the most critical for almost every part of deep sea mining projects. The scale of the miner correlates to the production of the project and may determine revenue for the company. Also the sizes of the miner, especially the sizes of the track, highly influence the generated force from track-soil interaction. However since no actual mining example has been built yet and detailed calculation of vehicle design with regard to the production of deep sea mining is out of the scope of this study, we can only assimilate the data from current prototypes. A joint venture of Mitsubishi Heavy Industry, Kayaba System Machinery and Sumitomo Metal Mining proposed a prototype miner with length of 7 m, width of 3.2 m and height of 3.5m, aiming for the SMS excavation in peripheral waters near Okinawa, Japan (Ishiguro et al., 2013). Prototypes from Nautilus Inc., though detailed sizes not known publicly, has same level of scales (Lipton, 2008). Chinese 1000m deep sea miner mainly used for mining of PMN also has 6.2m of track length and 3.5m of thread width (Dai et al., 2009). Thus here we choose to set our virtual miner with almost the same level of size, a track length of 6m, thread width of 5m and track width of 0.6m. More detailed sizes are listed in table 1.2.

3.3.3 Example of Parameter Optimization: Mass of the Vehicle and Static Sinkage

One of the most important design considerations for the subsea miner is the vehicle mass, which directly influence the sinkage during real excavation. There exist two widely accepted analytical pressure-sinkage models, Bekker's model and Reece's model (Wong, 2010). Here we use Bekker's model for rough estimate of vehicle mass because Reece's model is suitable for homogeneous soil and requires more data for accurate estimation. According to equation 1.19 and soil parameters in table 1.1, we can tell that with a controlled soil bearing capacity and contact area, the higher of the vehicle weight, the deeper the sinkage. A pressure-sinkage curve with different levels of bearing capacity is shown in figure 8. The upper limit of the sinkage can be determined with the consideration that the maximum sinkage depth may not surpass the height of chassis. If sinkage is greater than the vehicle ground clearance and vehicle belly may come into contact with the terrain surface, then corresponding soil resistance will increase dramatically by belly drag (Wong, 2009). We assume to avoid this circumstance on account of the miner safety and effectiveness of its motion.

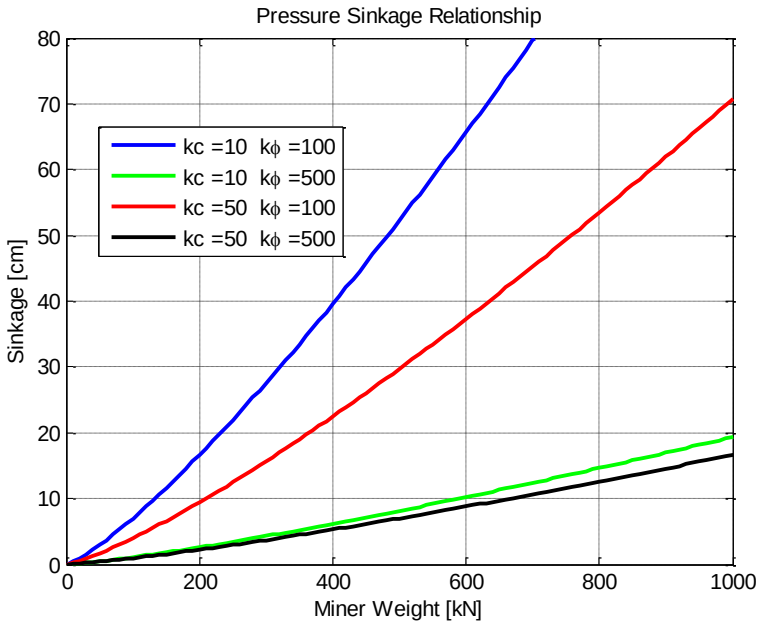

Figure 3.8. Pressure-sinkage curves with different soil parameters, sinkage exponent is 0.8 in this case.

Unit for k_c and k_ϕ are [kN/m^{n+1}] and [kN/m^{n+2}] respectively.

Assuming that the ground clearance of the subsea miner is 0.5m, we test the pressure-sinkage model with two different sets of modulus. $\mathbf{k_c}$ = {10 , 50} and $\mathbf{k_\phi}$ = {100 , 500}[1], which resulted into four different pressure-sinkage curves. Results are shown in figure 8, in which vehicle weight up to approximately 450 kN. With a safety factor of 3.0, the proper vehicle weight can be around 150 kN, which is roughly 30 metric tons of weight in water (the buoyance will reduce some of the vehicle weight in the water). This deduction coincides with the weight estimations in current prototyping (Ishiguro et al., 2013).

Mass Center

To simplify the dynamic analysis for subsea miner, the mass center locates together with the geometric center of the miner on X-Y plane. Asymmetric mass center, especially on lateral direction, would easily introduce unbalanced traction force, which is detrimental for vehicle stability. Although there exists reference to support adjustment of center of buoyance on the small scale underwater vehicle, thus change of center of mass on longitudinal direction, could improve its gradeability and effectively avoid turnover when it works on steep slopes (Lee et al., 2011), the accurate value for move of center of buoyance for a specific miner remains unknown for a specific crawler. Therefore we chose to control the potential influence introduced by variation of center of mass and focus more on the human performance in this study. Detailed location of center of mass is represented in table 1.2.

Matlab code for soil-traction interaction

(describing the red block in figure 3.4).

```
function [Flong, Fdel, Rc, Rblong,Flat, Rblat, Mt, Mc, Mb, Ma, slip] =
fcn(state,input, trigger,c, phi,p, xi, yi_l, L, H, n, D, ns, kc, kphi, W, c0,
c1,c2,B, Kr, Kc, gamma,h,K,E,kw)

% This function computes:
% longitudinal and lateral traction force, bulldozing resistance, compaction
% resistance and additional forces with
% given local relative points on the track (xi, yi_l, -H);
% xi: position of center of each track segment on local x coordinate
% yi_l: position of center of each left track segment on local y coordinate,
% tao1: longitudinal stress
% tao2: lateral shear stress

% Need to define soil parameters:
% kw(shear displacement where maximal shear stress occurs)
% E(ratio between residue shear stress and maximal shear stress)
% c (soil cohesion) p(vehicle's normal pressure) u  Cd(material constant)
phi(internal friction
% angle) L(track length) H(height of COM) n(number of roadwheels) beforehand
% phi  = 10/ 180*pi;
% c = 6*1e3;

vel_gl   = state(4:6); % vehicle speed in local coordinate
theta1 = state(7);     % pitch
theta2 = state(8);     % roll
theta3 = state(9);     % yaw
omega  = state(10:12); % angular speed

% rotation matrix
R= [cos(theta2)*cos(theta3), cos(theta1)*sin(theta3) +
cos(theta3)*sin(theta1)*sin(theta2), sin(theta1)*sin(theta3) -
cos(theta1)*cos(theta3)*sin(theta2);
     -cos(theta2)*sin(theta3), cos(theta1)*cos(theta3) -
sin(theta1)*sin(theta2)*sin(theta3), cos(theta3)*sin(theta1) +
cos(theta1)*sin(theta2)*sin(theta3);
                 sin(theta2),                                          -
cos(theta2)*sin(theta1),
cos(theta1)*cos(theta2)];

vel_bf  = R*vel_gl;     % local velocity
vel_bf1 = vel_bf(1);
vel_bf2 = vel_bf(2);
vel_bf3 = vel_bf(3);
omega1  = omega(1);
omega2  = omega(2);
omega3  = omega(3);
step = L/(n-1);         % length of a single track segment
delA = step*D;          % contact area of a single track segment

taomax1 = c+p*tan(phi);  % longitudinal maximum shear stress
taomax2 = c+p*tan(phi);  % lateral maximum shear stress

% Local speed of each track segment
v_track = [vel_bf1-H*omega2-yi_l'*omega3; vel_bf2+xi'*omega3+H*omega1;
vel_bf3+yi_l'*omega1-xi'*omega2];

% slip speed of each track segment
is = v_track-[input*ones(size(xi')); zeros(size(xi')); zeros(size(xi'))];

if input<0.001   %deadzone threshold
        s1   =  zeros(size(is(1,:)));  % longitudinal slip
        slip =  0;
        s2   =  zeros(size(is(1,:)));  % lateral slip
```

```
else
        s1 =  -is(1,:)/input.*(L/2-xi');  % longitudinal slip
        slip  =  -is(1)/input;
        s2 =  -is(2,:)/input.*(L/2-xi');  % lateral slip
end

id = ((L/2-xi')-abs(s1))<0;          % slip distance cannot exceed physical range
s1(id)  =sign(s1(id)).*(L/2-xi(id)');
id = (D/2-abs(s2))<0;                % slip distance cannot exceed physical range
s2(id)  = sign(s2(id))*D/2;

if trigger <1   % to check whether the slip event was triggered.
     tao1    = sign(s1)*taomax1.* ( (1-exp(-abs(s1)/K))) ;  % 'Ductile type soil
shear stress-shear displacement relationship'
     tao2    = sign(s2)*taomax2.* ( (1-exp(-abs(s2)/K))) ;
else
     tao1    = sign(s1)*taomax1*(0.8).* ( (1-exp(-abs(s1)/K))) ;  % 'Ductile type
soil shear stress-shear displacement relationship'
     tao2    = sign(s2)*taomax2*(0.8).* ( (1-exp(-abs(s2)/K))) ;
end

Flong = tao1*delA;   % longitudinal traction force
Flat  = tao2*delA;   % lateral traction force
Mt = -Flong.*yi_l'+Flat.*xi'; % rotary torque from traction force


% compaction force
Rc = -sign(v_track(1,1))*1/((ns+1)*(D^(1/ns))*(kc/D+kphi)^(1/ns))*
(W/2/L/1000)^(1+1/ns)*1000;  %Opposite direction of track speed
Mc = Rc*(-B/2);

% Bulldozing resistance
z0   = (W/2/D/L/1000/(kc/D+kphi))^(1/ns);   % static sinkage depth, Bekker 1969
zd1  = c0*((p/1000)^c1)*(abs(s1).^c2)/100;           % dynamic sinkage, Muro 1991
zd2  = c0*((p/1000)^c1)*(abs(s2).^c2)/100;           % slip [cm], p[Kpa] zd[cm]
z1   = z0+zd1;         % total longitudinal sinkage
z2   = z0+zd2;         % total lateral sinakge

Rblong = -sign(v_track(1,1))*D*(0.67*c*z1*Kc+0.5*z1.^2*gamma*Kr); % longitudinal
bulldozing force
Rblat =  sign(s2)*D.*(0.67*c*z2*Kc+0.5*z2.^2*gamma*Kr);           % lateral
bulldozing force
Mb    = -Rblong.*B/2 +Rblat.*xi';  % torque induced by bulldozing force

% Additional forces because of the grousers
AddF_max = 2*step*h*c+W/2/(n-1)/pi*tan(phi)*(h/D*acot(h/D));
if trigger <1  % to check whether slip is triggered
    Fdel  = sign(s1)*AddF_max.*(1-exp(-abs(s1)/K));
else
    Fdel  = sign(s1)*(0.8)*AddF_max.*(1-exp(-abs(s1)/K));
end

Ma  = -Fdel.*B/2;  % torque by additional traction force

end
```

Appendix IV –Pilot Study

The pilot study of this experiment took two periods. At the first period, the experiment setting required the subject to press an external button to switch between full automation and manual control in supervisory control mode, which led to an extremely unbalanced result in obstacle avoidance (figure 4.1). A subject (*Male, age: 25*) was tested in this setting, where he ran into every single obstacles under supervisory control. Thus this initial experiment setting was abandoned latter, and replaced with a much smoother switch approach for the second period of testing and the actual experiment.

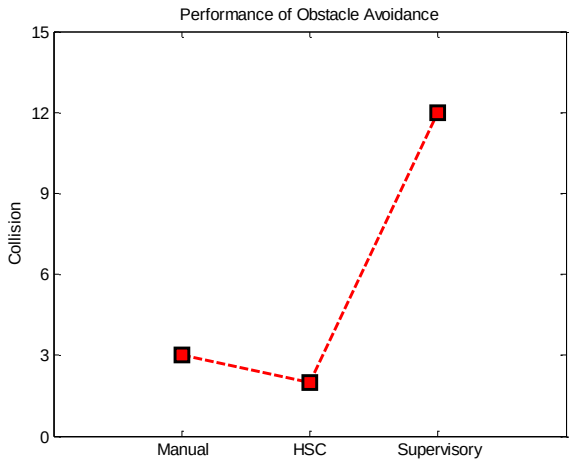

Figure 4.1. A subject's performance of obstacle avoidance with the initial experiment setting (clumsy supervisory switch).

For the latter pilot study, two subjects (Age: 24 and 27), one male and one female, both Master students from Delft University of Technology, were recruited for a pilot study to check the reliability of the whole experiment settings before the actual experiment. No statistical results can be drawn from the pilot study, but it helped to unveil the main effects in actual measurements. The differences of the experiment setting between this pilot study and the actual experiment are:

1. In supervisory control, the subject can return the control authority back to full automation anytime regardless of the lateral deviation, while the subjects needed to drive the vehicle back to the optimal path with absolute lateral deviation less than 0.6m in actual experiment.
2. The optimal speed set for supervisory control is 0.8m/s in the pilot study, as with that in HSC.

The simulated vehicle's trajectories during 12 obstacles controlled by these two subjects are shown in figure 4.2.

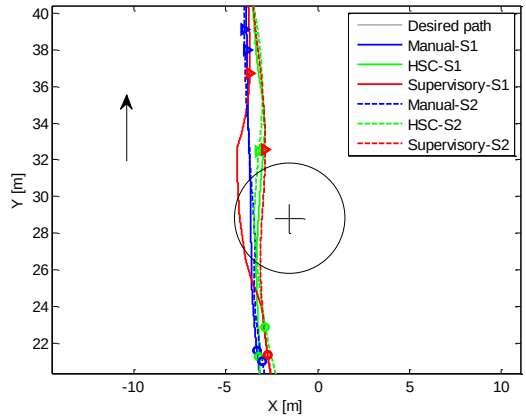
Desired path
Manual-S1
HSC-S1
Supervisory-S1
Manual-S2
HSC-S2
Supervisory-S2
Y [m]
X [m]

(a)

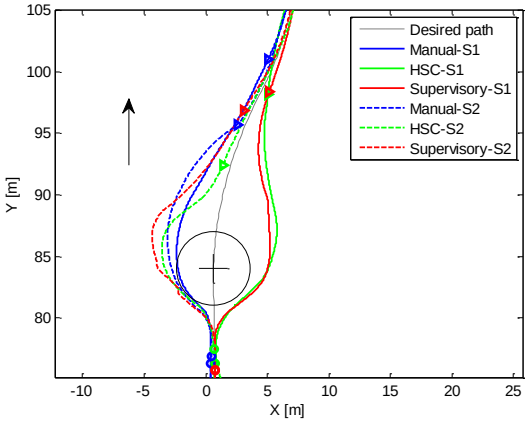
Desired path
Manual-S1
HSC-S1
Supervisory-S1
Manual-S2
HSC-S2
Supervisory-S2
Y [m]
X [m]

(b)

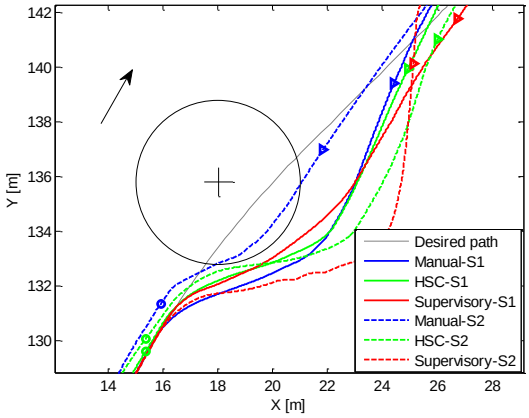
Desired path
Manual-S1
HSC-S1
Supervisory-S1
Manual-S2
HSC-S2
Supervisory-S2
Y [m]
X [m]

(c)

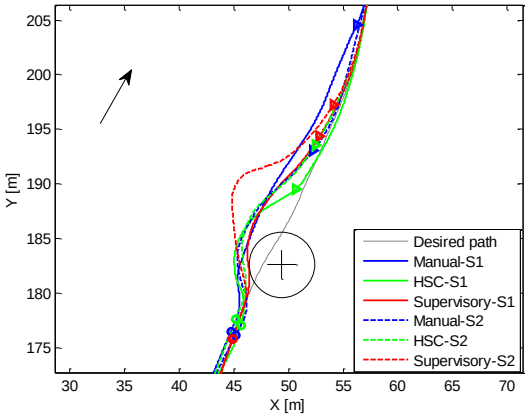
Desired path
Manual-S1
HSC-S1
Supervisory-S1
Manual-S2
HSC-S2
Supervisory-S2
Y [m]
X [m]

(d)

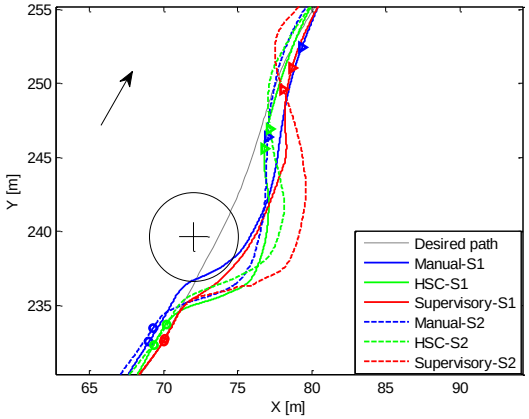
Desired path
Manual-S1
HSC-S1
Supervisory-S1
Manual-S2
HSC-S2
Supervisory-S2
Y [m]
X [m]

(e)

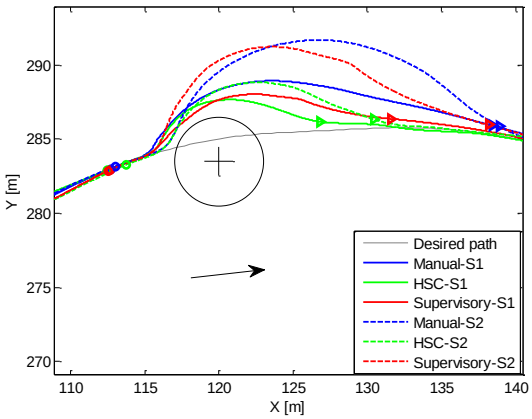
Desired path
Manual-S1
HSC-S1
Supervisory-S1
Manual-S2
HSC-S2
Supervisory-S2
Y [m]
X [m]

(f)

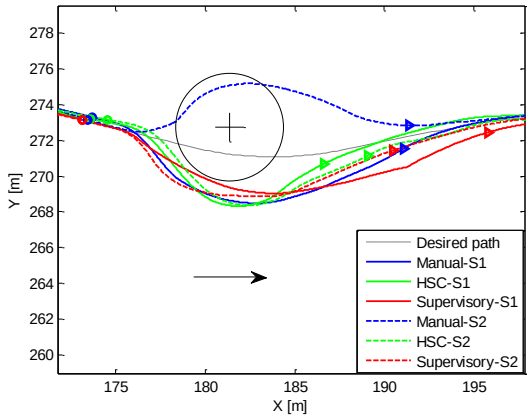

(g)

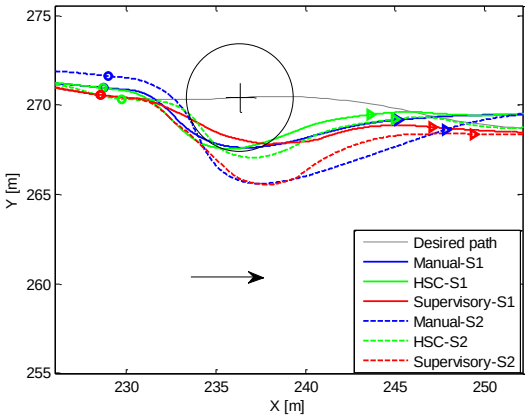

(h)

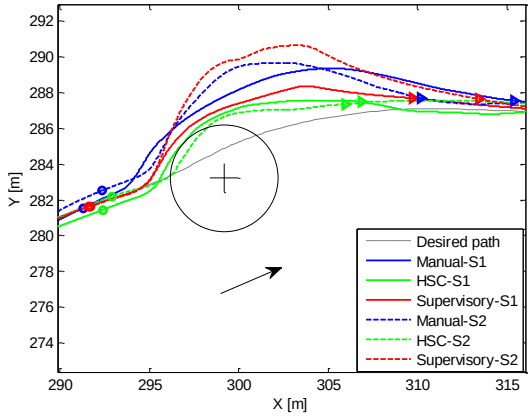

(i)

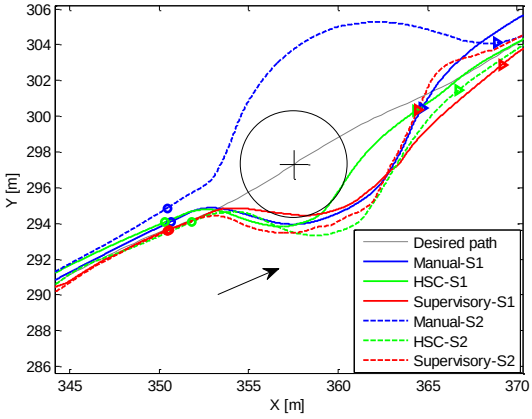

(j)

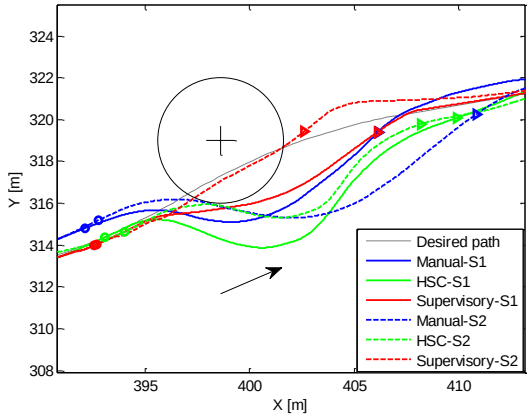

(k)

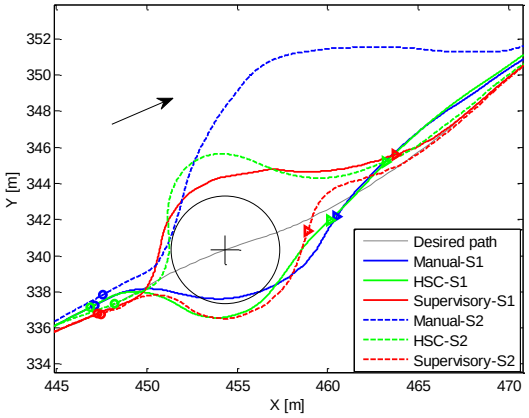

(l)

Figure 4.2. The simulated vehicle's trajectory in avoiding 12 obstacles, with solid lines represent the performance of the 1st subject while the dashed lines represent the 2nd subject. These circle markers label the moment when the corresponding obstacle appeared on the screen. And the triangular markers illustrate the place where the corresponding obstacle avoidance ends. The obstacle was drawn within a solid circle with radius of 3m. The black arrows represent the heading direction of the optimal path.

If a trajectory overlaps with the corresponding circle, it was recognized as a collision. According to figure 4.2, among those successful avoidances, the simulated vehicle seemed to spend less length during obstacle with respect to the optimal path in HSC than the other two experimental conditions. Regardless of these trajectories which overlap with the obstacle, these green triangular markers appear on the trajectories ahead of these red and blue ones in the majority of the cases. Therefore there might exhibit a tendency that the subjects could recover back to the optimal path faster in HSC than the other two conditions. Another phenomenon is that the subjects had a preference on the direction to avoid the obstacles where the obstacle locates aside of the optimal path. Otherwise their steering maneuvers were quite random for obstacles just on the optimal path (e.g. figure 4.2-b, l).

Figure 4.3 illustrates the root mean square of the lateral deviation during normal path tracking between obstacles. Averagely speaking, both subjects benefited from the two assist conditions compared to manual control. However their reactions towards HSC and supervisory control were different from each other. Subject 2 apparently made better use of the guidance in HSC than subject 1. However the full automation in supervisory control further decreased the lateral deviation than HSC for the 1st subject, which didn't exhibit significantly for the 2nd subject.

Figure 4.4 shows the total number of collisions triggered by two subjects under three experimental conditions. It was because the transition between manual and automation mode in supervisory control had been changed, the collision number in supervisory control decreased dramatically, and even less than manual control for both subjects. As a conjecture to be further tested in the actual experiment, the subjects could pay more attention to the intermittently popped-up obstacles in supervisory control since they did not need to generate physical effort in steering the vehicle, which resulted into less collision if they could regain the control authority easily during steering such a slow dynamic system.

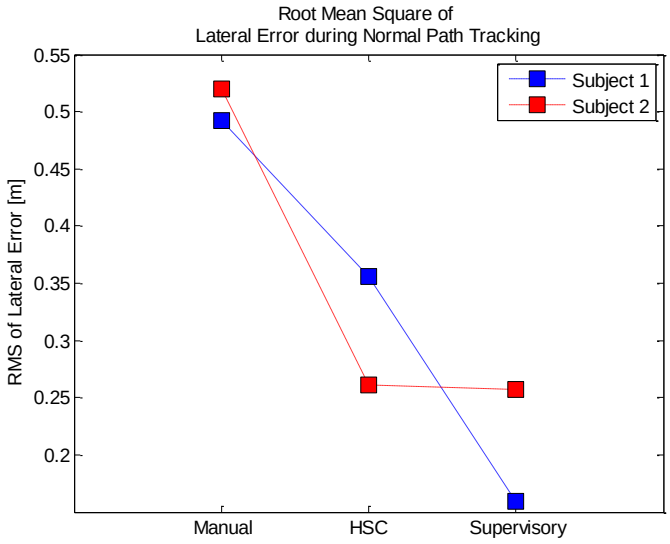

Figure 4.3. Root mean square of the lateral deviation between obstacles when steered by two subjects. Dashed line is for highlighting the comparison, does not mean any linear relationship between conditions.

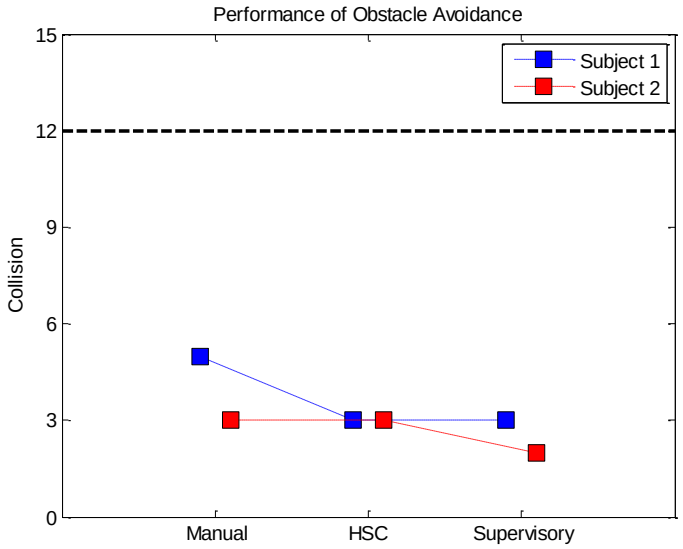

Figure 4.4. Total number of collisions run by each subject under different experimental conditions. The black dashed line represents hypothetically maximum collisions if the vehicle is run completely under full automation.

The response accuracy and reaction time for two subjects were shown in figure 4.5 and 4.6, respectively. There existed an obvious difference between different task modules. Both subjects had less accuracy with obstacles and during slip events than normal operation between obstacles, regardless of the experiment conditions. Similar to the results found for lateral deviation, the subject's different acceptance of the two assist conditions was also reflected on their performance in the secondary task. Theoretically the assist conditions could relieve the subject's mental workload so that the performance of secondary task between obstacles should be improved. While the first subject's accuracy between obstacles increased with the level of automation, the second subject exhibited a relatively constant and high accuracy during normal operation between obstacles. Meanwhile, unlike the second subject, the first subject could still perform a slightly higher accuracy in HSC than that in manual control even within obstacle avoidances. Thus it was questionable whether the higher of the automation level, the higher of the mental workload during unexpected events, as shown by the accuracy of the secondary task.

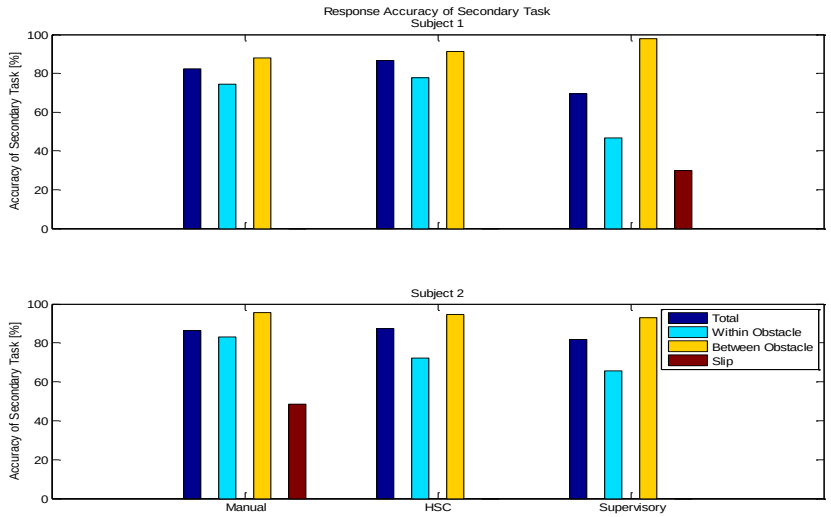

Figure 4.5. Responding accuracy of secondary task by two subjects. *Upper:* 1st subject. *Bottom:* 2nd subject. The data is categorized by different task modules. The dark blue bars represent the accuracies in total, within obstacles in light blue, between obstacles in yellow, and slip in brown. 1st subject only experienced the slip event in supervisory control and 2nd subject only in manual control.

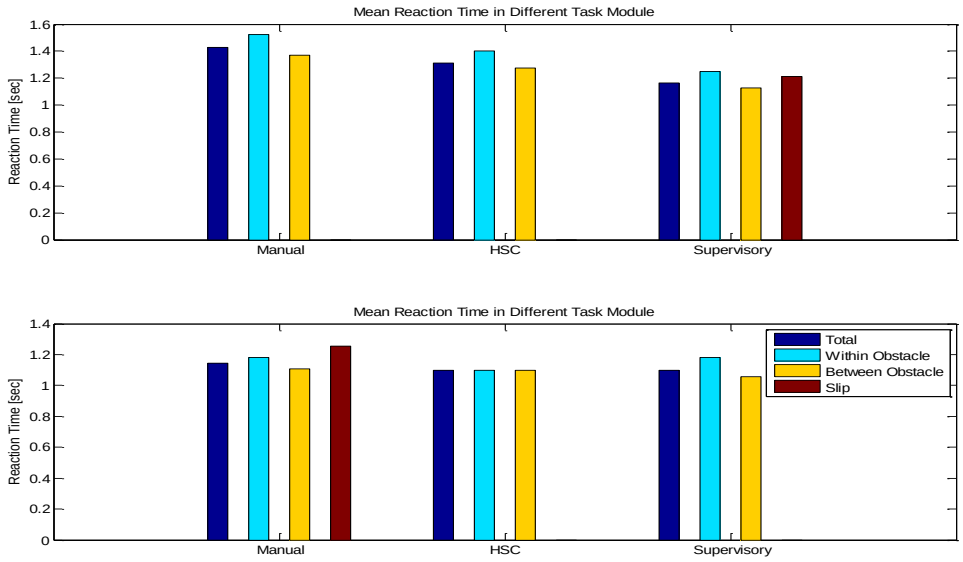

Figure 4.6. Reaction time of the secondary task by two subjects. *Upper:* 1st subject. *Bottom:* 2nd subject. The data is categorized by different task modules. The coloring manner is the same with figure 4.5.

The subjects' different reaction towards the assist conditions also continued in the reaction time of answering the secondary task. The first subject's reaction time towards the secondary task is noticeably decreased with the increase of the automation level, for both operations between and within obstacles. However the second subject's reaction time was not affected by the assist conditions with the same level as for the first subject.

To sum up, the first subject made better use of the guidance in steering the vehicle, regarding improvement of both accuracy and reaction time in answering the secondary task,

figure 4.5,4.6), while the second subject benefited more specifically from HSC in primary steering task (figure 4.3).

During the pilot study we found that there might exist a difference in the length the subject spent in avoiding the obstacle between three conditions (figure 4.2), however the subjects could return the control authority back to the automation system once they just pass the obstacle, such that the rest parts actually will be finished by the automation (figure 4.7). Thus in the actual experiment the subjects can only retrocede the control authority once they've driven the vehicle back to the optimal path with absolute tolerance at 0.6m, same with the tolerance used to identify the ending of an obstacle avoidance. In addition, because the total time to complete the task was an interesting metric to compare the effects between three experimental conditions, the reference speed for supervisory control was set to full thrust in actual experiment.

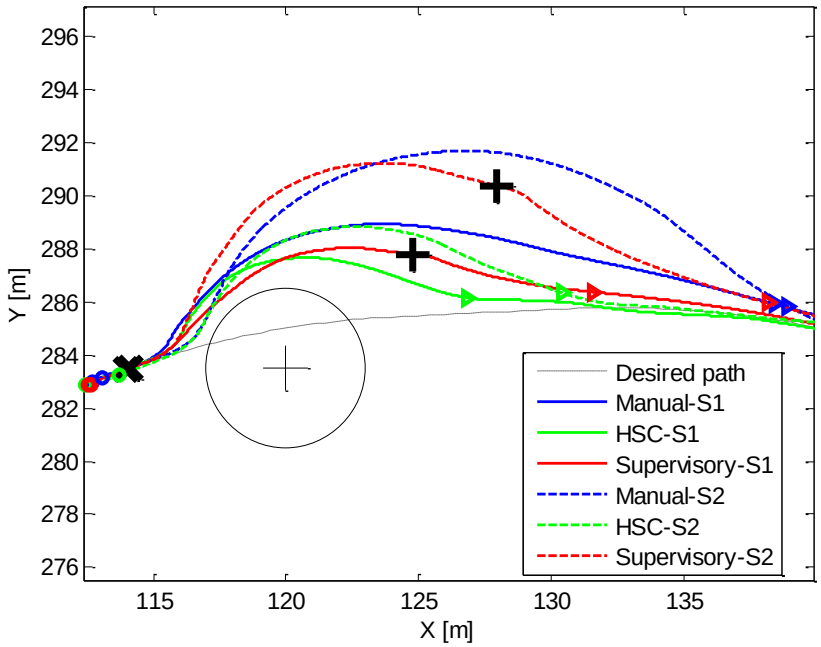

Figure 4.7. Two subjects performance in avoiding the 6th obstacle, all contents are similar to figure 4.2-f, besides two types of markers. The black cross makers represent the place where the subjects pulled back the handle to regain the control authority. The black plus signs depict the place where the subjects switched back to full automation. Both subjects returned the control authority back to the controller (plus signs) before the vehicle completely recovered to the optimal path (red triangles).

Appendix V – Task Instruction

Experiment: Haptic shared control in teleoperation of subsea crawler

First of all, thank you for your cooperation in this experiment. Below is the description of the tasks to be performed during the experiment and some safety considerations. If you are confused with any statement please do not hesitate to ask the experimenter.

The setting consists of two screens and two cranks, as showed in figure 1.

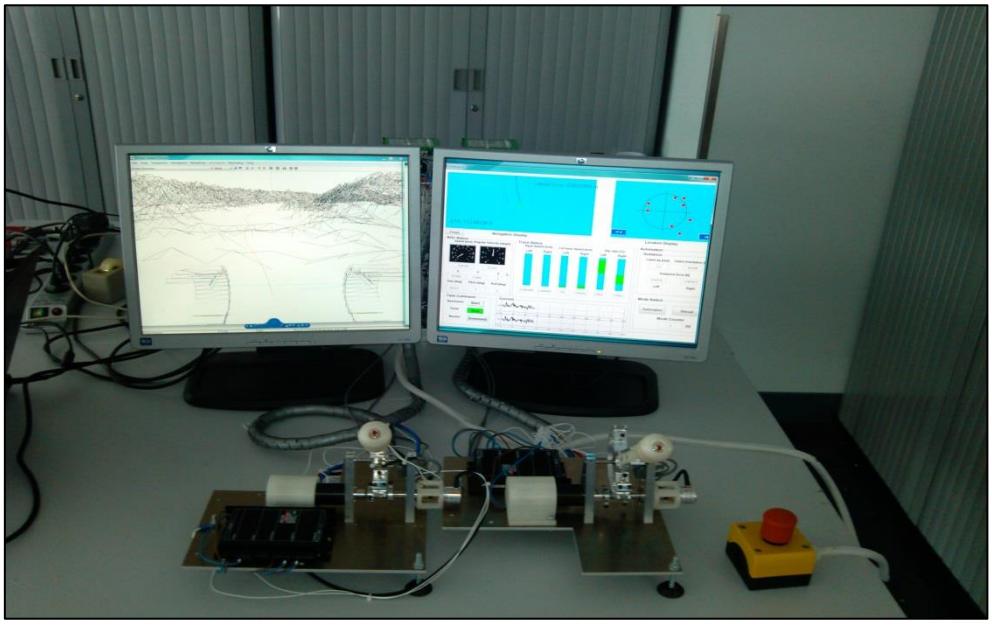

Figure 1. Experiment settings.

Figure2. guideline for handholding

Each of the two rotary cranks has one degree of freedom. **You need to grab the handle from the beginning till to the end of each trial.** Standard grab posture is shown in figure 2, where **your index finger should touch the concave surface of the handle as reference point**.

The red tactile switch on the top of the handle is for your input to respond to secondary task.

The whole experiment will be divided into two parts: Training section and experiment section.

In the first part you are required to do some training with visual feedback through augmented **3D display** (figure 3) of and **dashboard** (figure 4). You need to follow the pre-defined path (the red curve shown in 3D display) as close as you can with these two rotary cranks. Obstacles will show up during driving. You need to learn to first identify such an obstacle and then avoid it. Once you can control the lateral error (regardless of obstacle avoidance) and succeed in three consecutive obstacle avoidances, this will be regarded as completion of your training section.

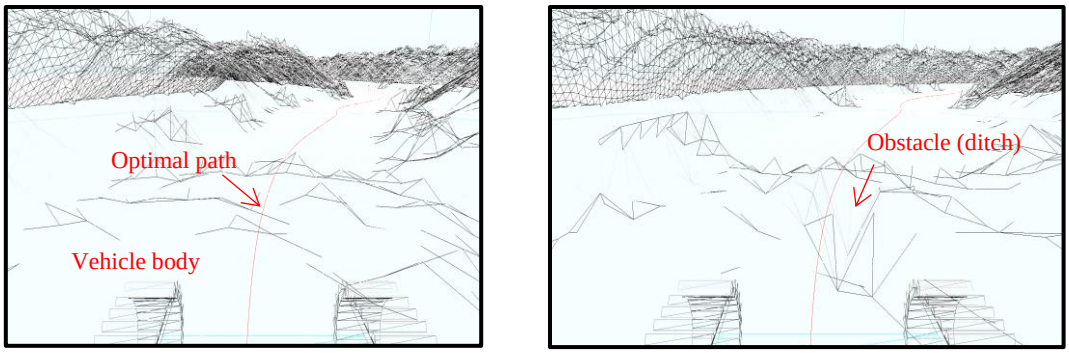

Figure 3. Augmented 3D display

Aside from the 3D representation, alternatively you can monitor the status of the vehicle based on information shown on dashboard. In addition, the secondary task is also shown on dashboard (figure 4). Information on dashboard is categorized as below:

A — Representation of vehicle position in global coordinate. Green dot illustrates the vehicle. Blue curve shows the predefined optimal path while those two parallel black curves are reference range for vehicle safety. (ETA: Estimated time of arrival)

B — Secondary task. The secondary task is tested throughout the whole experiment**. You need to identify the number of red dots in the black dashed circle (e.g. it's 4 in example). If the number is less or equal to 4, you are supposed to press the switch on the left handle, otherwise on the right handle.**

C — Speedometer, position and orientation of vehicle in numbers.

D — Status of the two tracks of the vehicle. First two color bars are the real inputs you insert onto the handle. The second two bars pertain to the recommended inputs calculated from automation (not necessarily correct). The last two are slip ratios of two tracks, which should be maintained on a low level.

E — Recommended speed, orientation of vehicle from automation system, and the guidance forces (not necessarily correct) .

F — Current speeds of surround seawater.

G — **Mode switches, which will be only activated in supervisory control.** You can tell the status of the system, either in manual control or full automation, based on the color of these two buttons. For example, in full automation, 'automation' will be in green while 'Manual' will turn into grey.

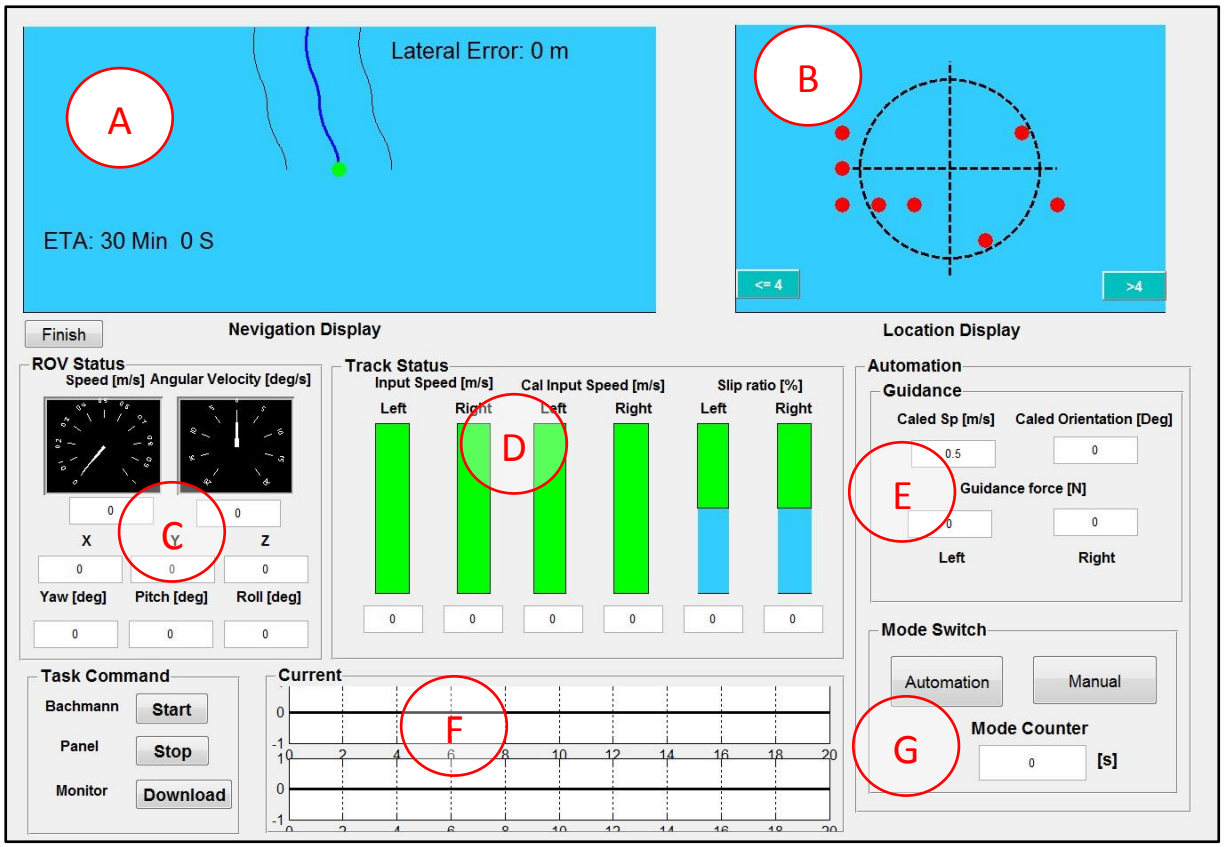

Figure 4. Details on dashboard.

In the second part, you will do the formal experiment section. Within this section you need to finish the path tracking task as in the training section and also accompanying secondary task **three times**, each will last for about 15 minutes. Each repetition is rendered in different conditions, namely manual control, haptic shared control and supervisory control. In manual control mode you directly control the motion of the vehicle. In haptic shared control mode, you will feel some guidance force through the rotary handles. **But this does not necessarily mean that you need to obey this guidance**. Always act naturally and try your best in both path tracking task and secondary task. In supervisory control, the vehicle will be in autonomous control mode and you only need to respond to the secondary task. However the automation system is not correct when encountering obstacles and slip, thus you need to intervene in the control loop once you feel necessary. Switch between automation and manual control is shown below:

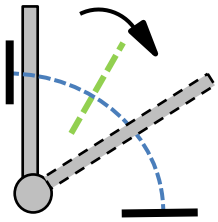

a. From automation to manual control, **pull back either of these two handles to less than 0.6 m/s for 0.5 seconds**, you can refer to 'D' part of the dashboard for your real input and indicators in 'G' section for system status.

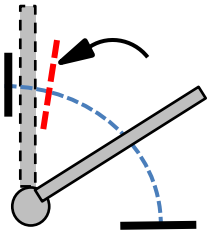

b. From manual control to automation, **push forward both two handles to exceed 0.9m/s for at least 0.5 seconds once the vehicle recovers back to the optimal path with less than 0.6m of absolute lateral deviation**, you can refer to 'D' part of the dashboard for your real input and indicators in 'G' section for system status.

Figure 5. Switch between automation and manual control.

Keep in mind that the order of aforementioned three conditions is only for explanation purpose, and is not the real order in actual experiment. For driving task, you are supposed to avoid all obstacles while keep as close to the optimal path as possible. This means that after you have avoided the obstacle, you should swiftly get back to the centerline. In addition, the whole time to complete the task is also a measurement to evaluate your performance. Thus as long as you can ensure obstacle avoidance and lateral error to the optimal path, you should drive as quickly as you can during the experiment. Last but not least, please be aware that the vehicle driving task is more important than secondary task.

If you have any questions regarding the experiment protocol, please do not hesitate and ask the experimenter directly. If you have any further questions about this experiment after your participation, please contact Kang Wang (K.Wang-3@student.tudelft.nl).

If you do not have further questions and feel ready to do the experiment, please do sign the informed consent before the actual experiment.

Good luck and enjoy the experiment.

Appendix VI – Reference

Abbink, D. a., & Mulder, M. (2009). Exploring the Dimensions of Haptic Feedback Support in Manual Control. *Journal of Computing and Information Science in Engineering*, *9*(1), 011006. doi:10.1115/1.3072902

Bekker, M. G. (1969). *Introduction to Terrain-Vehicle System*. Ann Arbor, Michigan: The University of Michigan Press.

Choi, J., Hong, S., Kim, H., & Lee, T. H. (2003). An Experimental Study on Tractive Performance of Tracked Vehicle on Cohesive Soft Soil. In *ISOPE* (pp. 139–143).

Dai, Y., Liu, S., Li, L., & Li, Y. (2010). Development of a fast simulation model for dynamic analysis of the 1000 m deep ocean mining system. *World Journal of Modelling and Simulation*, *6*(2), 83–96.

Dai, Y., Liu, S., Li, L., Li, Y., Wang, G., & Cao, X. (2009). Virtual Prototype Modeling and Fast Dynamic Simulation of the Complete Integrated Sea Trial System for Deep-Ocean Mining. *2009 International Conference on Computer Modeling and Simulation*, 244–250.

Griffiths, P., & Gillespie, R. B. (2005). Sharing Control Between Human and Automation Using Haptic Interface : Primary and Secondary Task Performance Benefits. *Human Factors*, *47*(3), 574–590.

Hong, S., Choi, J.-S., Kim, H.-W., Won, M.-C., Shin, S.-C., Rhee, J.-S., & Park, H. (2010). A path tracking control algorithm for underwater mining vehicles. *Journal of Mechanical Science and Technology*, *23*(8), 2030–2037.

Hong, S., Kim, H. W., & Choi, J. (2002). Transient Dynamic Analysis of Tracked Vehicles on Extremely Soft Cohesive Soil. In *ISOPE* (pp. 100–107).

Ishiguro, S., Yamauchi, Y., Odaka, H., & Akiyama, S. (2013). Development of Mining Element Engineering Test Machine for Operating in Seafloor Hydrothermal Deposits. *Mitsubishi Heavy Industries Technical Review*, *50*(2), 21–26.

Janosi, Z., & Hanamoto, B. (1961). The Analytical Determination of Drawbar Pull as a Function of Slip for Tracked Vehicles in Deformable Soil. In *First International Conference on the Mechanics of Soil-Vehicle Systems*. Torino, Italy.

Kim, H., Hong, S., & Choi, J. (2004). A Study on Prediction Model of Tracked Vehicle for Straight Maneuvering on Soft Soil. In *The Fourteenth International Offshore and Polar Engineering Conference* (Vol. 1, pp. 83–89).

Kim, H., Hong, S., Choi, J., & Yeu, T. (2005). Dynamic Analysis of Underwater Tracked Vehicle on Extremely Soft Soil by Using Euler Parameters. In *The Sixth ISOPE Ocean Mining Symposium* (pp. 141–148).

Kitano, M., & Jyozaki, H. (1976). A theoretical Analysis of Steerability of Tracked Vehicles. *Journal of Terramechanics*, *13*(4), 241–258.

Le, A. T. (1999). *Modelling and control of tracked vehicle*. The University of Sydney.

Lee, C., Kim, H., Hong, S., & Kim, S. (2011). A Study on the Driving Performance of a Tracked Vehicle on an Inclined Plane according to the Position of Buoyancy. In *The Ninth ISOPE Ocean Mining Symposium* (pp. 104–109).

Li, L., & Li, S. (2010). Simulation and mechanical characteristics of terramechanics of the surface soil on deep-sea bed (in Chinese). *Engineering Mechanics*, *27*(11).

Lipton, I. (2008). Mineral Resource Estimate Solwara 1 Project Bismarck Sea Papua New Guinea for Nautilus Minerals Inc.

Murakami, H., Watanabe, K., & Kitano, M. (1992). A Mathematical Model for Spatial Motion of Tracked Vehicles on Soft Ground. *Journal of Terramechanics*, *29*(1), 71–81.

Wills, B. M. D. (1963). The measurement of soil shear strength and deformation moduli and a comparison of the actual and theoretical performance of a family of rigid track. *Journal of Agricultural Engineering Research*, *8*(2), 115–131.

Wong, J. Y. (2001). *Theory of Ground Vehicles* (3rd ed.). Wiley.

Wong, J. Y. (2009). Development of high-mobility tracked vehicles for over snow operations. *Journal of Terramechanics*, *46*(4), 141–155.

Wong, J. Y. (2010). *Terramechancis and Off-road Vehicle Engineering*.

Wu, H., Chen, X., Gao, Y., He, J., Ding, L., & Xu, Y. (2008). Research on Effects of Grounding Pressure Distribution of a Type of Seabed Tracked Vehicle on Traction Force. In *The Eighteenth International Offshore and Polar Engineering Conference* (Vol. 8, pp. 73–77).